

INRIM - Politecnico di Torino

Ph.D. in Metrology: Measuring Science and Technique



Ph.D. Thesis

# Laboratory measurements of building acoustics at low frequencies: a modal approach

Andrea Prato

**Supervisor**

Dr. Alessandro Schiavi

**Academic supervisor**

Prof. Arianna Astolfi



*To Physics and Music, my greatest passions.*



# Abstract

The current international request to extend standard laboratory measurements of building acoustics (airborne and impact sound insulation and reverberation time) to frequencies below 100 Hz requires a deep study on the involved physical phenomenon and a proper procedure in order to get repeatable and reproducible results. In typical laboratory volumes (50-80 m<sup>3</sup>) and at low frequencies (50-100 Hz), the acoustic field is non-diffuse due to the presence of standing waves or resonant modes in the small laboratory rooms. In space and frequency domains, the sound field is characterized by large fluctuations of sound pressure levels, different from diffuse field condition, characterized by uniform sound field in both domains and is assumed from 100 Hz on in laboratory standard procedures. Under such conditions, standard sound insulation measurements and reverberation time descriptors are not adequate to correctly characterize the insulating property of partitions or flooring systems or the reverberation times of laboratory (or ordinary dwelling) rooms. For this reason, a new measurement approach based on resonant frequencies, or room modes, the so-called modal approach, is introduced. Resonant modes provide deterministic quantities in non-diffuse field and are responsible of most annoyance.

For airborne sound insulation, the standard sound reduction index is not representative of sound insulation as it is based on sound power measurements, which is still undefined for non-diffuse acoustic field. In the coupled system room-partition-room, in addition to natural resonant modes of each system component, the transmission of modes from the source to the receiving room is observed. The modal approach allows to evaluate the sound insulation by the determination of the sound transmission loss of a single source room mode passing into the receiving room through the partition. Such characteristic is the base of the new descriptor: the modal sound insulation. It is defined as the difference between the maximum sound pressure levels (evaluated in the corners of rectangular rooms) of source room modes that occur in both source and receiving rooms. Starting from the classical modal theory, a proper normalization term, corresponding to receiving room volume, is also introduced and presented together with a new method, based on the envelope of room frequency responses, to extend the results to the whole low frequency range, due to the discrete nature of modal sound insulation. Fur-

thermore, the uncertainty budget is analysed. From scale model measurements, normalization term results to be negligible and problems due to source and receiving room modal match, cause of sound insulation underestimation, has to be solved in the future with a proper weighting procedure, based on the increase of modal sound insulation as function of modal overlap degree (Kohlrausch-Williams-Watts function), experimentally evaluated in the scale model.

The modal approach is also applied to impact sound insulation and impact noise reduction measurement: new procedure and descriptors are introduced and first experimental tests on three different mass-spring systems are shown. Results agree with theoretical basis and validate such approach.

In the end, the modal approach is used for the measurement of reverberation time in small rooms, in terms of modal reverberation time. Two different methods are evaluated on the base of their mathematical relation: the direct and indirect methods. The first is based on the measurement of the direct modal sound decay, whereas the second evaluates the modal decay starting from the measurement of the half bandwidth of the resonant peak. For both methods, different sound signals are compared and suitable procedures are applied. First experimental tests show a good agreement between the two methods and their mathematical relation is confirmed.

# List of symbols

$c$	speed of sound ( $\text{m s}^{-1}$ )
$f$	frequency (Hz)
$f_0$	mass-spring system resonant frequency (Hz)
$f_n$	$n$ -th mode frequency (Hz)
$f_s$	Schroeder frequency (Hz)
$k$	wavenumber ( $\text{rad m}^{-1}$ )
$k_n$	$n$ -th mode wavenumber ( $\text{rad m}^{-1}$ )
$l$	axial modal integer (-)
$m$	tangential modal integer (-)
$n$	oblique modal integer (-)
$n_f$	eigenfrequency density (-)
$p$	sound pressure (Pa)
$p_0$	reference sound pressure (Pa)
$q$	partition modal integer (-)
$r$	partition modal integer (-)
$s$	experimental standard deviation (-)
$s'_{tot}$	dynamic stiffness ( $\text{MN/m}^3$ )
$t$	time (s)
$v$	vibrational velocity ( $\text{m s}^{-1}$ )
$v_n$	normal velocity ( $\text{m s}^{-1}$ )
$x$	space coordinate (m)
$y$	space coordinate (m)
$z$	space coordinate (m)
$A$	equivalent sound absorption area ( $\text{m}^2$ )
$A_n$	$n$ -th mode amplitude (Pa)
$C$	standing wave amplitude in rectangular room (Pa)
$D$	airborne sound insulation (dB), flexural stiffness ( $\text{N m}^2$ )
$D_{modal}$	modal sound insulation (dB)
$D_{modal,nV}$	normalized modal sound insulation (dB)
$G$	coupling factor (-)
$I$	sound intensity ( $\text{Pa m s}^{-1}$ )
$L$	room length (m)

$L_{modal}$	modal impact sound pressure level (dB)
$L_n$	normalized impact sound pressure level (dB)
$L_p$	sound pressure level (Pa)
$M$	surface mass ( $\text{kg m}^{-2}$ )
$MOF$	modal overlap factor (-)
$N_f$	number of eigenfrequencies (-)
$Q_0$	source total air outflow amplitude ( $\text{m s}^{-1}$ )
$Q_n$	total air outflow amplitude of the $n$ -th source ( $\text{m s}^{-1}$ )
$R$	sound reduction (dB)
$RSS$	residual sum of squares (-)
$S$	surface ( $\text{m}^2$ ), microphone sensitivity (V/Pa)
$T$	reverberation time (s), output voltage (V)
$T_n$	modal reverberation time (s)
$U$	expanded uncertainty (-)
$V$	volume ( $\text{m}^3$ )
$W_1$	incident sound power ( $\text{J s}^{-1}$ )
$W_2$	transmitted sound power ( $\text{J s}^{-1}$ )
$Z$	wall impedance ( $\text{Pa s m}^{-1}$ )
$\delta_n$	modal damping ( $\text{rad s}^{-1}$ )
$\psi_n$	spatial distribution function (-)
$\rho_0$	air density ( $\text{kg m}^{-3}$ )
$\sigma$	standard deviation (-)
$\tau$	transmission coefficient (-)
$\omega$	angular frequency ( $\text{rad s}^{-1}$ )
$\omega_n$	$n$ -th mode angular frequency ( $\text{rad s}^{-1}$ )
$\Delta f_{-3dB}$	resonant frequency half bandwidth (Hz)
$\Delta f$	modal overlap degree in frequency (Hz)
$\Delta L$	improvement of impact sound insulation (dB)
$\Delta L_{modal}$	improvement of modal impact sound insulation (dB)
$\Delta x$	difference between source and receiving room $x$ dimension (cm)
$\Lambda_n$	modal distribution constant (-)

# Contents

<b>1</b>	<b>Introduction</b>	<b>13</b>
1.1	State of the art, aims and objectives . . . . .	13
1.2	Overview . . . . .	18
<b>2</b>	<b>Theory</b>	<b>19</b>
2.1	Acoustic field in enclosed spaces . . . . .	19
2.1.1	The wave theory . . . . .	19
2.1.2	Normal modes in rectangular rooms with rigid boundaries .	22
2.1.3	Modal sound field in rectangular rooms with non-rigid boundaries . . . . .	28
2.2	Airborne sound insulation . . . . .	29
2.2.1	Sound insulation in diffuse field condition . . . . .	29
2.2.2	Sound insulation in non-diffuse field condition . . . . .	32
2.3	Modal reverberation time . . . . .	35
2.4	Impact sound insulation . . . . .	39
<b>3</b>	<b>Preliminary measurements</b>	<b>43</b>
3.1	Instrumentation: measurement devices and setup . . . . .	43
3.2	Characterization of acoustic source . . . . .	47
3.3	Modal qualification of airborne sound insulation laboratory rooms .	48
3.3.1	Spatial distribution of source and receiving room natural modes . . . . .	49
3.3.2	Spatial distribution of source room transmitted modes into receiving room . . . . .	51
<b>4</b>	<b>Airborne sound insulation at low frequency: the modal approach</b>	<b>53</b>
4.1	The modal sound insulation . . . . .	54
4.2	Normalization terms . . . . .	59
4.3	The extension to the whole low frequency band . . . . .	64
<b>5</b>	<b>Evaluation of uncertainty budget</b>	<b>67</b>
5.1	Type A and combined standard uncertainty of room modes . . . . .	67

5.2	Repeatability of modal sound insulation measurement . . . . .	73
5.3	Reproducibility of modal sound insulation measurement . . . . .	75
<b>6</b>	<b>Analysis of modal sound insulation in the scale model</b>	<b>79</b>
6.1	Measurement setup . . . . .	79
6.2	Evaluation of volume normalization term . . . . .	80
6.3	The influence of modal match . . . . .	85
6.4	Validation of the extension to the whole low frequency range . . . .	90
6.5	Reproducibility of different methods . . . . .	91
<b>7</b>	<b>The modal approach for reverberation time measurement</b>	<b>95</b>
7.1	Preliminary measurements . . . . .	97
7.2	Direct method . . . . .	100
7.2.1	Pink noise . . . . .	101
7.2.2	Sine waves . . . . .	104
7.2.3	Comparison between different source signals . . . . .	112
7.3	Indirect method . . . . .	113
7.4	A first comparison between proposed methods . . . . .	115
7.5	Spatial measurements . . . . .	117
7.5.1	Indirect measurement . . . . .	117
7.5.2	Direct measurement . . . . .	119
7.5.3	Comparison between direct and indirect measurements . . . .	119
<b>8</b>	<b>The modal approach for impact sound insulation measurement</b>	<b>121</b>
8.1	The modal impact sound insulation . . . . .	122
8.2	Experimental measurements . . . . .	122
8.2.1	Test elements . . . . .	123
8.2.2	Measurement procedure . . . . .	123
8.2.3	Impact source: tapping machine or heavy/soft impact ball . . . .	124
8.2.4	Results and observations . . . . .	125
<b>9</b>	<b>Conclusions and future works</b>	<b>129</b>
	<b>Appendices</b>	<b>133</b>
<b>A</b>	<b>The modal sound insulation: comparison between sweep and noise signals</b>	<b>135</b>
<b>B</b>	<b>Normalization terms</b>	<b>139</b>
<b>C</b>	<b>Matlab scripts</b>	<b>143</b>
C.1	Extension of modal sound insulation envelope to one-third octave bands . . . . .	143

C.2 Calculation of resonant peak half bandwidth . . . . . 146

**Bibliography** . . . . . **150**



# Chapter 1

## Introduction

### 1.1 State of the art, aims and objectives

In recent years an increasing interest in building acoustics measurements and building components characterization at low frequencies (i.e. below 100 Hz, and typically from 50 Hz) has been observed. The consideration of low frequency noise has become more and more important because there is an increasing occurrence of sound sources with low frequency content, like technical equipment inside and outside of buildings, increased traffic volume and 'improved' video and audio equipment in dwellings. Also, more and more renewable energy sources like heat pumps, decentralised combined heat and power stations and wind turbines contribute to low frequency sound impact on people [1, 2]. Simultaneously, newer multilayer building elements, developed to be cheaper and lighter and eventually to have a better thermal insulation, tend to have resonance frequencies below 100 Hz, which become more and more disturbing under these circumstances. Former buildings consisted mostly of homogeneous heavyweight walls and floors, which do not have particular insulation problems at low frequencies [3]. Nevertheless, at present time, effective protection systems against low frequencies noise are still an open challenge both for researchers and components manufacturers.

Low frequency noise is in particular harmful since, on one hand, it propagates over long distances outdoors and, on the other, it coincides with poor sound insulation in buildings [4]. Main effects caused by noise, in particular at low frequencies, are temporal and permanent threshold shifts [5], pressure in the ear [6], impaired task performance or sleep disturbance [7]. More severe effects at higher sound levels are for example headache, feeling of irritation and stress [8]. It is not yet clear, whether some of the symptoms are psychosomatic. It is also not yet clear, whether the effects of low-frequency noise can be traced back solely to cochlear stimulation or other sound transmission paths [9]. The large number of isolated facts listed above are known, but they do not yet reveal cause-and-effect principles, which could be applied for practical purposes, such as legal requirements.

Currently, human perception is almost exclusively regarded in terms of selected equal-loudness contours, which are highly controversial at low frequencies and can be seen from a more than 10 dB difference of equal loudness contours at 50 Hz in the (new) ISO 226:2003 [10] (revised in 2014) and DIN 45631 [11] standards. Levels below the hearing threshold can also provoke reactions. So, for example, perception of low frequency noise takes place even below 20 Hz, but it is no longer perceived as tones [12]. Above the hearing threshold, the perceived loudness increases steeply at low frequencies but the upper limit of tolerability remains constant. Thus, small changes of sound pressure levels may cause dramatic effects. This makes it difficult to set adequate insulation requirements. The lack of knowledge and measurement methods prevents the formulation of requirements, extended to low frequencies, and subsequently the development of optimised building products and technical equipment, although low frequency problems are increasing. According to a survey by the German Federal Environment Agency (Umweltbundesamt) in 2011 [13] only 12.5% of the population are not disturbed by noise whereas about 60% are essentially or highly disturbed. Protection against noise in general is a basic requirement of the EU environmental legislation as well as of the regulations for building products, The EU regulation No 305/2011 [14] (repealing the former Council Directive 89/106/EEC) lists "protection against noise" as one of the seven basic requirements for construction works, saying "The construction works must be designed and built in such a way that noise perceived by occupants or people nearby is kept to a level that will not threaten their health and will allow them to sleep, rest and work in satisfactory conditions" or the directives of World Health Organization, "Excessive noise seriously harms human health and interferes with peoples daily activities at school, at work, at home and during leisure time. It can disturb sleep, cause cardiovascular and psychophysiological effects, reduce performance and provoke annoyance responses and changes in social behaviour" [15].

In Building Acoustics, noise below 100 Hz has been more or less neglected up to now, because the established measurement methods for sound insulation require smooth sound fields, which don't increasingly exist in rooms at such low frequencies. At present, minimum sound insulation requirements for buildings in European countries do not take into account frequencies below 100 Hz (apart from Sweden) [16]. Being aware of this situation, the COST Action TU0901 "Integrating and Harmonizing Sound insulation Aspects in Sustainable Housing Constructions" was established in 2010. COST is an intergovernmental framework for European Cooperation in Science and Technology, allowing the coordination of nationally-funded research at European level. COST TU0901 WG1 has just submitted a document N066, where it is recommended to extend all building acoustic evaluations down to 50 Hz, the present voluntary lower limit of measurements in standards. Much lower frequencies were discussed but not included due to a lack of applicable measurement procedures there. Unfortunately the existing acoustical measurement procedures are not suitable and accurate enough in order to achieve

repeatable and reproducible building acoustics measurements in the low-frequency range (50-100 Hz). Typically building acoustics measurements (airborne sound insulation, impact sound insulation and reverberation time) lead to unacceptable high uncertainties when applied to frequencies below 100 Hz [17-23]. On the basis of this, standardized laboratories, involved in building acoustic measurement, have to be opportunely qualified in order to guarantee proper characterizations below 100 Hz. At present, the measurement of sound pressure levels and sound insulation in building acoustics is based on the existence of diffuse sound fields, which requires small wavelengths compared with the dimensions of the involved rooms and building elements. This assumption aims at a high comparability of measurement results, even if they were obtained from diverging measurement conditions. This works fairly well down to about 100 Hz but represents an abuse below. At lower frequencies, single vibration modes determine the results, leading to a high spatial spread of sound pressure levels and a high dependence of sound reduction values on details of the situation, which makes it difficult for example to characterize the performance of building components. On the basis of these conclusions, laboratory measurements are fundamental in order to provide a first characterization of acoustic performance of building components at low frequency with proper measurement methods to improve the actual standards and to be, in the future, applicable for in-situ measurements.

Standard measurements are historically performed by measuring sound pressure levels in the frequency range between 100 Hz and 5000 Hz in one-third-octave bands. The performance of airborne sound insulation of vertical partitions is quantified by the sound reduction index ( $R_W$ ), based on sound power ratios which are derived from measured field quantities like sound pressure under diffuse field condition (i.e. short wavelength with respect to room dimensions). The measurement procedure, as stated in the new ISO 10140-2:2010 [24] standard, is widely known. Less known is the acoustical performance of building components in non-diffuse field condition, such as for frequencies below 100 Hz. Standardized airborne sound insulation laboratories, in which volume ranges between 50 m<sup>3</sup> and 80 m<sup>3</sup>, are characterized by a non-diffuse field (i.e. wavelengths equal or wider than room dimensions) below the Schroeder frequency, usually around 350 Hz. Anyway, for practical reasons, it is conventionally accepted a condition of diffuse field from 100 Hz on. Generally speaking, measurements of sound insulation in diffuse field condition (such as classical transmission loss as stated in former ISO 140 standard series) are possible since the sound pressure in the enclosed volumes of the rooms is space-time independent. This condition is not true below the Schroeder frequency, and in particular below 100 Hz, in which the modal behaviour becomes dominant with stationary (and quasi-stationary) waves which entail large sound pressure level fluctuations [25]. Acoustical measurements carried out without the due caution below 100 Hz can lead to strongly inaccurate characterizations, since the distribution of the sound pressure in space and frequency domains is not uniform

in the enclosed and small volume. Currently it is not possible to correctly define the incident and transmitted sound power in such modal acoustic field according to standard approach. At this point a question arises: even if it is possible to determine the sound power emitted by a building element, how would it be correlated to the modal sound field and the real human perception? Would it be an accurate evaluation of sound insulation? Several authors in the past, closely related to a diffuse field approach, proposed different measurement methods to evaluate sound reduction index [26, 27], nevertheless some issues have to be deepened. In particular, measurement of the sound reduction index  $R_W$  at low frequencies is extremely variable from one laboratory to another (low reproducibility) [28, 29] and depends on several parameters that affect the modal composition of the sound field [30], such as the geometrical dimensions of the rooms, the location of the sound source, the geometry and the vibration properties of the interface, the room-panel-room modal coupling and the reverberation time, related to modal absorption, of the two rooms [31]. Actually, a new sound intensity measurement procedure has been recently proposed in order to achieve low frequencies airborne sound insulation in laboratory [32]. Nevertheless sound intensity approach is subjected to several practical complications, such as the presence of a totally sound absorbing surface on the opposite wall, in receiving room and, at this time, the lack of a standardized calibration procedure of the sound intensity probes. Since in new ISO 10140:2010 standard series it is stated to perform sound pressure level measurement rather than sound intensity one, a suitable procedure, united with a proper laboratory qualification, must be achieved. Besides, revision of ISO 717 standard [33, 34], which aims to redefine new single-number quantities for airborne sound insulation, includes low frequency range (50 Hz, 63 Hz and 80 Hz) without the introduction of a specific measurement procedure [35]. The attempt proposed in this thesis is to fill this gap providing both a theoretical analysis of the non-diffuse acoustical field and an exhaustive experimental survey in laboratory. Theoretical background of sound pressure modal behaviour, in source room and receiving room, the motion of the panel and the related interactions is discussed and the boundary conditions are properly analysed. As a consequence, from experimental measurements and data analysis, the possibility to define a correct sound insulation descriptor in agreement with non-diffuse field conditions is investigated. Once the non-diffuse field of the source room and receiving room is identified, the modal sound insulation ( $D_{modal}$ ), different from sound reduction index for diffuse field, is defined as the difference between the maximum sound pressure levels of source room modes that occur in both source (natural mode) and receiving rooms (transmitted mode) and can be represented as an indicator of modal sound transmission loss. Theoretical background, measurement procedures with related problems and introduction of a normalization term are discussed. Furthermore, a first rough method to extend sound insulation measurement to all frequencies between 44 Hz and 112 Hz (the lower and upper bounds of the 50 Hz and 100 Hz third octave bands respectively)

is also proposed and a one-third-octave band representation (from 50 Hz to 5000 Hz) as stated in ISO 717 revision is consequently possible.

As for airborne sound insulation, also impact sound insulation existing indexes described in ISO 10140-3:2010 [36] need to be reviewed and adapted in order to better describe the physical phenomenon in connection with the actual auditory perception of noise due to modal field and to ensure repeatable and reproducible laboratory values. Different authors have modelled the effect of the impact sound transmission by using low frequency modal analysis and provided a good prediction of the acoustic field generated in a rectangular room with a punctual sound source [37]. Based on these results and on the modal approach introduced for airborne sound insulation, technical and practical solutions, from a metrological and regulatory point of view, are provided to qualify the measurement laboratory for the characterization of the acoustic performance of a floor for frequencies below 100 Hz. For this purpose, a new index of impact sound insulation in non-diffuse field condition is introduced and first experimental measurements are performed.

The growing interest of the international scientific community to extend the conventional building acoustics comprehends also architectural acoustic measurements at frequencies below 100 Hz, which require detailed studies about the decay of the sound pressure and the reverberation time in small enclosures (30-200 m<sup>3</sup>). In such conditions, the standard measurement of reverberation times involves high measurement uncertainty caused by the presence of the acoustic modes in the room, responsible for the highest inconvenience for what concerns the quality of listening (rumble effect) or noise from other environments, as stated by different authors [38-40]. The reverberation time is defined as the time (in seconds) for the sound pressure to decay by 60 dB or, in terms of energy, is the time taken by the energy to decay of one-millionth from its initial value. This definition fits very well to the type of procedure described in ISO 3382-2:2008 [41], which provides a direct measurement of the sound pressure decay. The problem that emerges by this measure is the non-linearity of the decay with a broadband analysis (one-third octave band as stated in the ISO Standard) due to the presence of more resonant frequencies in one band, each with its particular decay. At frequencies below 100 Hz in such rooms, in fact, non-diffuse sound field conditions are reached: this field has the particularity of being homogeneous neither in frequency nor in space. This means that, by analysing the frequency spectrum below 100 Hz, resonant frequencies are evident and their peaks are well spaced and their spatial distribution inside the room is not uniform. Furthermore human sound perception in non-diffuse field is mainly affected by resonance modes, which entail many problems for acoustic comfort or quality of listening, especially in recording studios, small concert halls or open-space offices. Therefore, the measurement of reverberation time at low frequency is preparatory and necessary for the acoustic treatment of listening and working rooms. The Directive ISO 3382, which describes how to measure reverberation times in ordinary rooms (especially in small dwellings) with interrupted noise

or integrated response to the impulse, does not provide a measurement method for frequencies below 100 Hz. The peculiarity of such sound field has to be considered due to its non-diffuse nature, i.e. the presence of standing waves into the internal system. For this purpose, a modal approach also for reverberation time measurement is applied, resulting in measuring reverberation times for single resonant frequencies: the modal reverberation time. It is, firstly, measured with two different methods: the first is a direct measurement of the reverberation time, based on the guidelines of ISO 3382, but with different measurement positions and source signals; the second one is the indirect method, based on the measurement of the half bandwidth of resonance modes in the considered low frequency range, which is related to the modal damping and, as a consequence, to the modal reverberation time.

## 1.2 Overview

In Chapter 2, the theoretical basis of non-diffuse sound field is described, as well as the physics of main building acoustics measurements (airborne sound insulation, reverberation time and impact sound insulation), their Standard procedures and the connections with non-diffuse acoustic field condition at low frequencies (50-100 Hz).

Chapter 3 describes the instrumentation setup and measurements devices and the modal qualification of airborne sound insulation chambers of INRIM laboratories.

In Chapter 4, 5 and 6, the modal approach is introduced for airborne sound insulation measurement in laboratory and a new descriptor with proper normalization term is proposed on the basis of theoretical calculation and experimental tests. The analysis of uncertainty is then performed for modal sound pressure level and modal sound insulation measurements. Finally, the modal approach in the scale model is evaluated in order to examine in depth normalization term previously introduced, to validate the extension of modal sound insulation to the whole low frequency range and to compare reproducibility standard deviations obtained from standard and modal approaches.

Chapter 7 is focused on the measurement of reverberation time in non-diffuse sound field at low frequencies with two methods (direct and indirect) and different source signals are analysed. A first uncertainty evaluation is also presented.

In the end, the impact sound insulation at low frequencies is dealt in Chapter 8. New descriptors according to the modal approach are introduced and first experimental evidences are shown.

# Chapter 2

## Theory

In this chapter a basic background theory about the sound propagation in enclosed spaces, i.e. in spaces containing homogeneous fluid, air, and completely delimited by rigid or partially rigid boundaries typical of building acoustics laboratory rooms, is described. Besides, a description of main building acoustic measurements involved in the research, related to ISO standards, is showed.

### 2.1 Acoustic field in enclosed spaces

#### 2.1.1 The wave theory

The starting point for the representation of sound field in a room is the classical wave theory [25, 42, 43]:

$$\nabla^2 p = \frac{1}{c^2} \frac{\partial^2 p}{\partial t^2} \quad (2.1)$$

where  $p$  is the sound pressure and  $c$  is the velocity of sound. Assuming a harmonic time law for the pressure with an angular frequency  $\omega$ , i.e.  $p = p_\omega(\mathbf{r})e^{i\omega t}$ , where  $\mathbf{r}$  represents the three spatial coordinates, the Helmholtz equation is obtained

$$\nabla^2 p_\omega(\mathbf{r}) + k^2 p_\omega(\mathbf{r}) = 0 \quad (2.2)$$

where  $k = \omega/c$  is the wavenumber. Furthermore, assuming that the room under consideration has locally reacting walls and ceiling as boundary conditions, the velocity component normal to any wall is

$$v_n = -\frac{1}{i\omega\rho_0} \frac{\partial p}{\partial n} \quad (2.3)$$

Replacing  $v_n$  with  $p/Z$ , where  $Z$  is the wall impedance, the previous equation becomes

$$Z \frac{\partial p}{\partial n} + i\omega\rho_0 p = Z \frac{\partial p}{\partial n} + ikc\rho_0 p = 0 \quad (2.4)$$

where  $\rho_0$  is the air density. The wave equation yields non-zero solutions fulfilling the boundary condition (Eq. 2.4) only for particular discrete values of  $k_n$ , called eigenvalues, where  $n$  represents a trio of integers. Each eigenvalue  $k_n$  is associated with a solution  $\psi_n(\mathbf{r})$ , which is the eigenfunction of the considered room, or *distribution function*. Providing a fixed value for  $k = \omega/c$ , i.e. the driving frequency of a sound source, it is possible to prove that eigenfunctions are mutually orthogonal:

$$\int \int \int_V \psi_n(\mathbf{r})\psi_m(\mathbf{r})dV = \begin{cases} V\Lambda_n & \text{for } n = m \\ 0 & \text{for } n \neq m \end{cases} \quad (2.5)$$

where  $V$  is the volume of the closed space and  $\Lambda_n$  is some dimensionless constant depending on the shape of the function  $\psi_n$ . It is possible to evaluate acoustical properties of the room knowing all the eigenvalues and eigenfunctions. Now, considering, for the real case, a distribution of sound sources over the room volume represented by a density function  $q(\mathbf{r})$  and a driving frequency  $\omega$ , the Helmholtz equation modifies in the following way:

$$\nabla^2 p_\omega(\mathbf{r}) + k^2 p_\omega(\mathbf{r}) = -i\omega\rho_0 q(\mathbf{r}) \quad (2.6)$$

with the same previous boundary equations. Since eigenfunctions form an orthogonal set of functions, source function can be expanded in series of  $\psi_n$ :

$$q(\mathbf{r}) = \sum_n Q_n \psi_n(\mathbf{r}) \quad \text{with} \quad Q_n = \frac{1}{V\Lambda_n} \int \int \int_V \psi_n(\mathbf{r})q(\mathbf{r})dV \quad (2.7)$$

Furthermore, also solutions  $p_\omega(\mathbf{r})$  can be expanded in eigenfunctions:

$$p_\omega(\mathbf{r}) = \sum_n A_n \psi_n(\mathbf{r}) \quad (2.8)$$

The insertion of both series in Eq. 2.6 leads to

$$\sum_n A_n (\nabla^2 \psi_n + k^2 \psi_n) = -i\omega\rho_0 \sum_n Q_n \psi_n \quad (2.9)$$

Using  $\nabla^2 \psi_n = -k_n^2 \psi_n$ , from Helmholtz equation, and equating term by term in the equation above, the following relations are obtained:

$$A_n (-k_n^2 \psi_n + k^2 \psi_n) = -i\omega\rho_0 Q_n \psi_n \quad (2.10)$$

$$A_n = i\omega\rho_0 \frac{Q_n}{k_n^2 - k^2} \quad (2.11)$$

Considering a point source at the point  $\mathbf{r}_0$  with an amplitude of total air outflow from the source  $Q_0$ , the source function can be represented by a delta-function:

$$q(\mathbf{r}) = Q_0\delta(\mathbf{r} - \mathbf{r}_0) \quad (2.12)$$

In this way,  $Q_n$  terms in Eq. 2.7 become

$$Q_n = \frac{1}{V\Lambda_n}Q_0\psi_n(\mathbf{r}_0) \quad (2.13)$$

Using Eq.s 2.13, 2.10, and 2.8, the sound pressure in a generic point  $\mathbf{r}$  of the room generated by a point source placed in  $\mathbf{r}_0$  at frequency  $\omega$  is

$$p_\omega(\mathbf{r}) = iQ_0\omega\rho_0 \sum_n \frac{\psi_n(\mathbf{r})\psi_n(\mathbf{r}_0)}{V\Lambda_n(k_n^2 - k^2)} \quad (2.14)$$

It is important to underline that the same sound pressure level is obtained exchanging source position  $\mathbf{r}_0$  with observation position  $\mathbf{r}$ . This is the so called *reciprocity theorem* which can be applied with advantage in room acoustics measurements.

Since boundary conditions are usually complex,  $k_n$  term can be expressed by

$$k_n = \frac{\omega_n}{c} + i\frac{\delta_n}{c} \quad (2.15)$$

Assuming that  $\delta_n \ll \omega_n$ , Eq. 2.14 becomes

$$\begin{aligned} p_\omega(\mathbf{r}) &= ic^2Q_0\omega\rho_0 \sum \frac{\psi_n(\mathbf{r})\psi_n(\mathbf{r}_0)}{V\Lambda_n(\omega_n^2 - \omega^2 + 2i\delta_n\omega_n)} \\ &= c^2Q_0\omega\rho_0 \sum \frac{\psi_n(\mathbf{r})\psi_n(\mathbf{r}_0)}{V\Lambda_n(2\delta_n\omega_n + i(\omega^2 - \omega_n^2))} \end{aligned} \quad (2.16)$$

This equation represents the transmission function of the room between the points  $\mathbf{r}$  and  $\mathbf{r}_0$ . Angular frequencies  $\omega_n$  are called eigenfrequencies, or *resonant frequencies*, or *natural modes* of the room. The equation shows that the steady-state pressure wave at a point  $(x, y, z)$  is the sum of the waves corresponding to the different normal modes of the room, each with amplitude proportional to the values of the standing wave at the source and at  $(x, y, z)$ . Larger sound pressure values are obtained for a driving frequency coincident with a resonant frequency  $\omega = \omega_n$ . The  $\delta_n$  term is defined as the damping constant of the  $n$ -th mode. Damping term regulates the amplitude, the width of the resonant peak curves (Fig. 2.1) and lowers the value of the resonant frequency (as seen from the maximum curve). This last behaviour can be neglected as the condition of  $\delta_n \ll \omega_n$  is assumed.

Therefore, for a sound source positioned at  $x_s, y_s, z_s$ , the mean-square sound pressure level at a receiver point  $x, y, z$ , that is associated with the  $n$ -th mode, represented by three indexes  $l, m, n$ , is calculated by

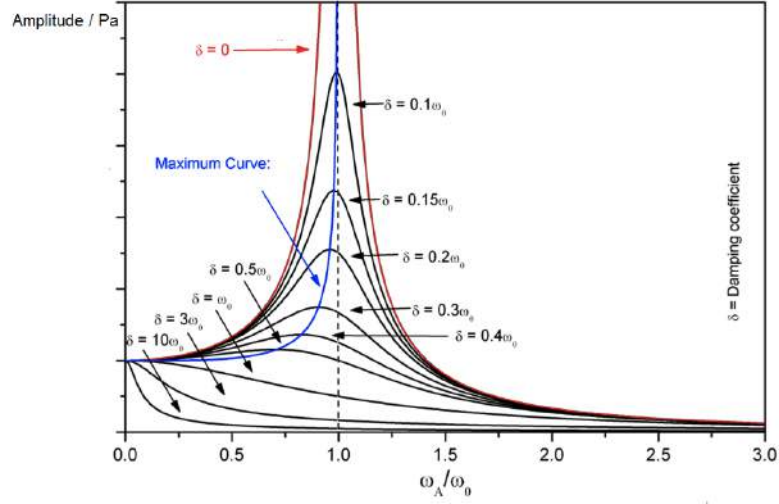


Figure 2.1: Resonant frequency amplitude as function of damping  $\delta_n$ .

$$\langle p_{l,m,n}^2(x, y, z, x_s, y_s, z_s) \rangle_t = \left| \frac{c^2 \omega \rho_0 Q_0 \psi_{l,m,n}(x, y, z) \psi_{l,m,n}(x_s, y_s, z_s)}{V \Lambda_{l,m,n} \sqrt{4\omega_{l,m,n}^2 \delta_{l,m,n}^2 + (\omega^2 - \omega_{l,m,n}^2)^2}} \right|^2 \quad (2.17)$$

This is the general expression of sound field for enclosed spaces which is valid for each room with any shape, volume and damping property. In the following Section, a particular case (rectangular room and rigid boundaries) is considered in order to provide a more intuitive explanation of the physical phenomenon involved, the *modal sound field*.

### 2.1.2 Normal modes in rectangular rooms with rigid boundaries

In order to provide a real and tangible explanation of a sound field in a common closed space, a rectangular room with rigid walls or boundaries and  $L_x, L_y, L_z$  dimensions is considered (Fig. 2.2).

In cartesian coordinates, the wave equation is written as

$$\frac{\partial^2 p}{\partial x^2} + \frac{\partial^2 p}{\partial y^2} + \frac{\partial^2 p}{\partial z^2} - \frac{1}{c^2} \frac{\partial^2 p}{\partial t^2} = 0 \quad (2.18)$$

Assuming an harmonic dependence on time, it can be written as (Helmholtz equation in cartesian coordinates):

$$\frac{\partial^2 p}{\partial x^2} + \frac{\partial^2 p}{\partial y^2} + \frac{\partial^2 p}{\partial z^2} - k^2 p = 0 \quad (2.19)$$

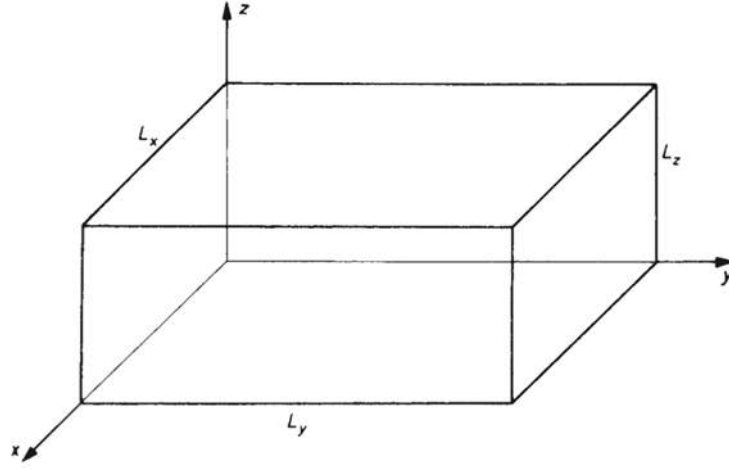


Figure 2.2: Dimensions of a rectangular room.

The acoustic pressure  $p$  can be expressed as the product of three components  $p_x, p_y, p_z$

$$p(x, y, z) = p_x(x)p_y(y)p_z(z) \quad (2.20)$$

In this case, Helmholtz equation becomes

$$\frac{1}{p_x} \frac{d^2 p_x}{dx^2} + \frac{1}{p_y} \frac{d^2 p_y}{dy^2} + \frac{1}{p_z} \frac{d^2 p_z}{dz^2} = -k^2 \quad (2.21)$$

and can be separated in three different equations

$$\frac{d^2 p_x}{dx^2} = -k_x^2, \quad \frac{d^2 p_y}{dy^2} = -k_y^2, \quad \frac{d^2 p_z}{dz^2} = -k_z^2 \quad (2.22)$$

with

$$k_x^2 + k_y^2 + k_z^2 = k^2 \quad (2.23)$$

and boundary conditions for rigid walls (i.e.  $|Z_x| = |Z_y| = |Z_z| = \infty$ )

$$\frac{dp_x}{dx} = 0 \quad \text{for } x = 0 \text{ and } x = L_x \quad (2.24)$$

and the same for  $p_y$  and  $p_z$  components.

Eq. 2.21 has a general solution

$$p_x(x) = A \cos(k_x x) + B \sin(k_x x) \quad (2.25)$$

According to boundary conditions (Eq. 2.24),  $B = 0$  and  $k_x L_x$  must be an integral multiple of  $\pi$ . The constant  $k_x$  must therefore assume one of the allowed values

$$k_x = \frac{n_x \pi}{L_x} \quad (2.26)$$

Similarly the allowed values of  $k_y$  and  $k_z$  are

$$k_y = \frac{n_y \pi}{L_y} \quad (2.27)$$

$$k_z = \frac{n_z \pi}{L_z} \quad (2.28)$$

Inserting these values in Eq. 2.23 resonant frequencies for a three-dimensional rectangular room are obtained:

$$f_n = \frac{kc}{2\pi} = \frac{c}{2} \left[ \left( \frac{n_x}{L_x} \right)^2 + \left( \frac{n_y}{L_y} \right)^2 + \left( \frac{n_z}{L_z} \right)^2 \right]^{1/2} \quad (2.29)$$

where  $n$  is the set of the three indexes  $n_x, n_y, n_z$  and defines the eigenfrequencies, or the modal frequencies, or simply natural modes of the room. The steady state eigenfunction (Eq. 2.20) associated with these eigenvalues is given by

$$p(x, y, z) = C \cos\left(\frac{n_x \pi x}{L_x}\right) \cos\left(\frac{n_y \pi y}{L_y}\right) \cos\left(\frac{n_z \pi z}{L_z}\right) \quad (2.30)$$

where  $C$  is the amplitude of the three-dimensional standing wave and it is necessary to add the time-dependence  $e^{i\omega t}$  in order to get the complete solution. The product of the three cosines is responsible of the large fluctuation of sound pressure in the room, i.e. in the space domain. The numbers  $n_x, n_y, n_z$  indicate the number of nodal planes perpendicular to the  $x$ -axis,  $y$ -axis,  $z$ -axis, respectively and their different combinations distinguish three types of modes: axial, tangential and oblique (Fig. 2.3 and 2.4).

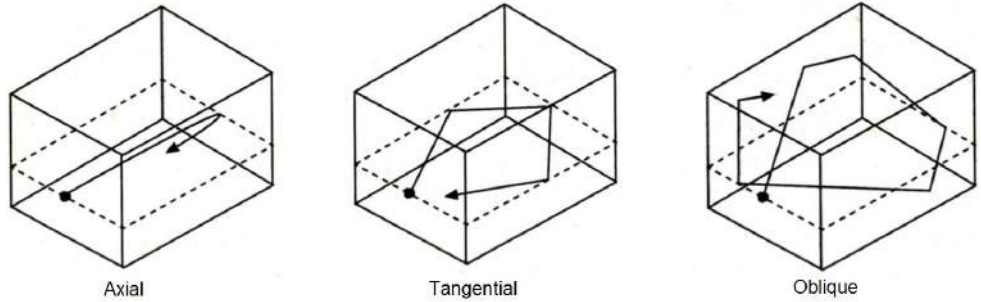


Figure 2.3: Representation of the three kinds of modes in a rectangular room.

- Axial modes correspond to waves which propagate along a Cartesian axis and two indexes are equal to 0;

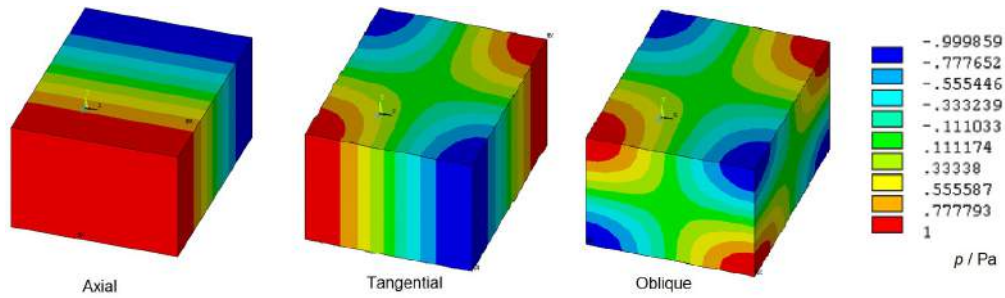


Figure 2.4: Sound pressure distribution in a rectangular space for different modes.

- Tangential modes correspond to waves which propagate in parallel to a pair of walls and are reflected by the other two couples of walls and are represented with an index equal to 0;
- Oblique modes are three-dimensional waves reflected by the other couples of walls and are represented by a set of indexes different from 0.

To show the modal distribution in the frequency domain, it is useful to introduce the following geometrical representation: wavenumbers  $k_x$ ,  $k_y$ ,  $k_z$ , are interpreted as Cartesian coordinates in a  $k$ -space. Each of the allowed values of  $k_x$ , given by Eq. 2.26 corresponds to a plane perpendicular to the  $k_x$ -axis. The same holds for the values of  $k_y$  and  $k_z$ , given by Eq- 2.27. These three equations therefore represent three sets of equidistant, mutually orthogonal planes in the  $k$ -space (Fig. 2.5).

Since for one eigenvalue these equations have to be satisfied simultaneously, each intersection of three mutually orthogonal planes corresponds to a certain eigenvalue. These intersections in their totality form a rectangular point lattice in the  $k$ -space. The lattice points corresponding to tangential and to axial modes are situated on the coordinate planes and on the axes, respectively. This representation allows a simple estimation of the number of eigenfrequencies which are located between the frequency 0 and some other frequency. Geometrically, Eq. 2.23 represents a spherical surface in the  $k$ -space with radius  $k$  enclosing a volume  $4\pi k^3/3$ . On the other hand, since the distance between a certain lattice point and its nearest neighbours is in the three coordinates directions  $\pi/L_x$ ,  $\pi/L_y$ ,  $\pi/L_z$ , the  $k$ -volume per lattice point is  $\pi^3/L_x L_y L_z = \pi^3/V$ . The number of lattice points enclosed in a sphere with radius  $k$ , which is equivalent to the number of resonant frequencies between 0 Hz and a generic frequency  $f$ , is given by:

$$N_f = \frac{\pi k^3/6}{\pi^3/V} = \frac{4\pi}{3} V \left( \frac{f}{c} \right)^3 \quad (2.31)$$

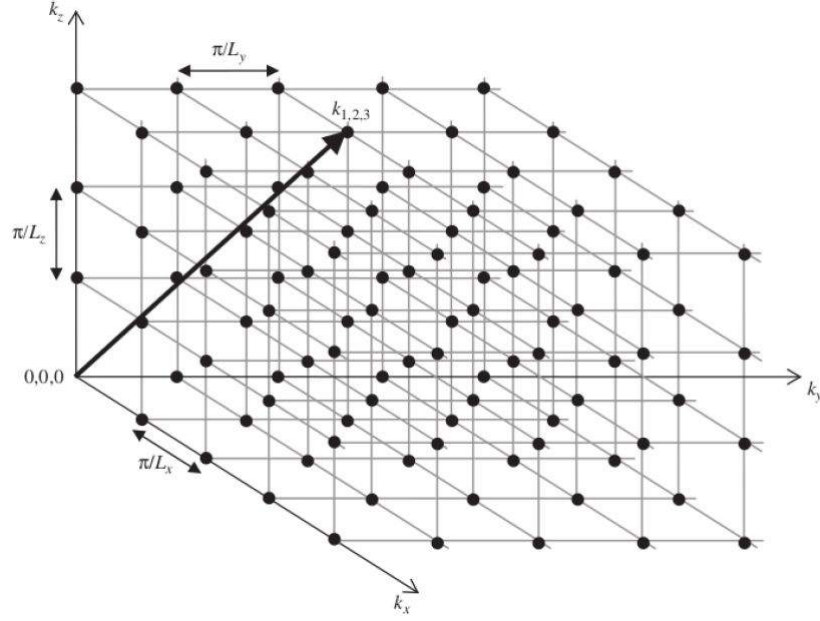


Figure 2.5: Modal lattice in the  $k$ -space.

The average density of eigenfrequencies  $n_f$ , i.e. the number of eigenfrequencies per Hz at the frequency  $f$  is

$$n_f = \frac{dN_f}{df} = 4\pi V \frac{f^2}{c^3} \quad (2.32)$$

On the basis of last equations, the *modal overlap factor MOF* is defined as the degree of overlap of two following modes in the frequency domain and is given by

$$MOF = \frac{\Delta f_{-3dB}}{\Delta f} = \Delta f_{-3dB} n_f \quad (2.33)$$

where  $\Delta f_{-3dB}$  is the half bandwidth corresponding to a 3 dB decrease from the peak of the resonant frequency and  $\Delta f$  is the average frequency spacing between mode frequencies (see Fig. 2.6).

When  $MOF \ll 1$  there is no overlap between two following modes and the frequency response is characterized by deep troughs between two modes. With increasing values of  $M$ , adjacent modes tend to overlap more and more until they cannot be distinguished from one another ( $MOF \gg 1$ ). The term  $\Delta f_{-3dB}$  is directly proportional to the modal damping (see Eq. 2.34) and inversely proportional to modal reverberation time  $T$  (see the following Section 2.3 for a deeper discussion):

$$\Delta f_{-3dB} = \frac{\delta_n}{\pi} = \frac{2.2}{T} \quad (2.34)$$

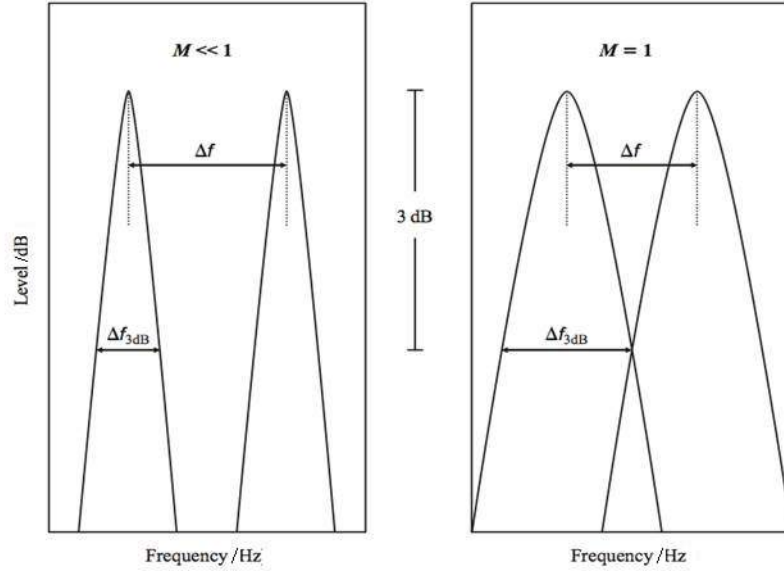


Figure 2.6: Different modal overlap ratios for adjacent modes,  $MOF \ll 1$  and  $MOF = 1$ .

In this way, Eq. 2.33 becomes

$$MOF = \frac{\Delta f_{-3dB}}{\Delta f} = n_f \frac{2.2}{T} = 8.8\pi V \frac{f^2}{c^3} \frac{2.2}{T} \quad (2.35)$$

The value  $MOF = 3$  has been conventionally defined as a limit value to distinguish the modal field ( $MOF < 3$ ) from the diffuse field ( $MOF > 3$ ); see Fig. 2.7.

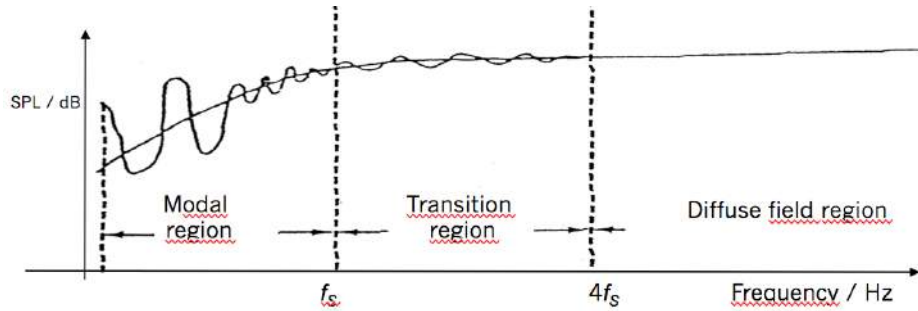


Figure 2.7: From modal to diffuse sound field in the frequency domain.

Inserting such value in Eq. 2.35 it is possible to define the cut-off frequency, or the Schroeder frequency  $f_s$  as

$$f_s \approx 2000 \sqrt{\frac{T}{V}} \quad (2.36)$$

The Schroeder cut-off frequency depends only on the reverberation time and room volume. For small rooms with volumes less than  $60 \text{ m}^3$  and typical reverberation time of  $1.5 \text{ s}$ , the Schroeder frequency is around  $300 \text{ Hz}$ . Below such frequency sound field is characterized by large fluctuation in space and frequency domain (modal field, or non-diffuse field), while above  $f_s$  the acoustic field is defined a diffuse field due to the almost uniform response in space and frequency.

### 2.1.3 Modal sound field in rectangular rooms with non-rigid boundaries

A theory for a generic room with non-rigid walls and a theory for a rectangular room with rigid walls have been discussed so far. Now, a rectangular room with a sound source and non-rigid boundaries is supposed, which represent the most common case for standard dwellings and for most of laboratory rooms. Basic starting equations, boundary conditions and solutions are the ones discussed previously, Eq. 2.9, 2.4, 2.17. The resonant frequencies associated to a rectangular room are given by Eq. 2.29 assuming that  $\delta_n \ll \omega_n$ . For a rectangular room spatial distribution functions  $\psi_{l,m,n}$  in Eq. 2.17 for receiver and source positions can be written, according to Eq. 2.30, as:

$$\psi_{l,m,n}(x, y, z) = \cos\left(\frac{l\pi x}{L_x}\right) \cos\left(\frac{m\pi y}{L_y}\right) \cos\left(\frac{n\pi z}{L_z}\right) \quad (2.37)$$

$$\psi_{l,m,n}(x_s, y_s, z_s) = \cos\left(\frac{l\pi x_s}{L_x}\right) \cos\left(\frac{m\pi y_s}{L_y}\right) \cos\left(\frac{n\pi z_s}{L_z}\right) \quad (2.38)$$

The set of the three indexes  $l, m, n$  can represent axial, tangential or oblique modes, according to their combination. It is evident that, for source and receiver points in the one of the eight corners of the room ( $x = 0, L_x; y = 0, L_y; z = 0, L_z$ );  $\psi_{l,m,n}(x_{corner}, y_{corner}, z_{corner}) = 1$ , and the mean-square sound pressure level (Eq. 2.17) reaches the maximum value. As a consequence, all axis, tangential and oblique modes have, in common, greatest energy at corners of rectangular room. This is a crucial aspect of the modal approach applied to the sound insulation measurement at low frequency discussed in Chapter 4.

Furthermore, for a rectangular room, the constant dimensionless term  $\Lambda_{l,m,n}$  can be seen as the reciprocal of the product of  $\epsilon_l \epsilon_m \epsilon_n$  (if  $l=0$ , then  $\epsilon_l=1$  else  $\epsilon_l=2$ ; if  $m=0$ , then  $\epsilon_m=1$  else  $\epsilon_m=2$ ; if  $n=0$ , then  $\epsilon_n=1$  else  $\epsilon_n=2$ ). In general  $\Lambda_{l,m,n}$  is equal to  $1/2$ ,  $1/4$  or  $1/8$  for axial, tangential or oblique modes respectively.

## 2.2 Airborne sound insulation

The airborne sound insulation of a partition between two rooms is defined as the ability to reduce the acoustic energy that propagates through air from the source room to the receiving room. When a wavefront bears on the surface of a partition, different phenomena appear: the wave energy is converted in a forced mechanical vibration; part of such mechanical energy is converted back into acoustic energy as transmitted (in the receiving room) and reflected acoustic radiation; another part is dissipated into thermal energy and a last part is structurally transmitted and radiated in the receiving room (*flanking transmission*).

A typical airborne sound insulation laboratory comprises two rooms: a source room and a receiving room separated by a test element. In laboratory, it is assumed that all sound is transmitted via the test element while the flanking transmission is neglected. Laboratory airborne sound insulation measurements are primarily used to compare the sound insulation provided by different test elements and to calculate the sound insulation *in situ*.

The transmission coefficient  $\tau$  is defined as the ratio of the sound power transmitted by the test element  $W_2$  to the sound power incident on the test element  $W_1$

$$\tau = \frac{W_2}{W_1} \quad (2.39)$$

The standard parameter used to define the sound insulation property of a partition is the so called *sound reduction index*, or transmission loss,  $R$ , in decibels that is expressed as

$$R = 10 \log_{10} \left( \frac{1}{\tau} \right) = 10 \log_{10} \left( \frac{W_1}{W_2} \right) \quad (2.40)$$

Around the fundamental resonant frequency of the partition  $f_0$ , the trend of sound reduction curve shows a dip (see Fig. 2.8). Before and after such frequency, sound reduction increases with a trend of 6 dB/Octave. Since most of partitions present a resonant frequency in the low frequency range ( $< 200$  Hz), it is possible to obtain non-zero values of sound insulation also for lower frequencies, i.e. in the frequency range of 50-100 Hz.

### 2.2.1 Sound insulation in diffuse field condition

By assuming that the sound fields in the source and receiving room are diffuse (i.e. above Schroeder frequency, see Section 2.1.2) it is possible to calculate the incident and the transmitted sound power from sound pressure level ( $L_p$ ) measurements in each room. To find these sound powers, the first step is to calculate the sound intensity incident upon any surface in a diffuse field, which is given by

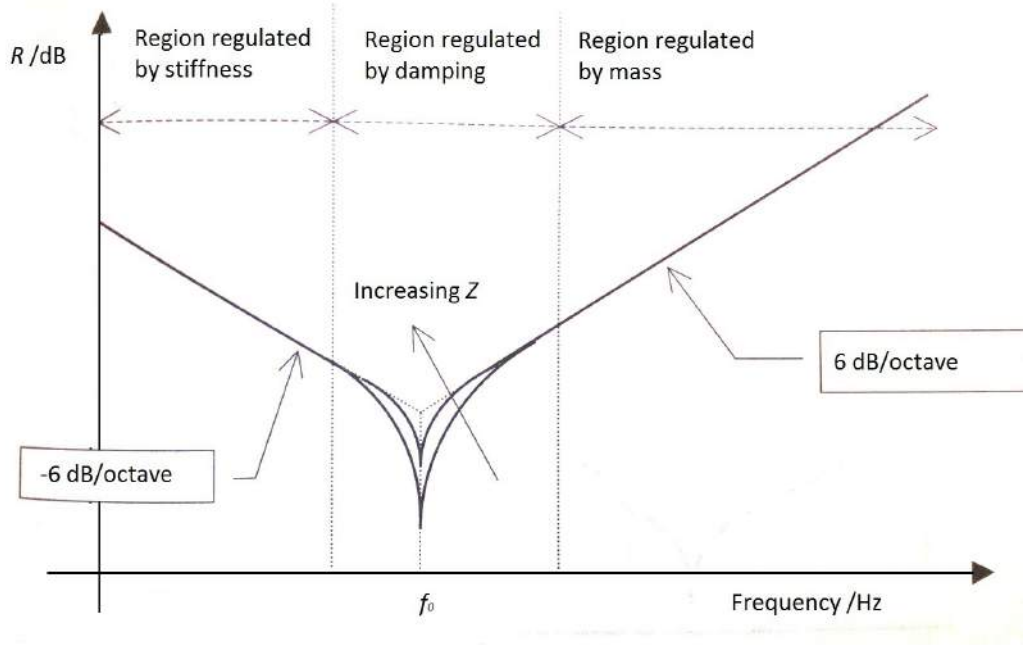


Figure 2.8: Trend of sound reduction curve,  $R$ , around the fundamental resonant frequency of the partition.

$$I_1 = \frac{\langle p_1^2 \rangle_{t,s}}{4\rho_0 c} \quad (2.41)$$

where  $\langle p^2 \rangle_{t,s}$  is the temporal and spatial average mean-square sound pressure in the diffuse field,  $\rho_0$  is the air density and  $c$  is the sound speed in air. The power that is incident upon the test element in the source room is

$$W_1 = I_1 S = \frac{\langle p_1^2 \rangle_{t,s}}{4\rho_0 c} S \quad (2.42)$$

where  $S$  is the area of the test element. The power transmitted through the partition to the equivalent absorption area  $A$  must equal the sound intensity in the receiving room. Rooms not only have absorbent surfaces, but they also contain absorbent objects (e.g. furniture, air). The absorption area  $A$  is defined as the ratio of the sound power absorbed by a surface or object to the sound intensity incident upon the surface or object and describes all the absorption in the room using a single area (unit of measurement,  $m^2$ ). Hence, for an absorption area  $A$ , in the receiving room the transmitted power is defined as

$$W_2 = I_2 A = \frac{\langle p_2^2 \rangle_{t,s}}{4\rho_0 c} A \quad (2.43)$$

Combining Eqs 2.39, 2.42 and 2.43 the following relation is obtained:

$$\tau \frac{\langle p_1^2 \rangle_{t,s}}{4\rho_0 c} S = \frac{\langle p_2^2 \rangle_{t,s}}{4\rho_0 c} A \quad (2.44)$$

and

$$\frac{1}{\tau} = \frac{\langle p_1^2 \rangle_{t,s}}{\langle p_2^2 \rangle_{t,s}} \frac{S}{A} \quad (2.45)$$

which is converted to decibels to give the sound reduction index (*SRI*)

$$R = 10 \log_{10} \left( \frac{\langle p_1^2 \rangle_{t,s}}{\langle p_2^2 \rangle_{t,s}} \right) + 10 \log_{10} \left( \frac{S}{A} \right) = L_{p1} - L_{p2} + 10 \log_{10} \left( \frac{S}{A} \right) \quad (2.46)$$

where  $L_{p1}$  and  $L_{p2}$  are the temporal and spatial average sound pressure levels in the source and receiving rooms respectively.

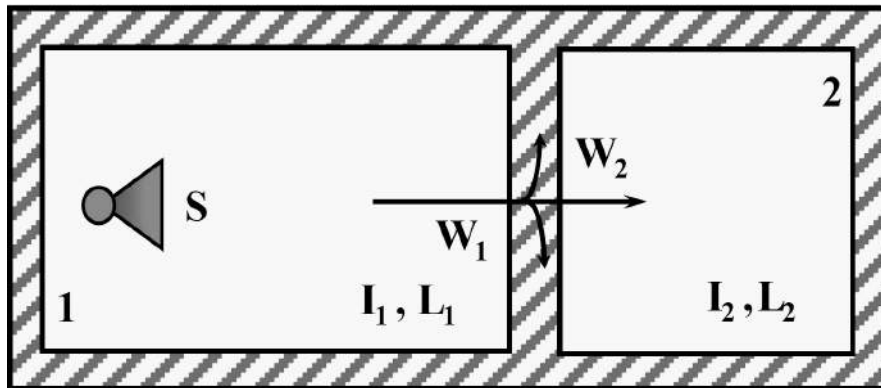


Figure 2.9: Outline sketch of a transmission suite for airborne sound insulation measurements.

Laboratory airborne sound insulation is regulated by ISO 10140-2:2010 standard which contains the guidelines to evaluate sound insulation property of a building element such as walls, floors, doors, windows, shutters, facade elements, glazing, small technical elements, etc. The measurements of *sound reduction index* (Eq. 2.46) are performed in laboratory test facilities in which sound transmission via flanking paths is suppressed. The test results can be used to compare the sound insulation properties of building elements, classify elements according to their sound insulation capabilities, help design building products which require

certain acoustic properties and estimate the *in situ* performance in complete buildings. Two horizontally or vertically adjacent rooms are used, the source room and the receiving room. The test element is mounted in an opening of about 10 m<sup>2</sup> in the partition between those rooms. In the source room, a diffuse sound field is generated by a moving loudspeaker or loudspeakers at two or more fixed positions. The average sound pressure levels are measured in the source and receiving rooms with continuously moving microphones 0.7 m distant from room boundaries, normally in the frequency range between 100 Hz and 5000 Hz. Although Schroeder frequencies can reach values of about 350 Hz for typical laboratory room volumes between 50 m<sup>3</sup> and 150 m<sup>3</sup>, the sound field in this frequency range is conventionally considered diffuse for practical reasons. The equivalent sound absorption area in the receiving room is calculated from reverberation time measurements by

$$A = \frac{0.161V}{T} \quad (2.47)$$

where  $V$  is the receiving room volume and  $T$  is the reverberation time of the receiving room (see Section 2.3), defined as the time required, in seconds, for the average sound in a room to decrease by 60 dB after a source stops generating sound.

### 2.2.2 Sound insulation in non-diffuse field condition

Sound transmission in non-diffuse field condition, i.e. for frequencies much lower than Schroeder frequency  $f_s$ , below 100 Hz for the small laboratory rooms, needs another scientific dissertation as diffuse field approximations (for example sound intensity formulation in Eq. 2.41) are not valid. As stated in Section 2.1.2, non-diffuse field is characterized by large fluctuation of sound pressure levels in space and frequency domains due to the presence of standing waves. For this reason, starting from *wave theory* (Section 2.1.1), a theoretical model is obtained for the study of the sound transmission between two rooms through the partition. Theory is based on C. H. Jo and S. J. Elliott work and supported by P. M. Morse studies [44-46]. Acoustic field in source and receiving rooms and motion of the panel can be written as modal expansions, solutions of the proper differential equations for each physical system (source room, partition and receiving room). The following boundary conditions are assumed for the theoretical model:

- rectangular rooms as boundary conditions in order to simplify solutions of equations;
- sound transmission only from source to receiving room since the opposite transmission can be neglected;
- no framework in the test opening in order to simplify coupling factors (Eq. 2.56 and 2.61);

- no flanking transmission (experimentally verified);
- simple acoustic source at a corner of source room, so source distribution term can be described by a simple harmonic source with an amplitude  $Q_0$  and the source distribution term  $\psi_{l,m,n}^{(1)}(\mathbf{r}_0) = 1$  (see Section 2.1.3).

### Acoustic field in source room

Sound pressure in the rectangular source room with dimensions  $L_x^{(1)}$ ,  $L_y^{(1)}$ ,  $L_z^{(1)}$ , at a frequency  $\omega$  in the point  $\mathbf{x}_1 = (x_1, y_1, z_1)$ , obtained from the "forced" (source) and "damped" (boundary absorption, Eq. 2.15) wave equation (Eq. 2.6) with the addition of the time dependence, can be described as (see Eq. 2.8)

$$p^{(1)}(\mathbf{x}_1, \omega, t) = \sum_{l_1 m_1 n_1=0}^{\infty} A_{l_1 m_1 n_1}^{(1)}(\omega) \psi_{l_1 m_1 n_1}^{(1)}(\mathbf{x}_1) e^{-i\omega t} \quad (2.48)$$

where  $l_1, m_1, n_1$  are the modal integers of source room and  $\psi_{l_1 m_1 n_1}^{(1)}$  is the modal distribution function (see Eq. 2.37):

$$\psi_{l_1 m_1 n_1}^{(1)}(\mathbf{x}_1) = \cos\left(\frac{\pi l_1 x_1}{L_x^{(1)}}\right) \cos\left(\frac{\pi m_1 y_1}{L_y^{(1)}}\right) \cos\left(\frac{\pi n_1 z_1}{L_z^{(1)}}\right) \quad (2.49)$$

Modal amplitudes are expressed by (see Eq. 2.10)

$$A_{l_1 m_1 n_1}^{(1)}(\omega) = \frac{\rho_0 c^2 \omega Q_0}{V_1 \Lambda_{l_1 m_1 n_1} [2\omega_{l_1 m_1 n_1} \delta_{l_1 m_1 n_1}^{(1)} + i(\omega^2 - \omega_{l_1 m_1 n_1}^2)]} \quad (2.50)$$

where  $\rho_0$  is the air density,  $c$  is sound speed,  $Q_0$  is the acoustic source volume velocity at frequency  $\omega$ ,  $V_1$  is the source room volume,  $\Lambda_{l_1 m_1 n_1}$  is 1/2, 1/4 or 1/8 for axial, tangential and oblique modes respectively,  $\delta_{l_1 m_1 n_1}^{(1)}$  is the modal absorption (or modal damping factor), and  $\omega_{l_1 m_1 n_1}^{(1)}$  is the resonant frequency of the related mode and is given by

$$\omega_{l_1 m_1 n_1}^{(1)} = \pi c \sqrt{\left(\frac{l_1}{L_x^{(1)}}\right)^2 + \left(\frac{m_1}{L_y^{(1)}}\right)^2 + \left(\frac{n_1}{L_z^{(1)}}\right)^2}. \quad (2.51)$$

### Velocity of the partition

The vibration of the partition with dimensions  $L_y^{(p)}$  e  $L_z^{(p)}$  is induced only by acoustic field in source room and the governing equation can be written as

$$D \left( \frac{\partial^2}{\partial y^2} + \frac{\partial^2}{\partial z^2} \right) \left( \frac{\partial^2}{\partial y^2} + \frac{\partial^2}{\partial z^2} \right) v + M \frac{\partial^2 v}{\partial t^2} = \frac{\partial p^{(1)}(\mathbf{x}_1, \omega, t)}{\partial t} \quad (2.52)$$

where  $D$  is the complex flexural stiffness of partition,  $M$  is the mass per unit area and  $v$  is the velocity of the partition.

The velocity of the partition in the point  $\mathbf{x}_p = (y_p, z_p)$ , can be expressed as series of structural modes:

$$v^{(p)}(\mathbf{x}_p, \omega, t) = \sum_{q,r=1}^{\infty} A_{qr}^{(p)}(\omega) \phi_{qr}^{(p)}(\mathbf{x}_p) e^{-i\omega t} \quad (2.53)$$

$q$  and  $r$  are partition modal integers and  $\phi_{qr}(\mathbf{x}_p)$  is the modal distribution function of the partition:

$$\phi_{qr}(\mathbf{x}_p) = 2 \sin \left( \frac{\pi q y_p}{L_y^{(p)}} \right) \sin \left( \frac{\pi r z_p}{L_z^{(p)}} \right). \quad (2.54)$$

Partition modal amplitudes, forced by source room acoustic field, neglecting receiving room influence, is given by:

$$A_{qr}^{(p)}(\omega) = \sum_{l_1 m_1 n_1=0}^{\infty} G_{l_1 m_1 n_1, qr}^{(1)}(\omega) A_{l_1 m_1 n_1}^{(1)}(\omega) \quad (2.55)$$

where  $A_{l_1 m_1 n_1}^{(1)}$  is the amplitude of the  $n$ -th source room mode and  $G_{l_1 m_1 n_1}^{(1)}$  is the source room-partition coupling factor given by

$$G_{l_1 m_1 n_1, qr}^{(1)}(\omega) = \frac{2\omega}{\Lambda_{l_1 m_1 n_1} \pi^2 i L_y^{(p)} L_z^{(p)} M [(1 + i\eta)\omega_{qr}^2 - \omega^2]} \cdot (1 - (-1)^{q+m_1}) (1 - (-1)^{r+n_1}) \cdot \frac{q}{(q^2 - m_1^2)} \frac{r}{(r^2 - n_1^2)} \quad (2.56)$$

where  $\eta$  is the hysteretic damping factor,  $M$  is the mass per unit area,  $\omega_{qr}^{(p)}$  is the resonant frequency of the related mode described by

$$\omega_{qr}^{(p)} = \pi^2 \sqrt{\frac{D}{M}} \left[ \left( \frac{q}{L_y^{(p)}} \right)^2 + \left( \frac{r}{L_z^{(p)}} \right)^2 \right] \quad (2.57)$$

### Acoustic field in receiving room

Sound pressure field in the receiving room with dimensions  $L_x^{(2)}, L_y^{(2)}, L_z^{(2)}$ , generated by the motion of the partition, is expressed by:

$$p^{(2)}(\mathbf{x}_2, \omega, t) = \sum_{l_2 m_2 n_2=0}^{\infty} A_{l_2 m_2 n_2}^{(2)}(\omega) \psi_{l_2 m_2 n_2}^{(2)}(\mathbf{x}_2) e^{-i\omega t} \quad (2.58)$$

where  $l_2, m_2, n_2$  are the modal integers of receiving room and  $\psi_{l_2 m_2 n_2}^{(2)}$  is the modal distribution function, similar to Eq. (2.49). Modal amplitudes are expressed by Eq. (2.59):

$$A_{l_2 m_2 n_2}^{(2)}(\omega) = \sum_{qr=1}^{\infty} G_{qr, l_2 m_2 n_2}^{(2)}(\omega) A_{qr}^{(p)}(\omega) = \quad (2.59)$$

$$= \sum_{qr=1}^{\infty} G_{qr, l_2 m_2 n_2}^{(2)}(\omega) \sum_{l_1 m_1 n_1=0}^{\infty} G_{l_1 m_1 n_1, qr}^{(1)}(\omega) A_{l_1 m_1 n_1}^{(1)}(\omega) \quad (2.60)$$

where  $G_{qr, l_2 m_2 n_2}^{(2)}(\omega)$  is the partition-receiving room modal coupling factor given by

$$G_{qr, l_2 m_2 n_2}^{(2)} = \frac{2S_p \rho_0 c^2 \omega}{V_2 \Lambda_{l_2 m_2 n_2} [2\omega_{l_2 m_2 n_2} \delta_{l_2 m_2 n_2} + i(\omega^2 - \omega_{l_2 m_2 n_2}^2)]} \cdot (1 - (-1)^{q+m_2}) (1 - (-1)^{r+n_2}) \frac{q}{(q^2 - m_2^2)} \frac{r}{(r^2 - n_2^2)} \quad (2.61)$$

where  $S_p$  is the partition surface, while all other terms have the same meaning of Eq. (2.50) and (2.51) for source room.

## 2.3 Modal reverberation time

At this point it is necessary to introduce the concept of reverberation time, previously mentioned. When a sound source present in a room suddenly stops to emit a sound signal, the sound energy decays because of the mechanisms of absorption present in the room. This phenomenon is called *reverberation*, and it is usually assessed by a decay curve, which is a graph of the sound pressure level over time. The reverberation time is defined as the time (in seconds) for the sound pressure level to decay by 60 dB or, in terms of energy, it is the time for the energy to decay to one-millionth of its initial value. This definition fits well to the

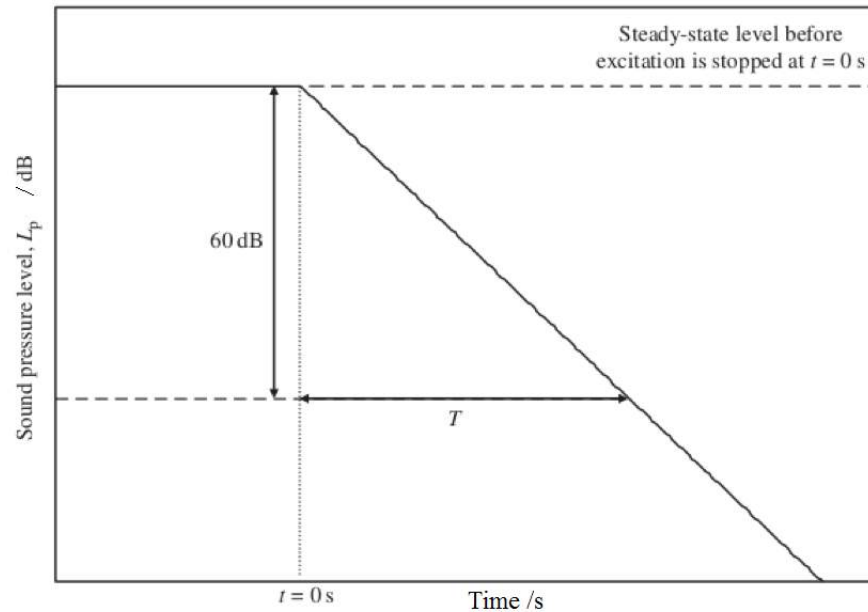


Figure 2.10: Ideal linear decay curve.

decay curve, which is obtained under diffuse field condition, in which the curves are obtained as shown in Fig. 2.10.

Most of the curves can be approximated by a straight line for all the 60 dB of decay, but it is not always true if high background noise is present. The definition of reverberation time thus needs to integrate also the case to obtain reverberation time by the use of a linear regression on a minor decay in terms of energy (e.g. 30 dB) or only on a part of the curve, in order not to necessarily consider a decay of 60 dB. Multiples of 60 (15, 20 or 30 dB) are used to calculate the  $T_x$ , where  $x$  is related to the value of  $\Delta L_p$  considered. It is however important to note that, even without considering the 60 dB decay, reverberation time must always be related to that value, so obtained reverberation time values from the "minor" decays have to be proportionally multiplied to get the time referred to a (hypothetical) decay of 60 dB. The first point used for the linear regression starts 5 dB below the beginning of the decay, in order not to consider possible interference due to the transient and the possible bias due to measurement instruments.

In diffuse field conditions (above the Schroeder frequency), as it has been seen before the behavior of sound field is statistical, and the frequency response of the room is flat. This is due to the fact that the room modes are not spaced, and the peaks corresponding to the resonant frequencies are so close as to be indistinguishable. In this case, therefore, the measurement of the reverberation time simply consists of averaging the decay of a certain frequency band (usually octave or third octave bands, usually from 100 Hz on), and curves similar to that

shown in Fig. 2.10, with a linear decay long enough to calculate  $T_{60}$ . In the case of non-diffuse field, the decay curve may not be approximated by a straight line across the entire range of the 60 dB decay. This is due to the fact that, given a certain frequency band, the shape of the curve depends on the room modes that fall in that octave or third octave band, and the interaction between them. An example is shown in Fig. 2.11: if within the considered frequency band, there are two modes (with different decay times), the decay curve presents two different slopes, and the decay of the band is non-linear. In this case it is more useful and physically correct to evaluate reverberation time of each single mode of the room ( $T_{n,60}$  or just  $T_n$ ).

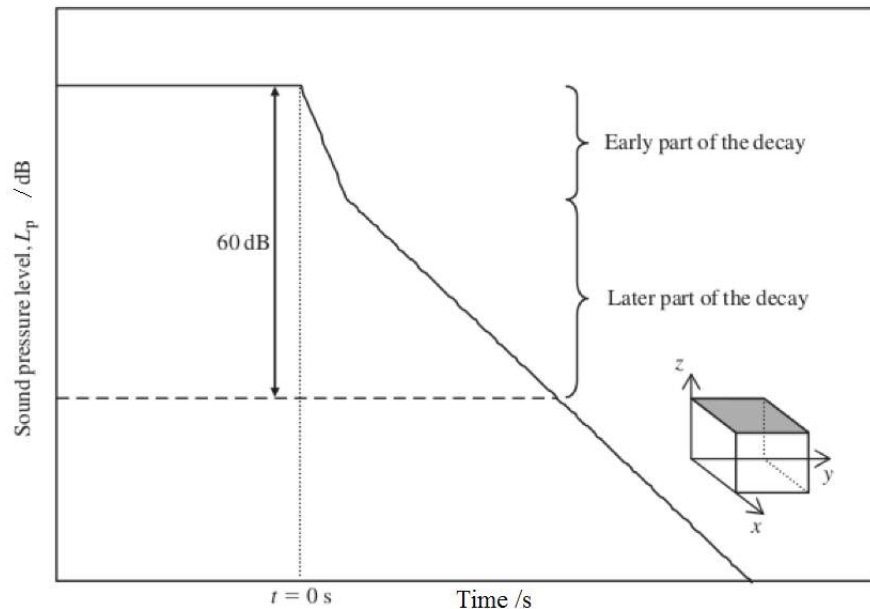


Figure 2.11: Non-linear decay curve due to the interaction of two modes in a third octave band.

Considering a rectangular room with reactive surfaces and dissipative properties, it is supposed to give energy to the resonant system via a sound source that emits a sinusoidal signal at a resonant frequency of the room. In reality, although the use of a source that emits a frequency different from a resonance, the source excites also modes close to the considered frequency as it supplies energy into the system according to its modal frequencies. When the source emission is interrupted, at time  $t = 0$ , the wave continues its path defined by that particular mode (see Fig. 2.3): part of its energy is reflected by the walls, and another part is dissipated from the air in the room.

Considering the decay of a single  $n$ -th mode, the squared sound pressure, proportional to its energy, becomes:

$$p^2(t) = p^2(0)e^{-2\delta_n t} \quad (2.62)$$

where  $\delta_n$  is the decay constant of the  $n$ -th mode, or the modal damping constant seen in Eq. 2.16 and gives information about the half bandwidth of the resonant frequency (Fig. 2.12) according to the formula:

$$\omega_1 = \omega_0 - \delta_n \quad (2.63)$$

$$\omega_2 = \omega_0 + \delta_n \quad (2.64)$$

$$\Delta\omega_{-3dB} = \omega_2 - \omega_1 = 2\delta_n \quad (2.65)$$

$$\Delta f_{-3dB} = \frac{\delta_n}{\pi} \quad (2.66)$$

as seen in Eq. 2.34.

In order to evaluate the reverberation time of a single mode after a 60 dB decay of the sound pressure level ( $T_n$ ), the following formulations are obtained [43]

$$L_{T_n} - L_0 = -60 = 10 \log_{10} \left( \frac{p^2(T_n)}{p^2(0)} \right) \quad (2.67)$$

$$\frac{p^2(T_n)}{p^2(0)} = e^{-2\delta_n T_n} = 10^{-6} \quad (2.68)$$

$$2\delta_n T_n = 6 \ln 10 \quad (2.69)$$

$$\delta_n = \frac{3 \ln 10}{T_n} \quad (2.70)$$

$$\Delta f_{-3dB} = \frac{\delta_n}{\pi} = \frac{3 \ln 10}{\pi T_n} = \frac{2.2}{T_n} \quad (2.71)$$

and so the modal reverberation time of a single mode can be expressed by

$$T_n = \frac{2.2}{\Delta f_{-3dB}} \quad (2.72)$$

where  $\Delta f_{-3dB}$  is the half bandwidth of the resonant frequency.

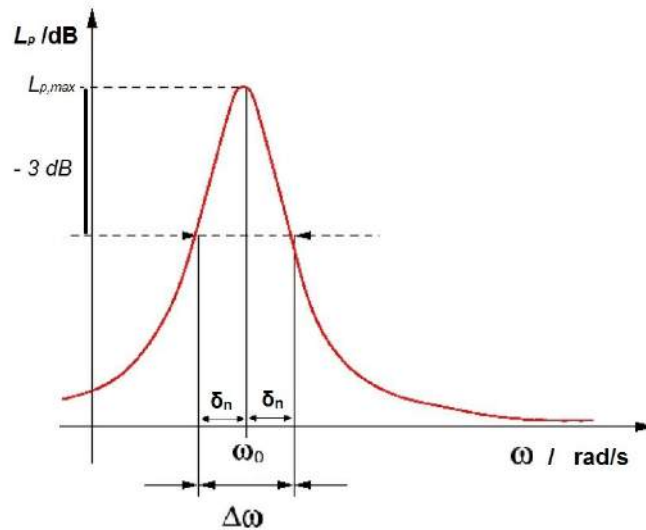


Figure 2.12: Half bandwidth of the  $n$ -th resonant frequency.

In this way a relation between the resonance width and the modal reverberation time is shown. Note how this *indirect* definition of the reverberation time is very well suited for modes which are easily identifiable and well spaced, i.e. in non-diffuse field condition. It is important to underline that the ISO regulations regarding the measurement of reverberation time (ISO 3382-2:2008) does not take into account the peculiarities of the sound field at low frequencies, but the last result opens the way to an *indirect* method of measurement that fits with the characteristics of the physical phenomenon.

## 2.4 Impact sound insulation

Impact sound insulation measurement evaluates the reduction of noise generated by an impact source on a floor structure. It is determined by impact sound level in the room below. For the airborne sound insulation the ratio of the sound power that is incident on the test element to the sound power transmitted by the same element is determined. As long as the sound transmission process from one room to the other is a linear process, it is possible to make measurements using loudspeakers with different sound power outputs and still obtain the same sound insulation value. To measure the impact sound insulation it is necessary to inject power into the floor using a structure-borne sound source. Although there are methods for measuring power input from different possible sources which are difficult and time-consuming to be accurately evaluated, a standardized and primary source is preferred: the ISO tapping machine, described in ISO 10140-5:2010 standard [47] and made of 5 hammers (0.5 kg each), that fall from a height of 40 cm every 100 ms (frequency of 10 Hz if all hammers are considered). Laboratory

measurement of impact sound insulation, described in ISO 10140-3:2010, requires measurement of the temporal and spatial average sound pressure level (SPL) in a room,  $L_p$  (see Section 2.2.1), when the floor above is excited by the tapping machine (Fig. 2.13).

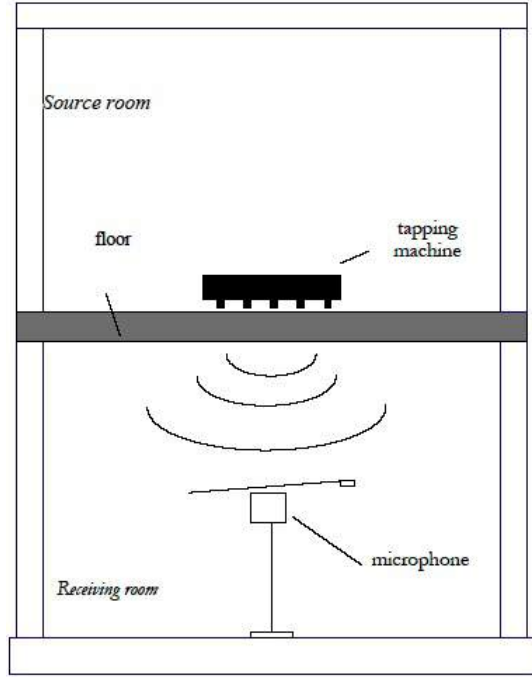


Figure 2.13: Laboratory measurement of impact sound insulation.

For a given sound power transmitted into the receiving room, the mean-square pressure in the room is inversely proportional to the absorption area  $A$  of that room. The normalized impact sound pressure level,  $L_n$  is therefore defined by using a reference absorption area  $A_0$  of  $10 \text{ m}^2$  for the receiving room to guarantee reproducible measurements in different laboratories.

$$L_n = L_p + 10 \log_{10} \left( \frac{A}{A_0} \right) \quad (2.73)$$

There are many different types of floor covering ranging from soft floor coverings to rigid walking surfaces. Another important variable in impact sound insulation measurements is the *improvement of impact sound insulation* due to the presence of a floor covering on the base floor or bare slab. The heavyweight base floor can generally be referred to as a 140 mm reinforced concrete slab; the exact details are given in ISO 10140-5:2010. The *improvement of impact sound insulation*  $\Delta L$  is measured using the ISO tapping machine and is defined as:

$$\Delta L = L_{n0} - L_n \quad (2.74)$$

where  $L_{n0}$  is the normalized impact sound pressure level for the ISO heavy-weight base floor without floor covering and  $L_n$  is the normalized impact sound pressure level with the floor covering.

The most common floor coverings can be divided in two categories: floating floors and resilient surface layers.

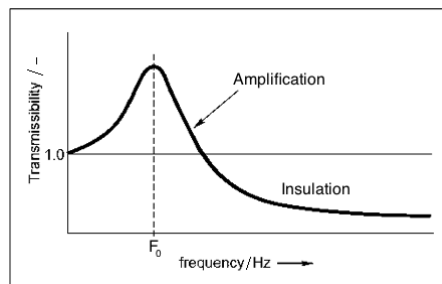


Figure 2.14: Transmissibility curve of the simple oscillator (damped mass-spring system).

For floating floors (a rigid floor covering on a resilient layer), i.e. a damped mass-spring system, motion transmissibility of the associated simple oscillator (Fig. 2.14) has a peak around the resonant frequency of the system given by [48]:

$$f_0 = \frac{1}{2\pi} \sqrt{\frac{s'_{tot}}{M}} \quad (2.75)$$

where  $s'_{tot}$  is the dynamic stiffness of the resilient layer and  $M$  is the mass per unit area of the floor covering.

Around the resonant frequency, noise level is amplified, entailing negative values of improvement of impact sound insulation ( $\Delta L < 0$ ). For frequencies below the resonance, transmissibility is equal to 1, so insulation values can be approximated to 0. The resonant frequency of the mass controls the starting insulation frequency while the damping controls the insulation curve slope. The same conclusions are valid for resilient surface layers except for the fact that there is no amplification of noise levels around the resonant frequencies which are deeply damped and that insulation curve slope are generally flatter.



# Chapter 3

## Preliminary measurements

### 3.1 Instrumentation: measurement devices and setup

A brief description of measurement devices used in the experimental tests is presented as follows. A measurement microphone, with its impedance adapter and preamplifier, and an external acquisition board with its analysis software, are used to record the acoustic signal. A different software, another external audio interface, a power amplifier and a loudspeaker are used for the generation of the source signal. The measurement devices shown below are the same for all building acoustics measurements in laboratory, except for scale model measurements.

#### Microphone

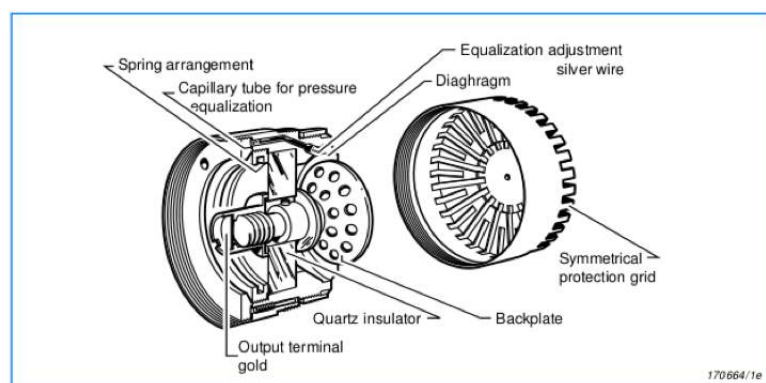


Figure 3.1: Microphone B&K 4165.

The Bruel & Kjaer 4165 is the 1/2" microphone used for measurements. Its frequency response is linear in a wide frequency range (10-1000 Hz), in particular

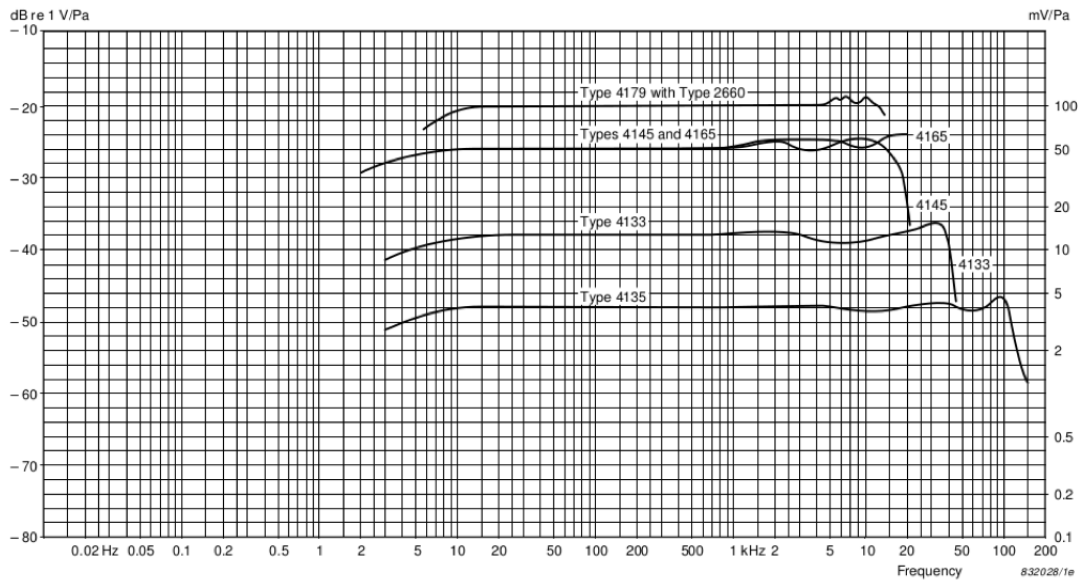


Figure 3.2: B&K 4165 frequency response.

in the low frequency range (20-200 Hz). Corner measurements reported in the following Chapters mean that the microphone is placed at a minimum distance of 5 cm from the three walls of the corner.

### Microphone preamplifier and power amplifier



Figure 3.3: G.R.A.S. 12AK and B&K 2706.

The microphone preamplifier is the G.R.A.S. 12AK, with gain set to 0 and linear filter. The power amplifier of the source signal is the Bruel & Kjaer 2706, with attenuation set to 0. The gain is set in order to get total sound pressure levels around 100 dB.

### Acoustic source and source signals

The acoustic source consists of a closed-box loudspeaker with a 15-inch cone in order to generate suitable low frequency sound pressure levels.



Figure 3.4: Closed-box loudspeaker.

Different source signals are used. In the case of sinusoidal signal, it is simply created by the software (described in the next section related to the generation and data acquisition) at the selected frequency. For the statistical noise signal, some clarifications are necessary. First, noise is defined as a signal with a particular spectral energy density function. Depending on the type of noise, such density function is different, therefore the amount of energy for each frequency band changes. Pink noise has the peculiarity to contain the same energy for constant percentage bands (i.e. third octaves or octaves), therefore the energy within the low frequency bands is greater than high frequency bands. This type of noise is structured to compensate for the sensitivity of the human ear at different frequencies and it is also used for the equalization of the sound fields in listening rooms or concert halls.

### Signal generation and data acquisition

For the generation of source signals, the Sound Forge audio editing software is used. The preamplification of source signal is controlled by the USB audio interface M-Audio Fast Track Pro. For what concerns the data acquisition, the National Instrument Sound and Vibration measurement suite, with its acquisition board



Figure 3.5: M-Audio interface and Nation Instruments acquisition board.

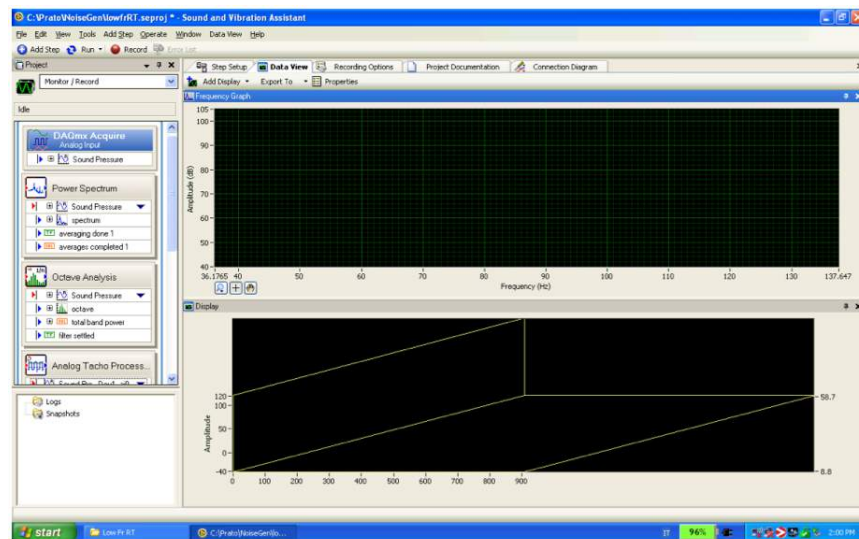


Figure 3.6: Nation Instruments - Sound and Vibration tool software.

are used. High resolution spectrum measurements (0.1 Hz or 0.25 Hz), obtained through temporal averages of sound pressure levels, are executed in order to detect resonant frequency curve. The types of averages used, depending on the source signal, are: the linear average for pink noise or sinusoidal signals and the peak hold for sweep signal (a signal in which the frequency increases or decreases with time and constant amplitude). The waterfall measurements, which represent the temporal evolution of the frequency spectrum, are used to determine the sound decay for reverberation time measurements. For this type of measurement, the ratio between the frequency resolution and the time resolution is constant, and, since the amount of computing power required to record a large number of spectra over time is very large, there are limitations: in this case, a spectrum every 0.1 s,

and a frequency resolution of 0.25 Hz are chosen. The plot of waterfall analysis is obtained by 3 dimensional graph (frequency, pressure level sound and time).

## 3.2 Characterization of acoustic source

To obtain an accurate measurement at low frequencies, it is necessary to use a sound source that could provide high sound pressure levels at frequencies above 30 Hz and has a frequency response as linear as possible at all frequencies. For this reason a closed-box loudspeaker, with a 15-inch speaker, described above, is used. In Fig. 3.7 the frequency response of the source, measured in free-field (outdoor on a meadow) at different distances (1 m, 2 m and 3 m from the center of the cone) with a pink signal, is shown. From 45 Hz to 112 Hz (the lower and upper bounds of 50 Hz and 100 Hz third octave bands respectively) there are differences in the order of 7 dB, which appear to be easily filled up with an equalization when performing measurements; while from 45 Hz to 200 Hz, there are differences around 15 dB, the limit of equalization.

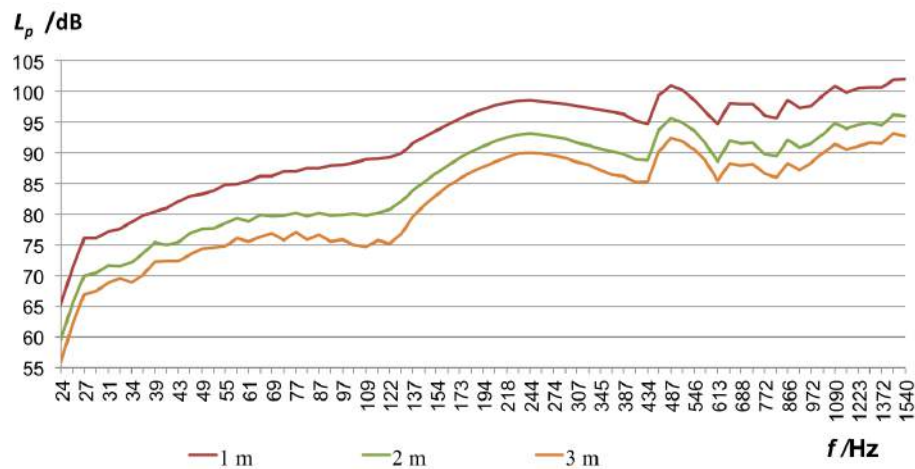


Figure 3.7: Loudspeaker frequency response at different distances.

Equalization process is necessary in order compensate modal behaviour of the loudspeaker cone as seen in the frequency response. In this way, evaluation of the natural modes of laboratory rooms is more accurate and possible errors in the detection of modes due to not linearized source signal are minimized. In Fig. 3.8, the loudspeaker frequency response in the low frequency range (30-400 Hz) with the application of equalization to the pink noise signal is shown.

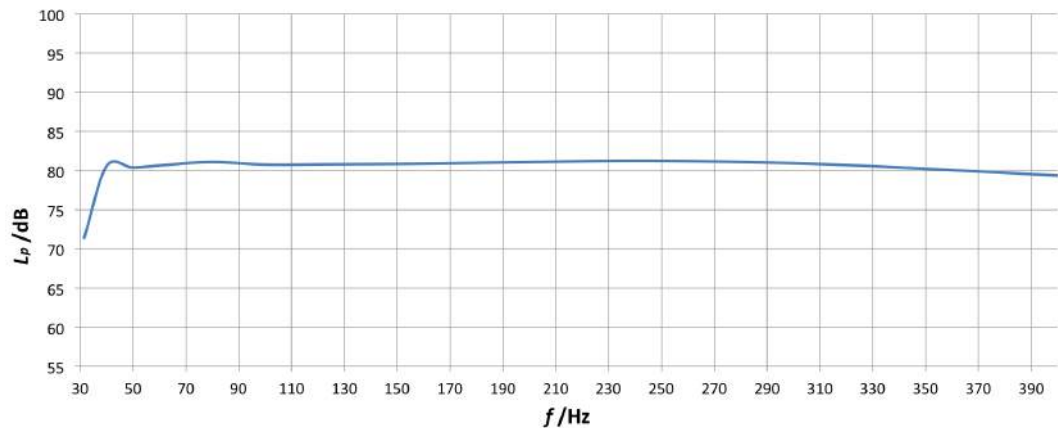


Figure 3.8: Linearized loudspeaker frequency response.

### 3.3 Modal qualification of airborne sound insulation laboratory rooms

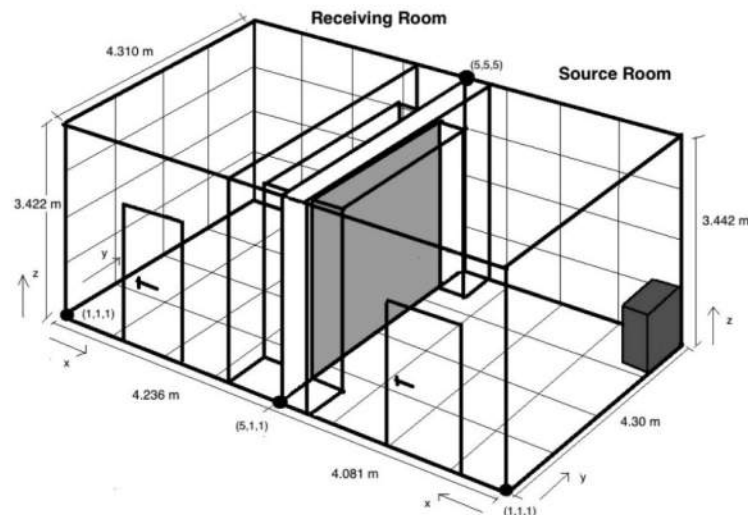


Figure 3.9: Ideal grid of 125 points in source and receiving rooms.

The laboratory for airborne sound insulation measurements consists of two rooms, source and receiving rooms, and the test element, as described in Section 2.2. The complexity of boundary conditions due to the coupling system (room-partition-room for airborne sound insulation measurements) makes necessary a deep study of modal behaviour of laboratory rooms. It consists in the determination of modal distribution in space and frequency domains of the source and receiving

rooms natural modes and the source room transmitted modes within the receiving room, according to the modal approach, previously touched on Chapter 1, and deepened in the following one. Source and receiving room dimensions are 4.300 m 3.858 m 3.442 m and 4.310 m 4.078 m 3.422 m, respectively, and volumes are around 60 m<sup>3</sup>. The geometry of the rooms is not perfectly rectangular due to the presence of a concrete framework around the test opening in order to reduce flanking transmissions. All measurements are executed with the loudspeaker, described above, placed at a corner of the room emitting the equalized pink noise signal to get high modal excitation. Rooms were subdivided in an ideal grid of 125 points (5x5x5 along the three axis and equally spaced) and punctual sound pressure level measurements,  $L_p$ , were performed (Fig. 3.9).

### 3.3.1 Spatial distribution of source and receiving room natural modes

Source and receiving room natural modes are evaluated separately. Such measurements are performed with a partition composed of expanded clay concrete blocks (10 cm thickness) covered with a 15 mm plaster layer. Since source and receiving rooms are not perfectly rectangular, theoretical calculations of resonant frequencies are different with respect to measured ones (Table 3.1).

Source room		Receiving room	
Theoretical modes /Hz	Measured modes /Hz	Theoretical modes /Hz	Measured modes /Hz
40.3	42.4	40.2	41.4
42.5	45.9	41.6	42.9
50.4	51.9	50.7	<b>50.9</b>
58.6	63.3	57.9	61.3
64.6	66.8	64.7	65.3
65.9	70.8	65.6	66.8
77.3	79.2	76.9	80.7
80.7	81.7	80.5	84.7
85.0	85.2	83.3	93.7
91.2	92.7	90.6	99.2
94.1	94.2	92.5	107.1
95.1	98.2	95.1	110.1
98.8	101.2	97.5	114.1
100.8	103.1	101.3	118.1
104.2	<b>105.1</b>	103.8	120.1

Table 3.1: The first 15 theoretical and measured natural modes. In bold, natural modes reported in Fig. (3.10) and (3.11).

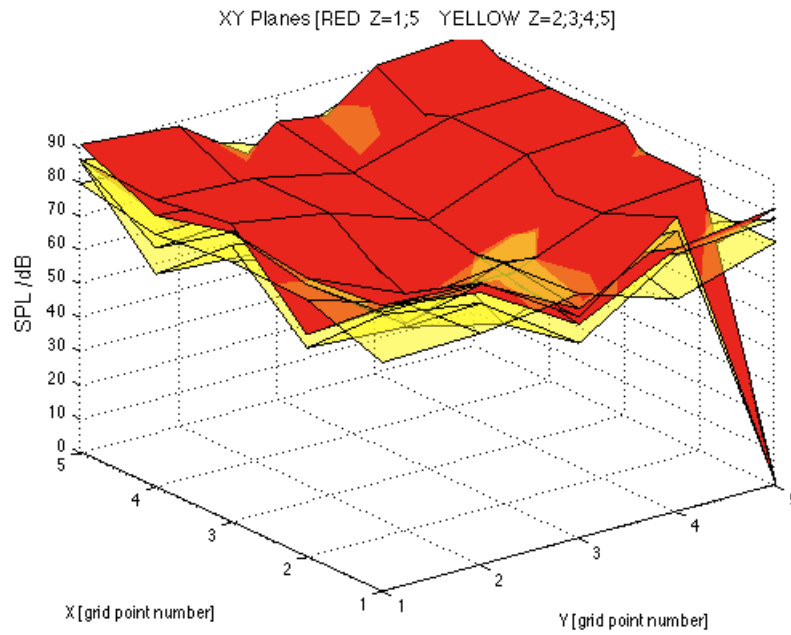


Figure 3.10: Spatial distribution of a source room natural mode (105.1 Hz).

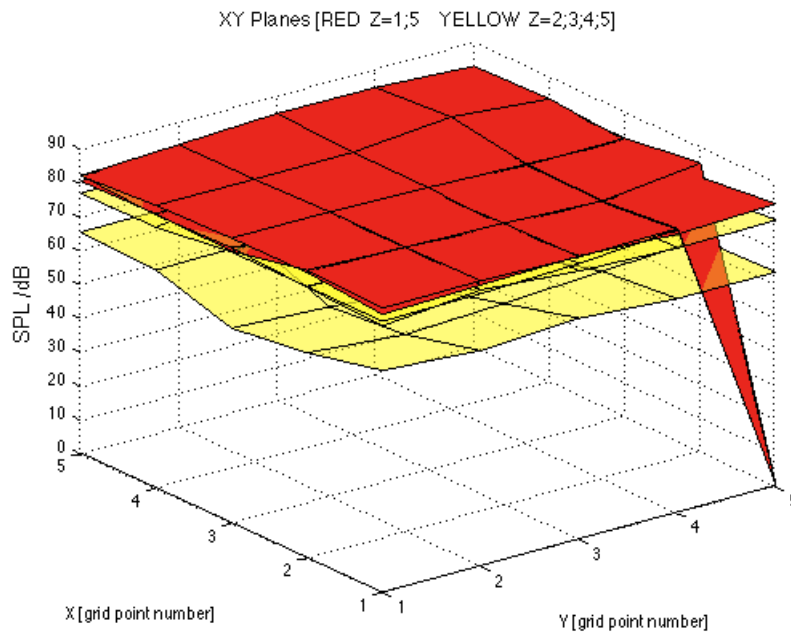


Figure 3.11: Spatial distribution of a receiving room natural mode (50.9 Hz).

In both chambers, modal sound field presents large SPL fluctuations in space with the highest values at corners of rooms for each resonant frequency as for perfectly rectangular room theoretical case. Examples of spatial distribution of source (105.1 Hz) and receiving room modes (50.9 Hz) are shown in Fig. 3.10 and 3.11 respectively. Dark grey planes correspond to floor ( $Z = 1$ ) and ceiling ( $Z = 5$ ) heights, light grey planes to intermediate ones ( $Z = 2; 3; 4$ ). Zero values of SPL are due to the presence of the loudspeaker (no measurement at that corner position).

### 3.3.2 Spatial distribution of source room transmitted modes into receiving room

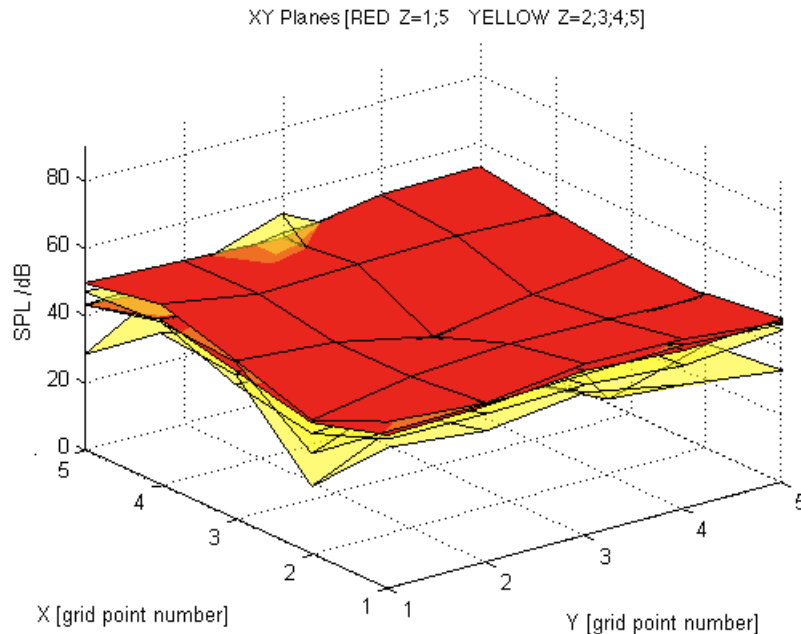


Figure 3.12: Spatial distribution of a source room natural mode transmitted into receiving room (70.25 Hz).

From the sound insulation modal theory (Section 2.2.2 and Chapter 1), source room natural modes are transmitted into receiving room. Since some source and receiving room eigenfrequencies are coincident in the frequency domain (similar room dimensions), spatial distribution of transmitted source room modes into receiving room is evaluated for non-coincident modes in order to avoid modal overlap. Measurements are operated with a different partition with respect to the previous one. It is composed as follows: plasterboard (12.5 mm), plaster layer (15 mm), perforated brick (8x24x24 cm), plaster layer (15 mm), expanded clay concrete blocks

(25x20x25 cm), plaster layer (15 mm), perforated brick (8x24x24 cm), plaster layer (15 mm), plasterboard (12.5 mm). As for the case of natural modes, transmitted modes are characterized by large sound pressure level fluctuations in space and highest levels at corners of room. In Fig. 3.12, an example of spatial distribution of a source room natural mode transmitted into receiving room is reported (70.25 Hz). It is important to underline that the use of a different partition, that changes source room  $x$  dimension with respect to the previous one, entails different eigenfrequencies (70.25 Hz source room mode does not appear in Table 3.1 for such reason).

## Chapter 4

# Airborne sound insulation at low frequency: the modal approach

As seen in Section 2.2, the standard descriptor of sound insulation, i.e. the sound reduction  $R$ , is related to the transmission coefficient  $\tau$  that is defined as the ratio of the sound power transmitted by the test element to the sound power incident on the test element. Assuming diffuse field, sound reduction is expressed as the difference between average sound pressure levels in the source and receiving rooms plus a term depending on equivalent absorption area,  $A$ . Application of such approach to non-diffuse field condition, strictly connected to boundary conditions entails low reproducibility values of sound insulation and it is not representative for the correct physical phenomena involved (low modal density, not uniform acoustic field in space and frequency domains). Furthermore, it is not possible to correctly define the incident and transmitted sound power in such modal acoustic field according to standard approach. Even if it could be possible to determine the sound power emitted by a building element how could it be correlated to the modal sound field and the real acoustics perception? Indeed, non-diffuse field represents a different physical phenomenon and has to be treated in a proper way in order to get reliable results with all connected problems (dependency on geometry of rooms and partition, modal absorption of walls, room volumes, modal match, etc). As described in Chapter 1, the evidence of transmission of source room modes into the receiving room through the partition, as showed and confirmed by experimental results [31], allows to introduce a new approach in the evaluation of sound insulation with respect to classical diffuse field one: the sound insulation property of a partition can be evaluated through a descriptor of modal sound transmission loss, i.e. the attenuation of source room modes passing through the partition into the receiving room. Such evaluation allows to shift from a statistical point of view in terms of average sound pressure levels, typical of diffuse field condition, to a discrete one, focused, in frequency domain, on source room modes and, in space, on the points of highest sound

pressure levels, or highest modal excitation (corners of rectangular rooms). From a perceptive point of view, such spatial positions are also representative of greatest annoyance and, in the perspective to evaluate the sound insulation property of a wall in the modal sound field, it is in accordance with such definition.

## 4.1 The modal sound insulation

Once localized highest modal excitation points, i.e. corners of laboratory rooms (Section 3.3), sound pressure level measurements are performed (closed-box loudspeaker emitting equalized pink noise at a corner of source room, 1/2" microphones at 7 corners of source room and at 8 corners of receiving room, see Section 3.1). Corner position means a distance of about 5 cm from all 3 neighbouring walls. Spectrum analysis is realized through FFT (frequency resolution of 0.25 Hz, temporal linear average of 60 s), instead of third octave bands, in order to identify all modes. Although Schroeder frequency is around 350 Hz in both chambers and a condition of diffuse field from 100-125 Hz on (one-third octave bands) is conventionally accepted as modal density is high enough, measurements and data analysis focuses on frequencies below 120 Hz (the upper bound of 100 Hz third octave band is 112 Hz). Different partitions are evaluated, but, for simplicity, only results related to a specific one are reported in order to focus only on the measurement procedure. The layered partition is composed as follows: plasterboard (12.5 mm), plaster layer (15 mm), perforated brick (8x24x24 cm), plaster layer (15 mm), expanded clay concrete blocks (25x20x25 cm), plaster layer (15 mm), perforated brick (8x24x24 cm), plaster layer (15 mm), plasterboard (12.5 mm). For each microphone position, a FFT spectrum is obtained (7 for source room, 8 for receiving room). In the perspective to work in condition of most annoyance, the highest sound pressure levels are selected for each frequency band in order to get 2 spectra, for source and receiving rooms respectively (Fig. 4.1).

Both spectra are characterized by a large number of modes (see Table 4.1 for further details in the following section). In particular, in the receiving room spectrum, a higher modal density is clear below 80 Hz due to transmission of source room modes. At higher frequencies, between 80 Hz and 86 Hz and around 101 Hz, some source room natural modes cannot be distinguished in the receiving room spectrum due to modal overlap or high absorption. Some eigenfrequencies are coincident with an error range of  $\pm 1$  Hz in both source and receiving rooms (localized on the same line in Table 4.1) and can be representative of modal transmission. Since some source and receiving room natural modes are similar or completely matching due to comparable dimensions of chambers, some source room transmitted modes and receiving room natural ones overlap, entailing an increase of modal sound pressure levels in the receiving room and, thus, an underestimation of modal sound insulation at such frequencies (e.g. 41 Hz, 66.25 Hz, 81.25 Hz, 85

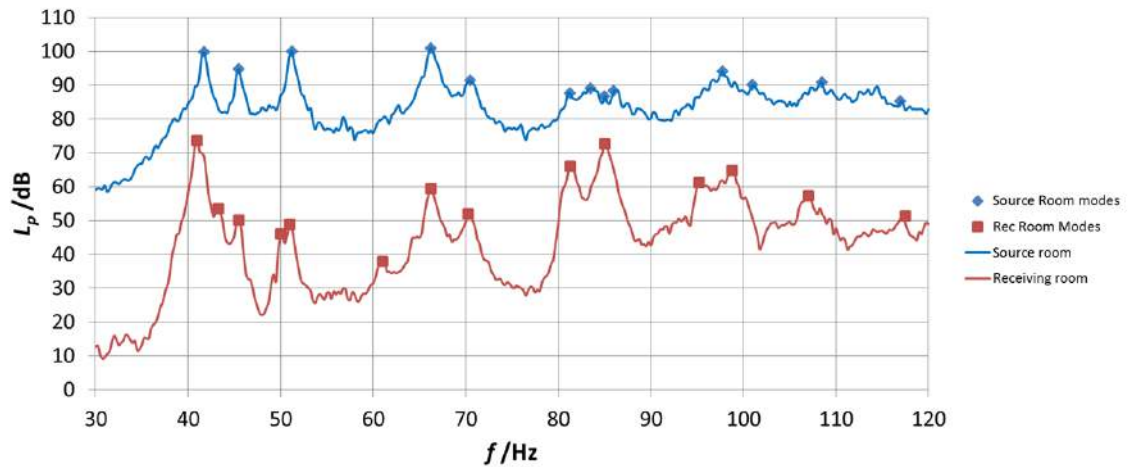


Figure 4.1: Source and receiving room spectra

Hz, 98.75 Hz, 107 Hz and 117.5 Hz). Only three source room transmitted modes can be distinguished from receiving room natural ones (e.g. 45.5 Hz, 51.25 Hz, 70.5 Hz).

A first rough analysis to evaluate a descriptor of sound transmission loss ( $D$ ) can be expressed by the difference between source ( $L_1$ ) and receiving ( $L_2$ ) rooms sound pressure level spectra (Fig. 4.2).

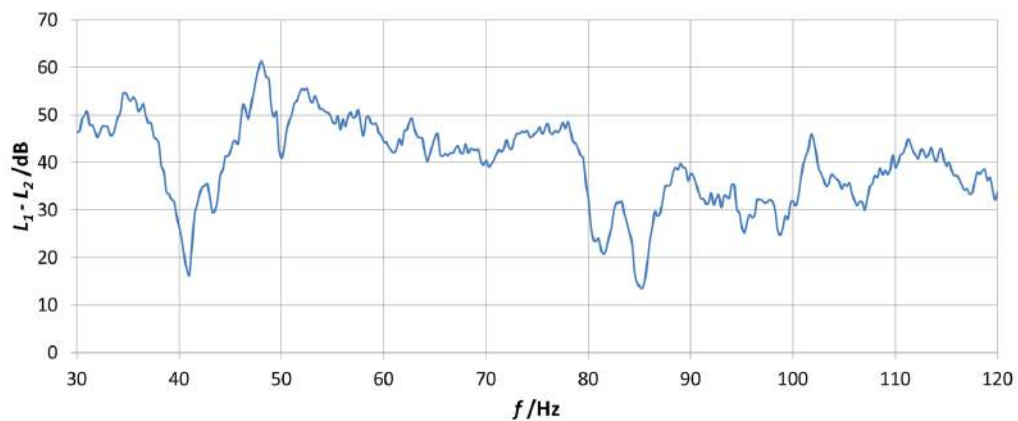


Figure 4.2: Sound pressure levels difference between source and receiving room.

The curve is characterized by large fluctuations due to low modal density and variable curve trends at not resonant frequencies. If the same measurements are performed in another laboratory with other dimensions, such curve would be different because of different modal composition and resonant half bandwidths (low reproducibility). For this reason, as for space domain, a point selection in fre-

quency is necessary in order to guarantee higher reproducibility values.

Point selection is based on the research of reliable modal sound transmission loss indicator. In the low frequency range, difference between the highest sound pressure levels of source room modes evaluated in the source and receiving room respectively can be considered as a descriptor of modal transmission loss, i.e. that particular property of the partition to prevent the transmission of a mode from one room to the other, as described in the introduction of this Chapter. Resonant frequencies, in addition, provide information about the resonant width  $\Delta f_{-3dB}$  related to modal absorption (see Eq. 2.63) and are stable in time. Such descriptor of sound transmission loss in non-diffuse field can be represented by the modal sound insulation ( $D_{modal}(f_n)$ ) which is defined as the sound pressure level difference between natural ( $L_{1,max}$ ) and transmitted ( $L_{2,max}$ ) source room modes ( $f_n = 2\pi\omega_n = 2\pi\omega_{l_1 m_1 n_1}$ ) evaluated in the positions of highest excitation (corners of laboratory rooms as stated in previous Chapter).

$$D_{modal}(f_n) = 20 \log_{10} \left( \frac{|p_{max}^{(1)}(x_{corner}, \omega_n, t)|}{|p_{max}^{(2)}(x_{corner}, \omega_n, t)|} \right) = L_{1,max_{corner}}(\omega_n) - L_{2,max_{corner}}(\omega_n) \quad (4.1)$$

where  $\omega_n = 2\pi f_n$ .

It is a discrete index as it refers just to source room resonant frequencies and provides an indication of sound transmission loss of a single mode passing through the partition from the source to the receiving room. Performing differences between the corresponding modal sound pressure levels, a representation of modal sound insulation ( $D_{modal}(f_n)$ ) is obtained (Fig. 4.3). Since some eigenfrequencies do not coincide perfectly (errors in the range of  $\pm 1$  Hz), source room resonant frequency values are used as  $x$ -coordinates in the representation of modal sound insulation curve as the transmission of source room natural modes has to be evaluated (Table 4.1).

Source room modes		Receiving room modes		$D_{modal}$
$f_n$ /Hz	$L_p$ /dB	$f$ /Hz	$L_p$ /dB	$D_{modal}$ /dB
41.75	99.7	<b>41</b>	73.6	26.2
		<b>43.25</b>	53.6	
45.5	94.7	45.5	50.1	44.6
		<b>50</b>	45.9	
51.25	100	51	48.9	51.1
		<b>61</b>	37.9	
66.25	100.9	<b>66.25</b>	59.4	41.4
70.5	91.3	70.25	51.9	39.4
81.25	87.6	<b>81.25</b>	66.1	21.6
83.5	89			
85	86.7	<b>85</b>	72.7	14.0
86	88.3			
		<b>95.25</b>	61.2	
97.75	94	<b>98.75</b>	64.8	29.2
101	90.1			
108.5	90.8	<b>107</b>	57.3	33.5
117	85.3	<b>117.25</b>	51.3	34.0

Table 4.1: Measured modes in source and receiving rooms [Hz] and difference between coincident modes ( $D_{modal}$ ). In bold, receiving room natural modes.

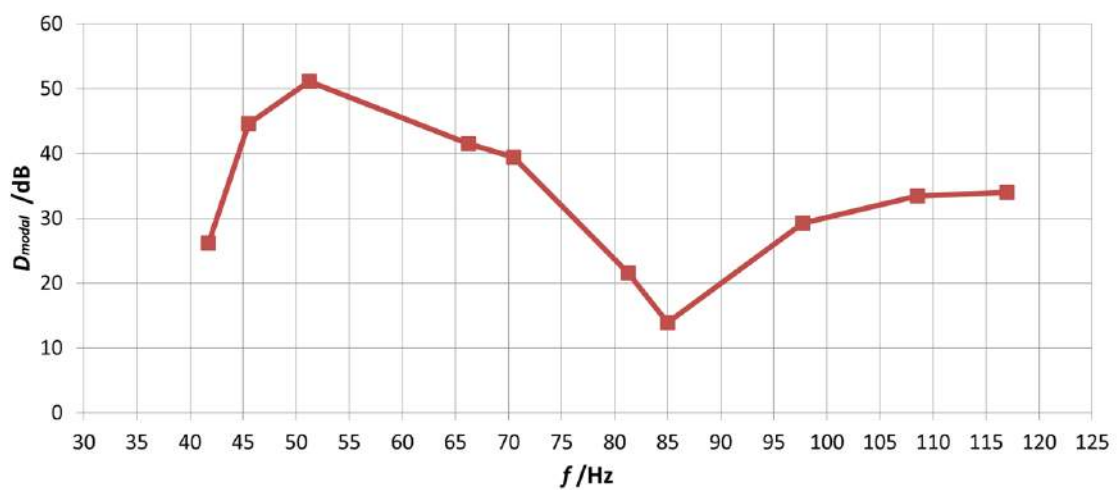


Figure 4.3: The modal sound insulation.

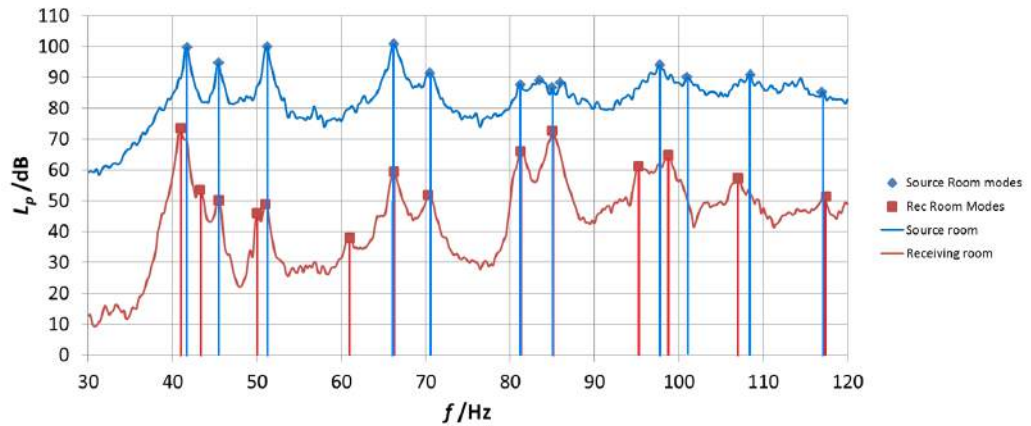


Figure 4.4: Source and receiving room spectra with indication of source and receiving room modes.

Since some natural source and receiving room modes are very close or equal (see frequencies in bold in Table 4.1) due to similar volumes, an overlap (or modal match) of source room transmitted modes and receiving room natural modes occurs in the receiving room spectrum (Fig. 4.4). Source and receiving rooms present 8 matching modes. Such problem could induce to an underestimation of modal sound insulation (see Chapter 6 for a deeper discussion and quantitative analysis).

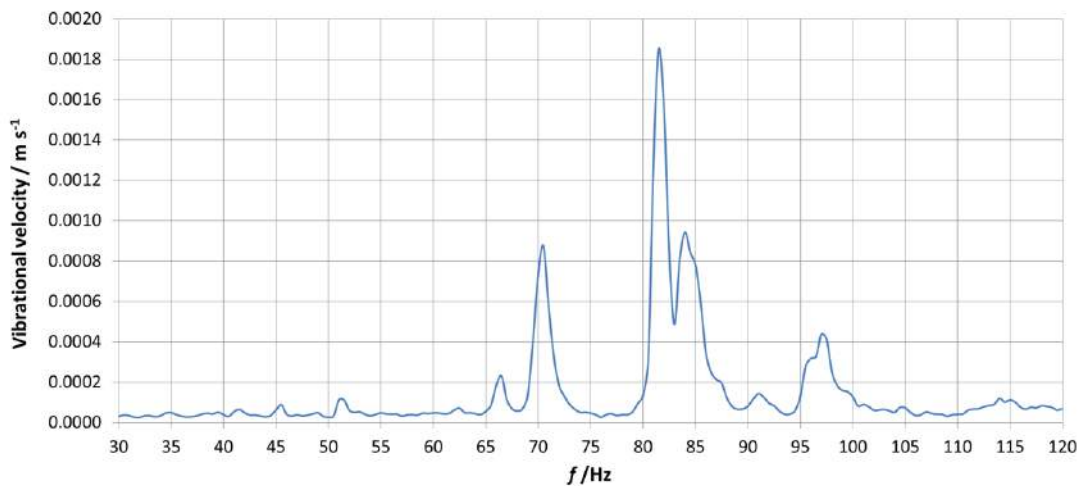


Figure 4.5: Structural modes of the partition.

The modal sound insulation curve provides an indication of modal transmission loss. In particular the curve presents a minimum at 85 Hz, which can be related to the resonant frequency of the partition (Fig. 4.5). Such comparison makes modal sound insulation measurement a significant sound transmission loss descriptor. Although the possibility to get a denser curve instead of considering

only source room modes, operations with non-resonant frequencies are not reliable sound transmission loss descriptors because of their variable and unpredictable behaviour. For this reason, the focus on source room modes can be considered the best choice to possibly get a reliable descriptor of modal sound insulation in order to get higher reproducibility values. High values of signal-to-noise ratio for each mode in the chambers make the influence of background noise negligible. Application of the correction for background noise level, according to ISO 10140–4:2010, does not show variations in the  $D_{modal}$  curve. Furthermore, two different sound source signals are tested: 30 s sweep from 20 Hz to 200 Hz and pink noise. In the first case, smoother source and receiving room spectra are obtained and consistent modal sound insulation values previously measured with pink noise signal (see Appendix A for further details).

## 4.2 Normalization terms

Reproducibility values of sound insulation measurements strongly depend on normalization terms. The modal sound insulation, see Eq. (4.1), aims to evaluate the transmission loss of a source room mode ( $f_n = 2\pi\omega_n = 2\pi\omega_{l_1m_1n_1}$ ) passing through the partition and directly depends on sound pressure levels measured at corners of source and receiving rooms, i.e. on the ratio between sound pressure in source and receiving rooms. Analytical and complete solution for sound pressure in source room can be obtained combining Eqs. (2.48), (2.49) and (2.50) while for sound pressure in receiving room Eqs. (2.58), (2.59), (2.56), (2.61) and (2.50). Modal sound transmission theory entails quite complex analytical solution of acoustic field and simple normalization terms associated to modal sound insulation cannot be obtained. Several consideration and approximation are necessary (see *Appendix B* for more details and calculations):

- Modal sound insulation derives from corner measurements of sound pressure levels ( $x_1 = 0, L_x, y_1 = 0, L_y, z_1 = 0, L_z$ ). For such reason, modal distribution functions for source ( $\psi_{l_1m_1n_1}^{(1)}$ ) and receiving room ( $\psi_{l_2m_2n_2}^{(2)}$ ) turns into 1 (see Eq. (2.49)).
- In the evaluation of modal sound insulation at a specific source room mode ( $\omega = \omega_{l_1m_1n_1}$ ), summation in the source room sound pressure equation can be reduced to one term since the others can be neglected. The same assumption can be transposed to receiving room sound pressure equation, although it is characterized by a product of three summations. We are considering just the highest term related to source room, partition and receiving room modal amplitudes. For  $\omega = \omega_{l_1m_1n_1}$ , source room sound pressure amplitude is the maximum ( $\omega_{l_1m_1n_1}^2 - \omega^2 = 0$ ) and receiving room pressure amplitude is the maximum when ( $\omega_{l_2m_2n_2}^2 - \omega^2$ ) is the minimum, i.e. when  $\omega_{l_2m_2n_2}^2$  is very close

to  $\omega^2 = \omega_{l_1 m_1 n_1}^2$ . Physically speaking, given a forced oscillation source at a specific source room mode  $\omega = \omega_{l_1 m_1 n_1}$ , influence of the other modes, which is mathematically given by summations, can be neglected with respect to the emitted one. The same reasoning is considered when a receiving room mode excited by a source room mode is taken into account. Such assumption is indirectly verified: the use of noise signal (excitation of all frequencies) or sine waves at specific source room modes (excitation of other modes is negligible with respect to emitted one), modal sound insulation results are very similar (see Appendix A).

- Reduction of summations to one term entails simplification of source room modal amplitude term  $A_{l_1 m_1 n_1}^{(1)}(\omega_{l_1 m_1 n_1})$  in the modal sound insulation equation (Eq. (4.1)), since it appears in both sound pressure terms (Eq. (2.48) and (2.58)).

Previous assumptions make  $D_{modal}$  depending on coupling terms (Eq. (2.56) and (2.61)) in which only partition and receiving room terms appear. Now, another step of simplification occurs: as partition property and dimensions are the same when sound insulation measurements are carried out in different laboratories as stated in ISO 10140–5:2010 and considering some coupling indexes terms in Eq. (2.56) and (2.61) equal to 1 (otherwise it is 0 but transmitted mode appears), modal sound insulation measurements in different laboratories depend only on receiving room volume  $V_2$  (influences of the other coupling indexes,  $\frac{q}{(q^2 - m_1^2)}$  and  $\frac{r}{(r^2 - n_1^2)}$ , and environmental parameters,  $\rho_0$  and  $c$ , are negligible). Fixing a standard value for receiving room volume ( $V_{2,0}$ ), normalized modal sound insulation becomes:

$$\begin{aligned}
 D_{modal,nV}(f_n) &= \\
 &= 20 \log_{10} \left( \frac{|p_{max}^{(1)}(x_{corner}, \omega_n, t)|}{|p_{0,max}^{(2)}(x_{corner}, \omega_n, t)|} \right) = \\
 &= 20 \log_{10} \left( \frac{|p_{max}^{(1)}(x_{corner}, \omega_n, t)|}{|p_{0,max}^{(2)}(x_{corner}, \omega_n, t)|} \cdot \frac{V_2}{V_2} \right) = \\
 &= 20 \log_{10} \left( \frac{|p_{max}^{(1)}(x_{corner}, \omega_n, t)| V_{2,0}}{|p_{0,max}^{(2)}(x_{corner}, \omega_n, t)| V_2} \right) = \\
 &= D_{modal} - 20 \log_{10} \left( \frac{V_2}{V_{2,0}} \right) \quad (4.2)
 \end{aligned}$$

where  $|p_{0,max}^{(2)}(x_{corner}, \omega_n, t)| \propto \frac{1}{V_{2,0}}$  is the normalized receiving room pressure term.

It is evident that receiving room volume is the main term that affect modal sound insulation descriptor. Reference standard receiving room volume is set on  $V_{2,0} = 50m^3$ , typical of a standard laboratory room. This reference value is just a proposal and has to be discussed and, eventually, modified.  $V_2$  is  $57 m^3$ . Introduction of normalization term in the modal sound insulation  $D_{modal,nV}$  entails a downward translation with respect to  $D_{modal}$  curve (see Fig. 4.6). Reproducibility measurements and evaluation of normalization terms are discussed in the following Chapters.

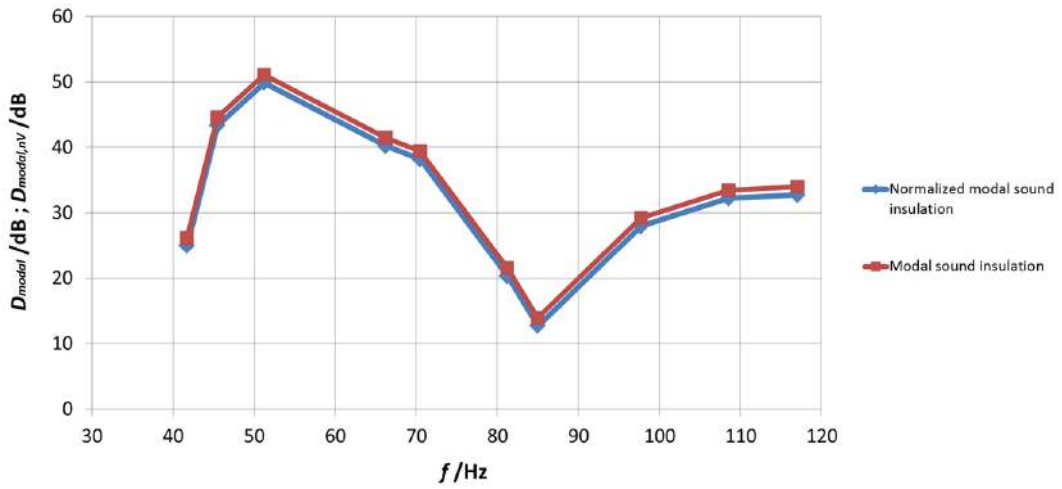


Figure 4.6: Comparison between  $D_{modal}$  and  $D_{modal,nV}$ .

As stated above, such operation is a first and simple normalization. As a matter of fact, since  $D_{modal}$  inversely depends on the modulus of the product of the coupling terms (Eqs. (2.56) and (2.61)), the influence of denominator terms in  $G_{qr,l_2m_2n_2}^{(2)}$  (Eq. 2.61) related to receiving room, i.e.  $|2\omega_{l_2m_2n_2}\delta_{l_2m_2n_2} + i(\omega^2 - \omega_{l_2m_2n_2}^2)|$ , the damping term and modal match term, respectively, are not negligible. As concerns the damping term, modal sound insulation could be affected by the presence of a sound absorber in the receiving room that could entail an underestimation of the sound pressure level of that particular source room transmitted mode in the receiving room and, as consequence, provide higher modal sound insulation values.

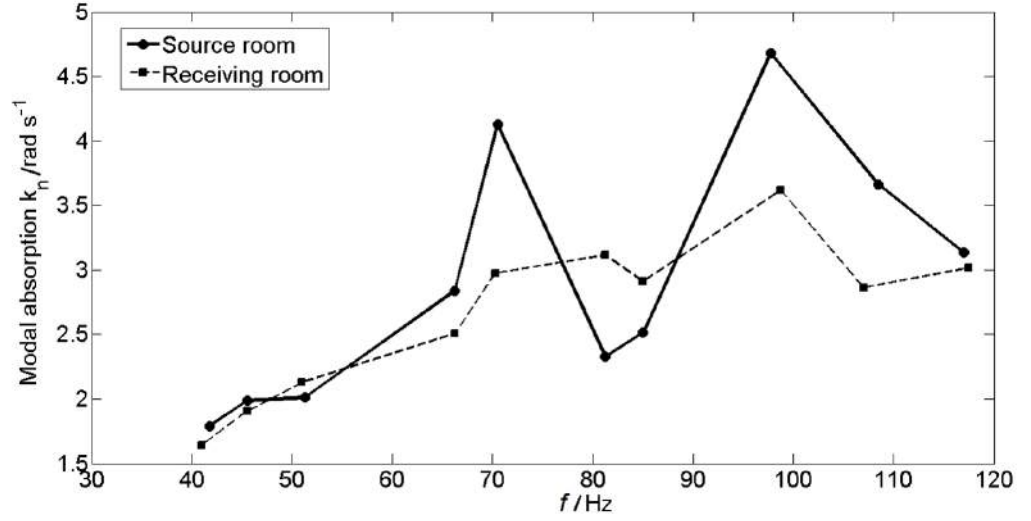


Figure 4.7: Modal dampings of source and receiving room modes.

In laboratory conditions, damping term effect is negligible: modal damping terms  $\delta_{l_1 m_1 n_1}$  or  $\delta_{l_2 m_2 n_2}$  are similar (see Fig. 4.7) since rooms are not equipped with particular low frequency absorbers (e.g. Helmholtz resonators) and are built with the same materials. Evaluation of modal dampings  $\delta_n$  is obtained by calculus of half bandwidth ( $\Delta f_{-3dB}$ ) by an interpolation of resonant peak with a Lorentzian function (an example is showed in Fig. 4.8). On the other hand, the modal match term ( $\omega^2 - \omega_{l_2 m_2 n_2}^2$ ) is not negligible except for, rarely in laboratory, very different source and receiving room modes, for which their mutual interaction is weak. Further and more detailed experimental results are reported in Chapter 6.

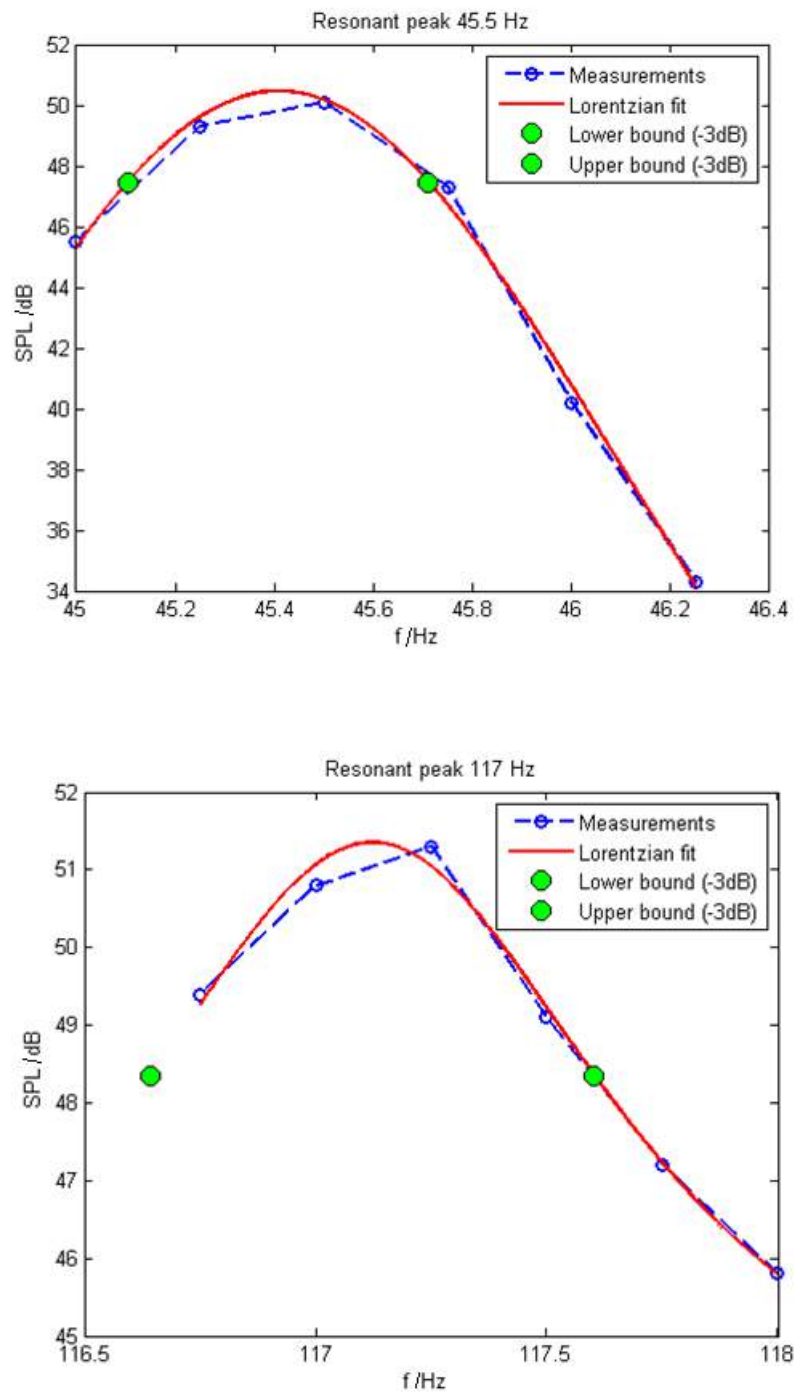


Figure 4.8: Evaluation of resonant half bandwidth  $\Delta f_{-3dB}$  through a Lorentzian fit (examples for receiving room 45.5 Hz and 117 Hz resonant frequencies).

### 4.3 The extension to the whole low frequency band

Because of the discrete nature of modal sound insulation, a new method is also introduced in order to extend it to the whole low frequency range in the 50 Hz, 63 Hz, 80 Hz and 100 Hz one-third octave bands (from 44 Hz to 112 Hz, the lower and upper bounds respectively). Considering a laboratory room with a different volume  $V$  and dimensions  $(L_x, L_y, L_z)$ , it is possible to assume that resonant frequencies can shift in frequency and move along the envelope of source and receiving room spectra, i.e. along the curve that connects, point-by-point, source resonance peaks (linear fit, Fig. 4.9) [49].

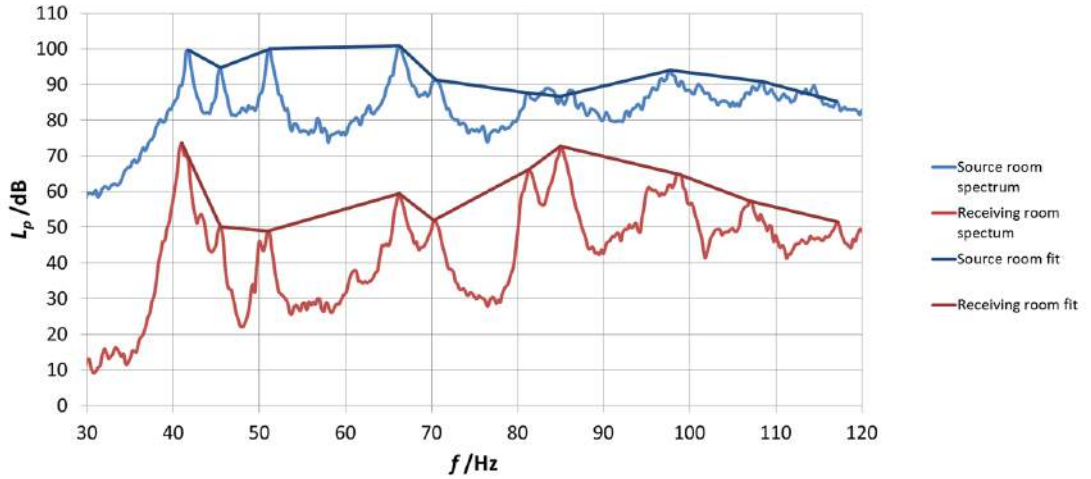


Figure 4.9: Envelope of source room resonant frequencies.

In this way, modal sound insulation (both for  $D_{modal}$  and  $D_{modal,nV}$ ) is extendible to the whole 44-112 Hz range (Fig. 4.10) and a third octave band representation is possible (Fig. 4.11). Furthermore, sound reduction integrated with modal sound insulation is shown (Fig. 4.12). It is important to underline that they refer to different measurement procedures and different physical meanings.

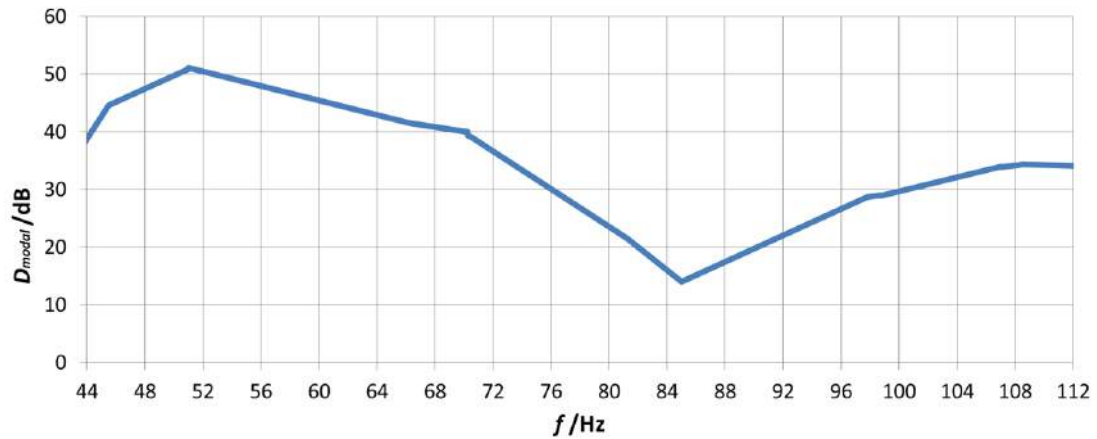


Figure 4.10: Extended modal sound insulation to the whole low frequency range.

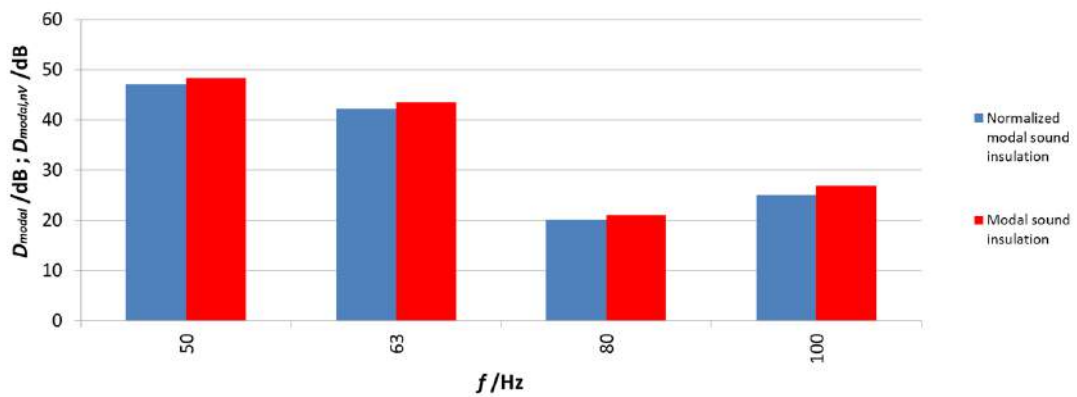


Figure 4.11: Third octave band representation of modal sound insulation.

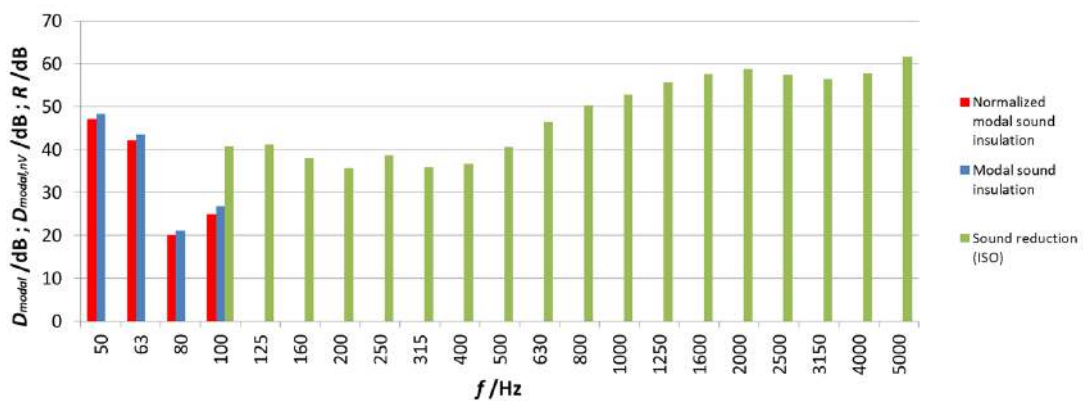


Figure 4.12: Sound reduction index ( $R$ ) integrated with modal sound insulation ( $D_{modal}$  and  $D_{modal,nV}$ ).



# Chapter 5

## Evaluation of uncertainty budget

In this Chapter, a first evaluation of uncertainty for measurement of room modes and modal sound insulation is reported as follows. Detailed results are deepened in each Section.

### 5.1 Type A and combined standard uncertainty of room modes

A first evaluation of room modes measurement uncertainty, based on GUM guideline [50], is performed in the receiving room of impact noise laboratory (3.618 m x 4.015 m x 3.498 m). The volume is about 51 m<sup>3</sup>. The temperature inside the chamber is 23.5 °C. The measurement setup consists of the devices described in Chapter 3.1. Source and microphone are placed in two different corners of the room. After calibrating the microphone and generating a pink noise signal from the source, a FFT spectrum analysis (linearly averaged for 60 second) of sound pressure level,  $L_p = 20\log_{10}(p/p_0)$ , is performed. Such measurement is repeated 4 times to evaluate type A uncertainty.

In Table 5.1 the measured modes are reported.

For simplicity, the statistical analysis is only extended to the first five resonant frequencies (42.9 Hz, 47.2 Hz, 50.2 Hz, 63.8 Hz, 66 Hz). In Table 5.2 and Fig. 5.1, sound pressure levels obtained from 4 consecutive measurements (repeatability) are shown.

Given  $n$  observations, the arithmetic mean of a quantity  $q$  is defined as:

$$\bar{q} = \frac{1}{n} \sum_{i=1}^n q_i \quad (5.1)$$

Variability of  $q_i$  observations is due to random effects that influence the measuring quantity. The experimental standard deviation of the probability distribution of  $q$  is given by

$f_n$ /Hz	$f$ /Hz
42.9	98.0
47.2	99.5
50.2	100.4
63.8	103.8
66.0	107.0
68.9	109.2
81.2	110.1
85.9	110.9
94.5	115.3

Table 5.1: Summary of measured modes.

$f_n$ /Hz	$L_{p1}$ /dB	$L_{p2}$ /dB	$L_{p3}$ /dB	$L_{p4}$ /dB
42.9	76.8	77.3	78.0	76.7
47.2	74.3	74.4	75.2	74.0
50.2	75.2	75.9	74.4	75.7
63.8	77.9	78.6	77.7	77.8
66.0	75.2	76.1	75.1	75.3

Table 5.2: Sound pressure levels of 4 repetitions for the first room modes.

$$s(q_i) = \sqrt{\frac{1}{n-1} \sum_{j=1}^n (q_j - \bar{q})^2} \quad (5.2)$$

The experimental standard deviation of the mean is given by

$$s(\bar{q}) = \frac{s(q_i)}{\sqrt{n}} \quad (5.3)$$

In Table 5.3, averages and repeatability standard deviations related to the 4 sound pressure level measurements (since level differences are less than 3 dB it is possible to perform the average of dB values instead of energetic average) associated to the five selected resonant frequencies are shown.

Assuming a normal distribution for a measurand  $q$ , the expanded uncertainty associated with  $q$  is given by:

$$U = t(\nu)s(q) \quad (5.4)$$

where  $t(\nu)$  is a factor associated to the t-Student distribution that depends on the number of degrees of freedom (in this case 3) and the significance to be hired;  $s(q)$  is the standard deviation. Assuming a confidence level of 95 % and a number

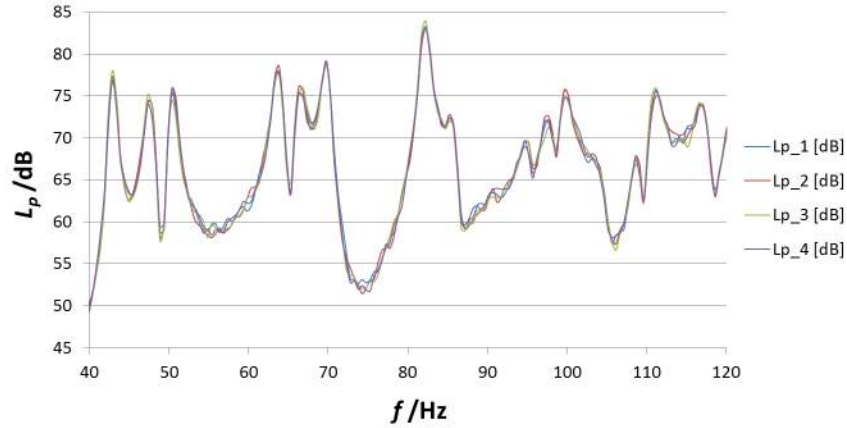


Figure 5.1: Sound pressure level spectra of 4 repetitions

$f_n$ /Hz	$\bar{L}_p$ /dB	$s(L_{p_i})$ /dB
42.9	77.2	0.6
47.2	74.5	0.5
50.2	75.3	0.7
63.8	78.0	0.4
66.0	75.4	0.5

Table 5.3: Average and experimental standard deviations of measured modes.

of degrees of freedom equal to 3 a value of  $t(\nu) \approx 3.18$  is obtained. In this way the expanded uncertainty for each frequency becomes (Table 5.4):

$f_n$ /Hz	$\bar{L}_p$ /dB	$U(L_p)$ /dB
42.9	77.2	1.9
47.2	74.5	1.6
50.2	75.3	2.1
63.8	78.0	1.3
66.0	75.4	1.4

Table 5.4: Type A expanded uncertainty of modal sound pressure levels

Now, the uncertainty contribution of measurement setup, through evaluation of combined uncertainty (with uncorrelated input quantities), is evaluated. In acoustics, sound pressures  $p$  are evaluated by output voltage  $T$ , knowing microphone sensitivity  $S$  ( $p = T/S$ ). In this way, sound pressure levels are given by:

$$L_p = 20 \log_{10} \left( \frac{p}{p_0} \right) = 20 \log_{10} \left( \frac{T}{S p_0} \right) \quad (5.5)$$

The output voltage from the microphone has a resolution, provided by the manufacturer, of  $1.19 \cdot 10^{-6}$  V. The sensitivity of the microphone, given by the manufacturer, is  $4.84 \cdot 10^{-2}$  V/Pa and its accuracy is  $5.57 \cdot 10^{-4}$  V/Pa. The uncertainty of a quantity  $y$  is given by:

$$u(y) = \sqrt{\sum_{i=1}^m u_i^2(y)} \quad (5.6)$$

where  $m$  is the number of variables in the model  $y$ ,  $u_i(y)$  is the uncertainty contribution due to the variable  $i$  and is expressed as

$$u_i^2(y) = c_i^2 u^2(x_i) \quad (5.7)$$

where  $c_i$  is the sensitivity coefficient and can be approximated by

$$c_i = \frac{\Delta y}{\Delta x_i} = \frac{(y + \Delta y) - y}{\Delta x_i} = \frac{[y(x_i + \Delta x_i)] - y}{\Delta x_i} \quad (5.8)$$

where  $\Delta x_i$  is an infinitesimal increment of variable  $i$ . In this specific case, since  $p_0$  is a reference value which is not associated to uncertainty, the uncertainty associated to  $L_p$ , for each of the five resonance frequencies selected, is given by:

$$u(L_p) = \sqrt{u_T^2(L_p) + u_S^2(L_p)} \quad (5.9)$$

where

$$u_T^2(L_p) = c_T^2 u^2(T) \quad (5.10)$$

$$u_S^2(L_p) = c_S^2 u^2(S) \quad (5.11)$$

$$c_T = \frac{\Delta L_p}{\Delta T} \quad (5.12)$$

$$c_S = \frac{\Delta L_p}{\Delta S} \quad (5.13)$$

For each selected frequency, output voltage  $T$  is measured, as shown in Table 5.5.

Using the uncertainty table and a coverage factor  $k$  equal to 3 for both variables,  $u^2(T)$ , which is a contribution of category B, and  $u^2(S)$ , which is a contribution of category A, are obtained. For example, the uncertainty table (Fig. 5.2), for a single mode (42.9 Hz), and the results of the calculations of the uncertainties, related to  $T$  (Table 5.6) and  $S$  (Table 5.7), are shown.

With 5 degrees of freedom and assuming a confidence level of 95% (corresponding to a coverage factor of approximately 2.57) for each frequency an expanded uncertainty associated to the corresponding  $L_p$  given in Table 5.8 is obtained.

$f_n$ /Hz	$T$ /V
42.9	$6.67 \cdot 10^{-3}$
47.2	$5.03 \cdot 10^{-3}$
50.2	$5.58 \cdot 10^{-3}$
63.8	$7.64 \cdot 10^{-3}$
66.0	$5.57 \cdot 10^{-3}$

Table 5.5: Output voltage for each selected mode.

	A	B	C	D	E	F	G	H	I	J	K	L	M	N	O	P	Q	R	S	T	
1																					
2	<b>T</b>	<b>Tensione in uscita</b>																			
3		Accuratezza																			
4		Risoluzione																			
5		Riproducibilità																			
6																					
7	<b>S</b>	<b>Sensibilità</b>																			
8		Accuratezza																			
9																					
10	<b>p<sub>0</sub></b>	<b>Pressione di riferimento</b>																			
11																					
12																					
13																					
14																					
15																					
16	Modello matematico																				
17	$y = L_p = 201 \log_{10} \left( \frac{p}{p_0} \right) = 201 \log_{10} \left( \frac{T}{S} \frac{p_0}{S} \right)$																				
18																					
19																					
20	Variabile x <sub>i</sub>		Cat A				Cat B		Parametri assegnati												
21	Simbolo	Valore	Note	U <sub>i</sub>	P <sub>g</sub>	v <sub>g</sub>	K <sub>g</sub>	S <sub>j</sub>	θ <sub>j</sub>	K <sub>s</sub>	v <sub>j</sub>	n <sub>g</sub>	n <sub>r</sub>	u <sup>2</sup> (x <sub>i</sub> )	c <sub>i</sub> =Δy/Δx	u <sup>2</sup> (y)	u <sup>2</sup> (y)/y				
22	T	6.70E-03	Acc	95%	100	2.0	0.0E+00			3	30	1	1	0.0E+00	1.3E+03	0.0E+00	0.0E+00				
23			Ris	95%	100	2.0	0.0E+00			3	100	1	1	1.2E-13	1.3E+03	2.0E-07	4.0E-16				
24			Ripr	95%	100	2.0	0.0E+00			3	30	1	1	0.0E+00	1.3E+03	0.0E+00	0.0E+00				
25	S	4.84E-02	Acc	95%	100	2.0	2.8E-04			3	5	1	1	7.9E-08	-1.2E+01	1.1E-05	2.6E-11				
26																					
27	y	76.8000	dB														Varianza di y, u <sup>2</sup> (y)		1.2E-05	2.6E-11	
28														Incertezza tipo di y, u(y)		3.4E-03					
29														Gradi di libertà di y, v(y)		5					
30														Livello di fiducia		95%					
31														Fattore di copertura (t di Student)		2.6E+00					
32														Incertezza estesa U(y)		8.7E-03		dB			
33																					
34																					
35																					
36	Calcolo dei coefficienti di sensibilità																				
37		Δx <sub>i</sub>	x <sub>i</sub> +Δx <sub>i</sub>	y+Δy	Δy	Δy/Δx															
38	T	1.00E-08	7E-03	8E+01	1.3E-05	1.3E+03															
39	0	1.00E+00	1E+00	-7.7E+01	-7.7E+01	-3.8E+01															
40	0	2.00E+00	2E+00	-7.7E+01	-7.7E+01	-3.8E+01															
41	S	3.00E+00	3E+00	4E+01	-3.6E+01	-1.2E+01															
42																					
43																					
44																					
45																					

Figure 5.2: Uncertainty table for 42.9 Hz mode.

$f_n$ /Hz	$u^2(T)$ /V <sup>2</sup>	$c_T$ /dB/V	$u^2_T(L_p)$ /dB <sup>2</sup>
42.9	$1.2 \cdot 10^{-13}$	$1.3 \cdot 10^{-3}$	$2.0 \cdot 10^{-7}$
47.2	$1.2 \cdot 10^{-13}$	$1.7 \cdot 10^{-3}$	$3.5 \cdot 10^{-7}$
50.2	$1.2 \cdot 10^{-13}$	$1.6 \cdot 10^{-3}$	$2.9 \cdot 10^{-7}$
63.8	$1.2 \cdot 10^{-13}$	$1.1 \cdot 10^{-3}$	$1.5 \cdot 10^{-7}$
66.0	$1.2 \cdot 10^{-13}$	$1.6 \cdot 10^{-3}$	$2.9 \cdot 10^{-7}$

Table 5.6: Uncertainty related to T.

The percentage ratio between the combined and the type A uncertainty of  $L_p$  (expanded uncertainty  $U(L_p)$ ) for each frequency (Table 5.9) shows a greater influence of type A uncertainty, due to random fluctuations in the repetition of the measurement, rather than to errors related to the measurement devices. As a

$f_n$ /Hz	$u^2(S) /(\text{V}/\text{Pa})^2$	$c_S$ /dB Pa/V	$u_S^2(L_p) /\text{dB}^2$
42.9	$7.9 \cdot 10^{-8}$	$-1.8 \cdot 10^2$	$2.5 \cdot 10^{-3}$
47.2	$7.9 \cdot 10^{-8}$	$-1.8 \cdot 10^2$	$2.5 \cdot 10^{-3}$
50.2	$7.9 \cdot 10^{-8}$	$-1.8 \cdot 10^2$	$2.5 \cdot 10^{-3}$
63.8	$7.9 \cdot 10^{-8}$	$-1.8 \cdot 10^2$	$2.5 \cdot 10^{-3}$
66.0	$7.9 \cdot 10^{-8}$	$-1.8 \cdot 10^2$	$2.5 \cdot 10^{-3}$

Table 5.7: Uncertainty related to  $S$ .

$f_n$ /Hz	$u(L_p) /\text{dB}$	$U(L_p) /\text{dB}$
42.9	$5 \cdot 10^{-2}$	$1.3 \cdot 10^{-1}$
47.2	$5 \cdot 10^{-2}$	$1.3 \cdot 10^{-1}$
50.2	$5 \cdot 10^{-2}$	$1.3 \cdot 10^{-1}$
63.8	$5 \cdot 10^{-2}$	$1.3 \cdot 10^{-1}$
66.0	$5 \cdot 10^{-2}$	$1.3 \cdot 10^{-1}$

Table 5.8: Combined expanded uncertainty of  $L_p$ .

matter of fact, the acoustic field is subject to fluctuations due to various factors (changes in temperature, density, speed of sound, speed of vibration of the source membrane) that can not be completely controlled, especially in building acoustics.

$f_n$ /Hz	$U_{comb}(L_p) / U_{typeA}(L_p) \%$
42.9	7.0%
47.2	8.0%
50.2	6.2%
63.8	10.2%
66.0	9.0%

Table 5.9: Ratio between combined and type A uncertainties.

## 5.2 Repeatability of modal sound insulation measurement

Repeatability measurements of modal sound insulation is performed (see Section 4.1). Since uncertainty of measurement devices is negligible, as seen before for modes measurement, modal sound insulation uncertainty is evaluated through repeatability measurements in terms of repeatability standard deviation, the traditional procedure of uncertainty assessment in building acoustics (ISO 12999-1:2014) [51]. The repeatability is defined as the closeness of the agreement between the results of successive measurements of the same measurand carried out under the same conditions of measurement [50]. 4 modal sound insulation measurements are performed on a heavyweight partition in laboratory rooms with a pink noise source signal. Results are reported in Table 5.10 and plotted in Fig. 5.3.

$f_n$ /Hz	$D_{modal_1}$ /dB	$D_{modal_2}$ /dB	$D_{modal_3}$ /dB	$D_{modal_4}$ /dB
42.00	8.3	8.2	6.28	7
51.50	17.9	20.4	18.8	20.0
66.25	21.1	22.9	22.6	23.0
70.25	14.6	16.0	16.5	15.4
84.25	9.7	10.0	9.9	10.1
97.75	7.5	6.6	7.9	6.7
105.50	7.8	8.0	9.8	9.0
109.50	21.9	22.2	21.4	21.9
113.00	28.9	25.1	24.2	25.3
$f_n$ /Hz	$\bar{D}_{modal}$ /dB	$s(D_{modal})$ /dB	$s(\bar{D}_{modal})$ /dB	$U(\bar{D}_{modal})$ /dB
42.00	7.4	1.0	0.5	1.5
51.50	19.3	1.2	0.6	1.8
66.25	22.4	0.9	0.4	1.4
70.25	15.6	0.8	0.4	1.3
84.25	9.9	0.2	0.1	0.2
97.75	7.2	0.6	0.3	1.0
105.50	8.7	0.9	0.5	1.5
109.50	21.9	0.4	0.2	0.7
113.00	25.9	2.1	1.0	3.3

Table 5.10: Repeatability results of modal sound insulation.

After the application of the extension to the whole low frequency range (according to Section 4.3), representation of modal sound insulation repeatability is depicted in Table 5.11 and Fig. 5.4.

Repeatability standard deviation values are within the limits fixed by ISO 12999-1:2014 for the low frequency third octave bands. Since volume normalization

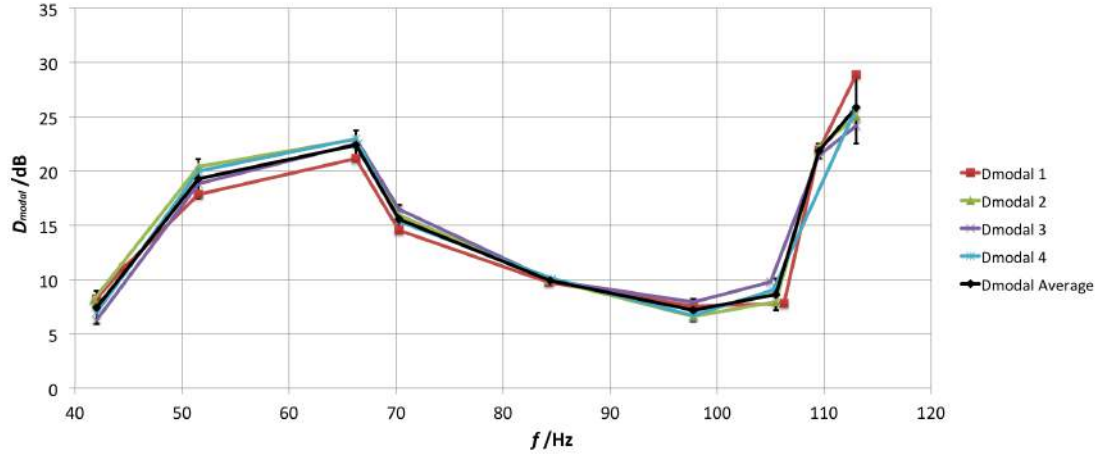


Figure 5.3: Modal sound insulation discrete curves of the 4 repetitions. Error bars correspond to repeatability expanded uncertainty of the mean for the 95% confidence level.

$f_n$ /Hz	$D_{modal_1}$ /dB	$D_{modal_2}$ /dB	$D_{modal_3}$ /dB	$D_{modal_4}$ /dB
50	15.4	17.7	15.9	16.8
63	19.6	21.8	21.1	21.7
80	10.7	10.9	11.1	11.0
100	8.8	8.5	9.6	8.7
$f_n$ /Hz	$\bar{D}_{modal}$ /dB	$s(D_{modal})$ /dB	$s(\bar{D}_{modal})$ /dB	$U(\bar{D}_{modal})$ /dB
50	16.4	1.0	0.5	1.6
63	21.0	1.0	0.5	1.6
80	10.9	0.2	0.1	0.3
100	8.9	0.5	0.2	0.7

Table 5.11: Repeatability results of modal sound insulation in one-third octave bands.

term in repeatability measurements is non influential (same laboratory rooms), it is evaluated separately in the next Section about reproducibility measurement.

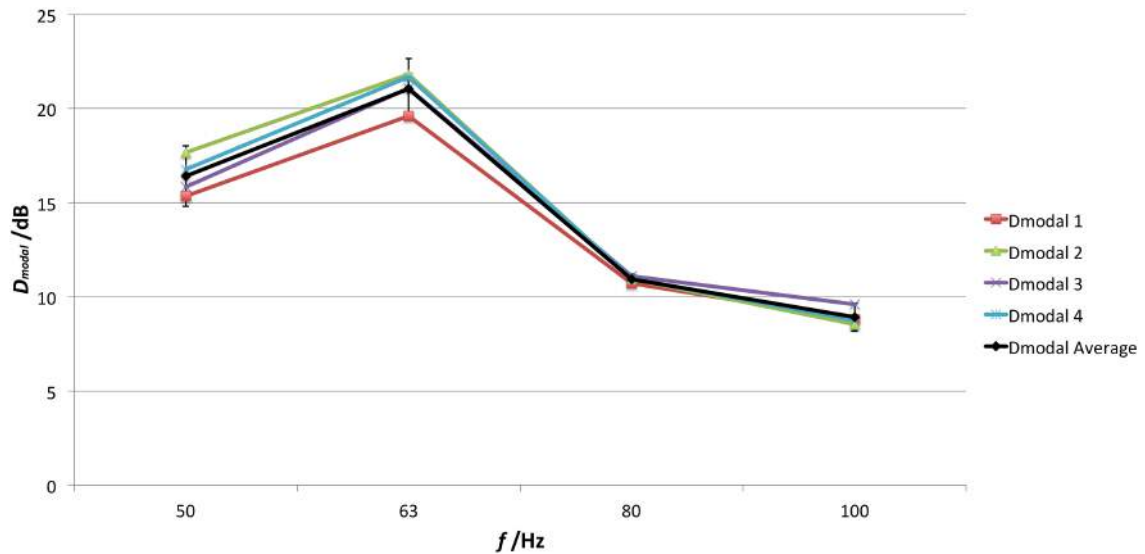


Figure 5.4: Modal sound insulation in one-third octave bands of the 4 repetitions. Error bars correspond to repeatability expanded uncertainty of the mean for the 95% confidence level.

### 5.3 Reproducibility of modal sound insulation measurement

A first reproducibility measurement of modal sound insulation is performed in the 2 airborne sound insulation INRIM laboratories on the same lightweight layered partition. Reproducibility is defined as the closeness of the agreement between the results of measurements of the same measurand carried out under changed conditions of measurement [50]. Results of discrete modal sound insulation values, with proper repeatability measurement to verify the dispersion (standard deviation), are reported in Tables 5.12, 5.13 and in Fig. 5.5, 5.6.

Results, extended in third octave bands, are reported in Table 5.14 and Fig. 5.7, 5.8. The qualitative trend of modal sound insulation is similar except for quantitative discrepancies. A good agreement is evident for 80 Hz and 100 Hz one-third octave bands, while for 50 Hz and 63 Hz one-third octave bands, the agreement decreases due to the presence of strong modal match with receiving room first modes (40-70 Hz). These modes are quite stable in time and frequency and are more influential than the volume normalization term which is not sufficient to increase reproducibility. In the following Chapter receiving room volume normalization term is discussed in depth. Inter-laboratory tests are necessary for a more accurate uncertainty and reproducibility assessment.

$f_n$ /Hz	$\bar{D}_{modal}$ /dB	$\bar{D}_{modal,nV}$ /dB
<b>42.00</b>	17.4	15.6
47.00	25.9	24.1
51.50	30.6	28.9
<b>66.75</b>	37.5	35.8
71.50	41.4	39.7
82.00	33.2	31.5
84.50	45.6	43.9
88.50	44.1	42.4
<b>96.00</b>	33.3	31.6
<b>99.25</b>	44.7	43.0
103.50	47.7	46.0
107.25	49.8	48.1
113.25	50.1	48.4

Table 5.12: Modal sound insulation in Lab. 1. In bold most influential matching modes.

$f_n$ /Hz	$\bar{D}_{modal}$ /dB	$\bar{D}_{modal,nV}$ /dB
<b>42.00</b>	18.4	16.7
45.00	12.9	11.2
52.00	33.6	31.8
<b>64.00</b>	20.5	18.8
<b>66.50</b>	27.5	25.8
69.00	30.5	28.8
86.25	43.4	41.7
96.50	36.3	34.6
107.75	51.7	49.9
<b>110.75</b>	34.9	33.2
<b>113.75</b>	37.2	35.5

Table 5.13: Modal sound insulation in Lab. 2. In bold most influential matching modes.

$f_n$ /Hz	Lab. 1		Lab. 2	
	$\bar{D}_{modal}$ /dB	$\bar{D}_{modal,nV}$ /dB	$\bar{D}_{modal}$ /dB	$\bar{D}_{modal,nV}$ /dB
50	30.3	28.6	22.9	21.4
63	35.5	33.8	25.8	24.1
80	39.1	37.4	38.2	36.5
100	43.2	41.5	39.1	37.5

Table 5.14: Reproducibility results of modal sound insulation in one-third octave bands in the 2 INRIM laboratories.

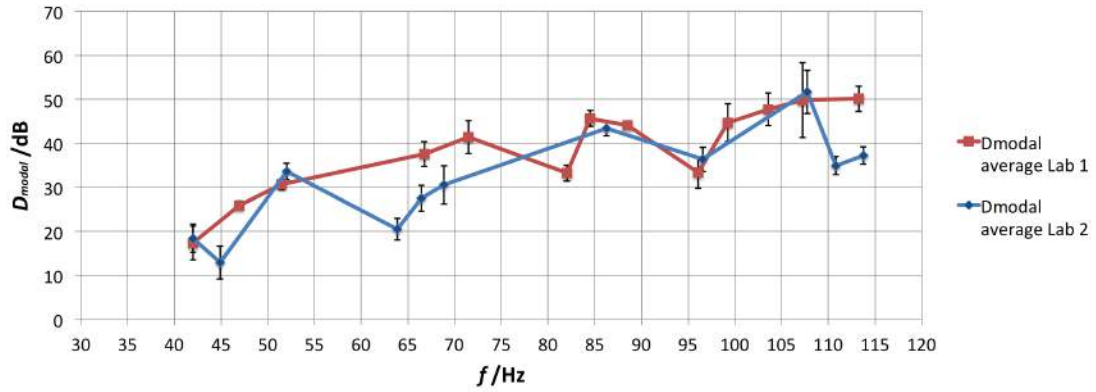


Figure 5.5: Modal sound insulation comparison in Lab.1 and 2. Error bars correspond to repeatability expanded uncertainty calculated for the 95% confidence level.

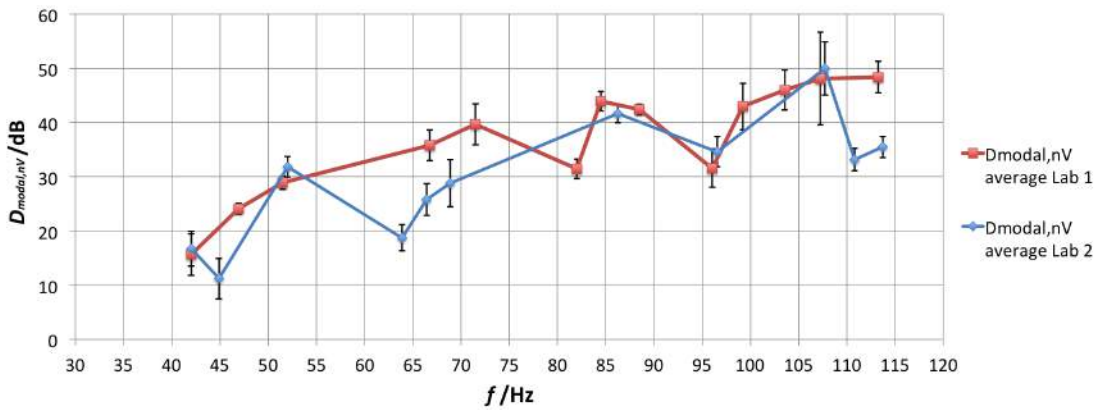


Figure 5.6: Normalized modal sound insulation comparison in Lab.1 and 2. Error bars correspond to repeatability expanded uncertainty calculated for the 95% confidence level.

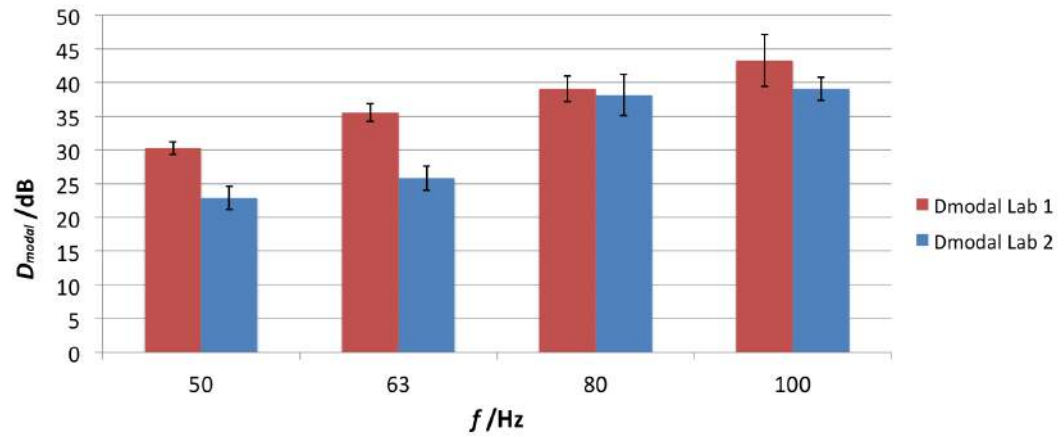


Figure 5.7: Modal sound insulation comparison in Lab.1 and 2. Error bars correspond to repeatability expanded uncertainty calculated for the 95% confidence level.

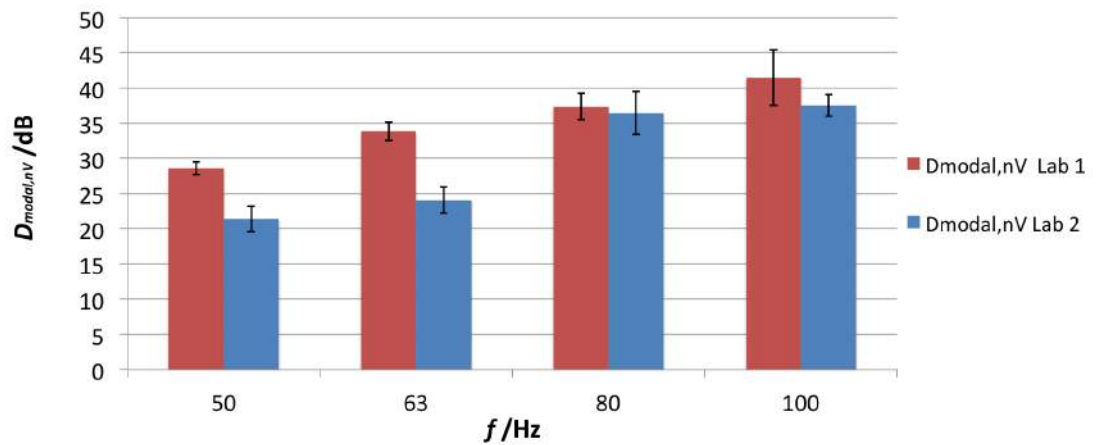


Figure 5.8: Normalized modal sound insulation comparison in Lab.1 and 2. Error bars correspond to repeatability expanded uncertainty calculated for the 95% confidence level.

# Chapter 6

## Analysis of modal sound insulation in the scale model

Modal sound transmission and insulation are evaluated in the 1:8 scale model at the Applied Acoustics Dept. in PTB (Braunschweig, Germany) [52]. In particular, it is necessary to investigate the validity of normalization term and the extension method to the whole low frequency range, to make a comparison of reproducibility measurements between standard and modal sound insulation descriptors and to evaluate the influence of modal match.

### 6.1 Measurement setup

The 1:8 scale model of an airborne sound insulation laboratory (a source and a receiving room) consists of 38 mm thick medium density fiber boards (Fig. 6.1).

The scale model is effectively used to carry out studies on the influence of geometric parameters: the basic idea of the investigation is to vary the size of source and receiving rooms to evaluate the influence of normalization term and to check the extension to the whole low frequency range through modal spectra envelope method mentioned in Chapter 4. For this reason, source and receiving room  $L_x$  dimension can be varied from 40 cm to 90 cm, shifting the mobile wall facing the test object, whereas  $L_y=45$  cm and  $L_z=38$  cm are fixed for both rooms. The test object, a gypsum board, is hung on a crane and fits the opening of the test facility. For what concerns instrumental devices, 1/4" microphones and an hexahedrons source of about 40 mm edge length, with one loudspeaker on each surface, are used for the generation and acquisition of the sound field (Fig. 6.2). Data acquisition and frequency analysis are provided by OROS Multi-channel Analyzer connected to a laptop with its own dedicated software.

Since the airborne sound field in the room has to be similar to the original case, the ratio between the wavelength and the room dimensions has to be constant.

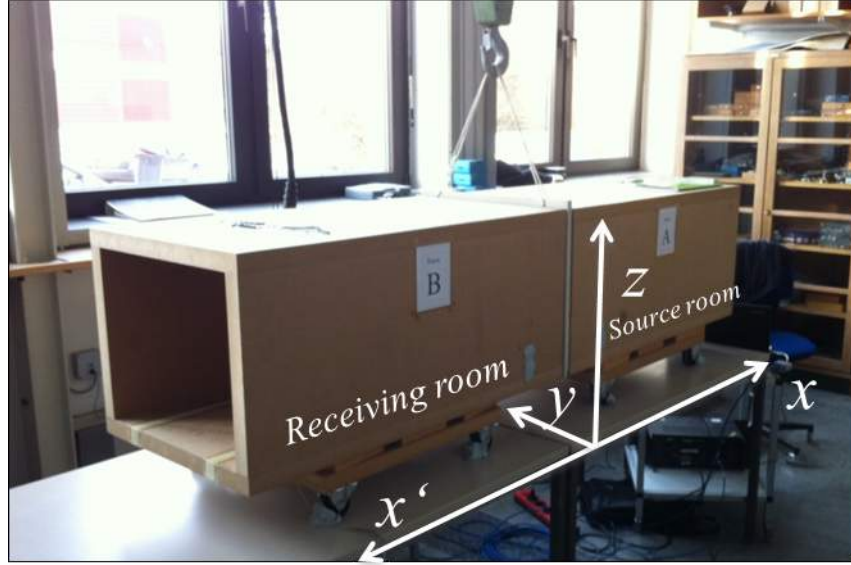


Figure 6.1: The 1:8 scale model of an airborne sound insulation laboratory.

This means that for the 1:8 scale model, a reduction by a factor of 8 is compensated by increasing the measurement frequency by the same factor. Therefore, low frequency range of 50-100 Hz corresponds to the 400-800 Hz range in the scale model. The same is obtained for the FFT spectrum resolution: if in laboratory measurements a resolution of 0.25 Hz is reached, in the scale model it corresponds to 2 Hz. The source signal used is a pink noise from 100 Hz to 1600 Hz. According to the modal approach, microphones and source are placed at the corners of the rooms (4 corners of each room are investigated).

## 6.2 Evaluation of volume normalization term

As stated in Chapter 4.2, normalized modal sound insulation is associated to the receiving room volume, according to Eq. 4.2. The validity of such term is checked by changing progressively the receiving room volume (volume variations from -30% to 60% with respect to source room volume), shifting the mobile wall from  $L_x=40$  cm to  $L_x=90$  cm with steps of 10 cm and performing modal sound insulation measurements, according to the procedure introduced in Chapter 4.1. To simplify the evaluation of normalization term, reference volume  $V_0$  is set to  $0.0684$  m<sup>3</sup>, i.e. the receiving room volume with  $L_x=40$  cm. Source room volume is left constant during all measurements and, in order to minimize modal match, at least for  $x$ -axis modes, its  $L_x$  dimension is fixed at 55 cm. In Fig 6.3, volume combinations of source and receiving room are shown.



Figure 6.2: The inner part of the scale model.

Highest modal sound pressure level spectra in source and receiving rooms are evaluated and shown in Fig. 6.4. Source room spectra are well overlapped as no volume change is performed. In receiving room spectra, the presence of natural and transmitted mode is evident. In particular, modes that depend on  $x$  dimension move in frequency and, approaching transmitted mode from source room due to similar  $x$  length (S50 and S60 curves), modal sound pressure level increases (e.g. around 318 Hz, 502 Hz, 556 Hz, 678 Hz and 828 Hz). Furthermore, modal match due to equal  $L_y$  and  $L_z$  lengths is clear and leads to the highest modal sound pressure levels in the receiving room for 394 Hz, 456 Hz, 596 Hz, 766 Hz resonant frequencies: in these cases, it is impossible to provide a real indication of sound insulation property of the partition due to such boundary conditions.

For each volume combination, modal sound insulation and normalized modal sound insulation values are obtained, depicted in Fig. 6.5, 6.6 and reported in Table 6.1. The lowest values are reached for matching modes, as sound pressure levels of source room transmitted modes are increased by receiving room modes. This leads to an underestimation of modal sound insulation. Whereas, for the other frequencies, modal sound insulation values are barely affected by modal match.

Analysis of standard deviations (from Table 6.1 and Fig. 6.7) shows no significant improvement of reproducibility with the introduction of volume normalization term. Such result raises a question about the assumptions and simplifications made in the modal approach theory (Chapter 4.2 and Appendix B) and the effective weight of volume term in modal sound insulation measurements. Particular attention has to be paid to modal sound insulation values of matching resonant

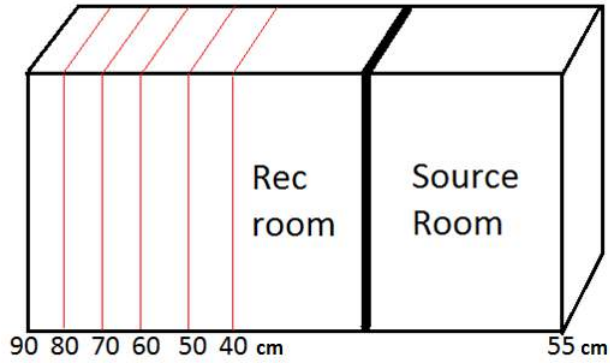


Figure 6.3: Volume combinations of source and receiving rooms.

$f_n$ /Hz	$\bar{D}_{modal}$ /dB	$s_{D_{modal}}$ /Hz	$\bar{D}_{modal,nV}$ /dB	$s_{D_{modal,nV}}$ /dB
318	35.2	4.5	31.3	4.6
394	6.1	1.2	2.2	2.5
456	4.7	1.6	0.8	1.3
502	30.6	5.2	26.7	5.9
556	29.9	4.7	26.0	5.2
596	13.9	3.1	10.0	2.1
678	30.1	5.3	26.2	5.6
736	34.3	3.7	30.4	4.5
766	13.7	2.2	9.8	1.3
828	28.2	6.1	24.3	5.9
856	32.8	0.8	26.2	1.5
904	16.5	3.1	12.6	1.5
952	22.5	8.0	17.1	6.6
986	18.5	3.6	14.6	4.1

Table 6.1: Averages and standard deviations of modal sound insulation ( $D_{modal}$ ) and normalized modal sound insulation ( $D_{modal,nV}$ ).

frequencies: low sound insulation values are obtained as expected and also lower standard deviations are gathered. This is an evidence of the fact that matching modes are very stable in time and it is the most influential parameter in the evaluation of modal transmission loss of a wall test specimen, through the modal sound insulation descriptor.

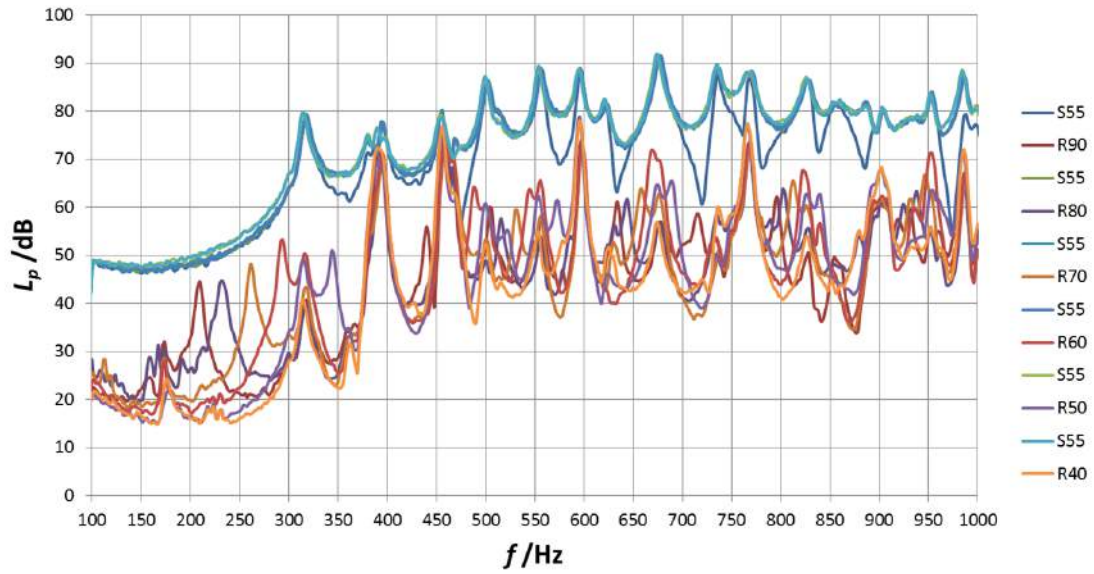


Figure 6.4: Highest modal sound pressure level spectra in source (S) and receiving (R) rooms with different volume combinations.

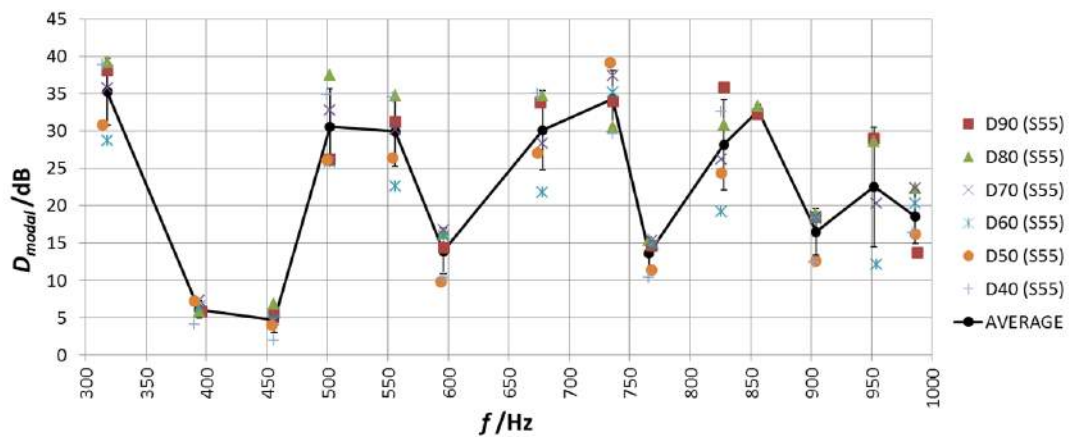


Figure 6.5: Modal sound insulation values obtained with different room combinations. Averages and standard deviations (error bars) are shown in black.

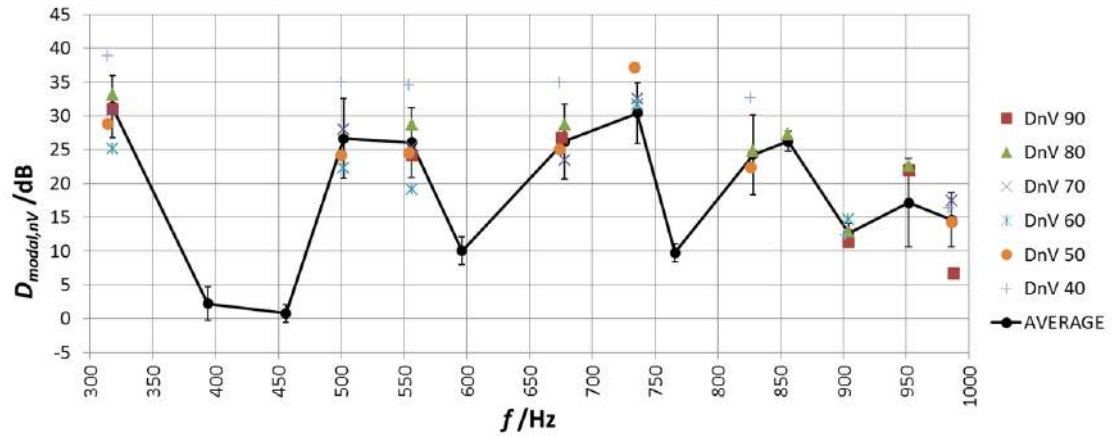


Figure 6.6: Normalized modal sound insulation values obtained with different room combinations. Averages and standard deviations (error bars) are shown in black.

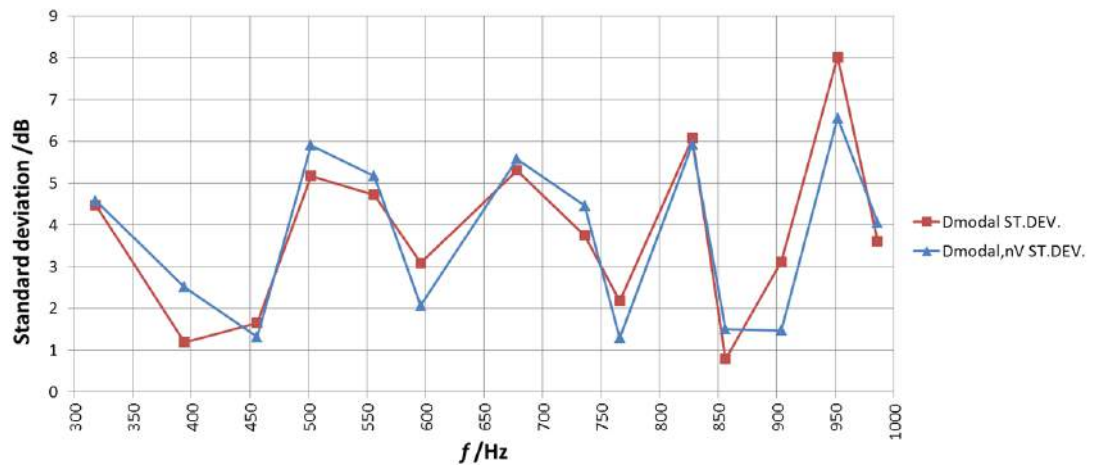


Figure 6.7: Comparison between standard deviation of modal sound insulation and normalized modal sound insulation.

## 6.3 The influence of modal match

Since scale model does not have the possibility to change  $L_y$  and  $L_z$  lengths in both rooms, modes associated to those dimensions are the same and modal match strongly influences modal sound insulation measurements as seen above. An attempt to exclude from the analysis perfectly matching modes or the most overlapped ones (e.g. 394 Hz, 456 Hz, 596 Hz, 766 Hz, ) is made to provide a real indication of modal transmission loss of the partition. Results of such selection are depicted in Fig. 6.8. The selection of low matching modes, representative for a real description of modal transmission loss of the wall test, provides higher values of modal sound insulation with respect to the previous ones (Fig. 6.5).

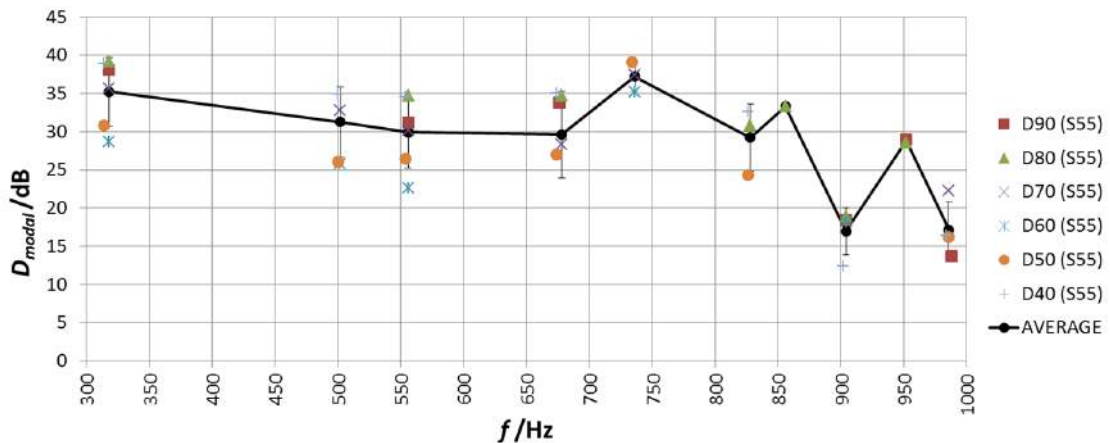


Figure 6.8: Modal sound insulation curve after the exclusion of matching modes or most overlapped ones.

It is clear how receiving room modes increase their level when source room transmitted modes approach (see as example receiving room spectra for 318 Hz in Fig. 6.4). Selection of modes entails also a decrease of modal sound insulation standard deviations for the remaining resonant frequencies as shown in Fig. 6.9, and this confirms the goodness of modal selection.

Influence of modal overlap or modal match due to volume coupling is clearer in the following measurement: fixing  $L_x$  of source room at 90 cm, modal sound insulation measurements are performed with receiving room  $L_x$  at 40 cm and 90 cm. Modal sound pressure levels in the receiving room increase due to volume coupling (Fig. 6.10). As an example, in the first case, first axial source room transmitted mode (196 Hz associated to  $L_x=90$  cm) is not influenced by a natural receiving room mode whereas, in the second case, perfect modal match entails an increase of 30-35 dB of modal sound pressure level at such frequency.

On the basis of this experimental evidence, the influence of receiving room natural modes to source room transmitted modes as function of the modal overlap

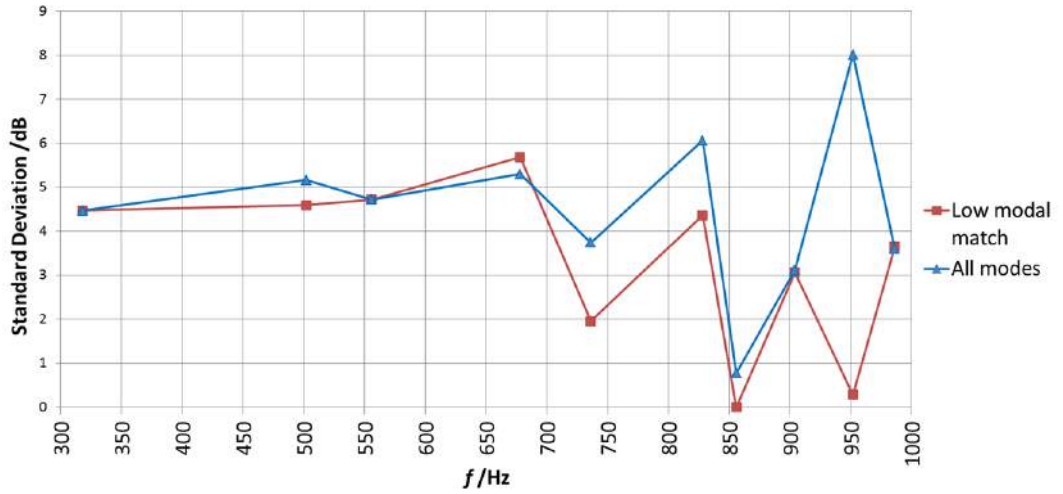


Figure 6.9: Comparison of modal sound insulation standard deviations calculated with all modes and after selection of low matching modes.

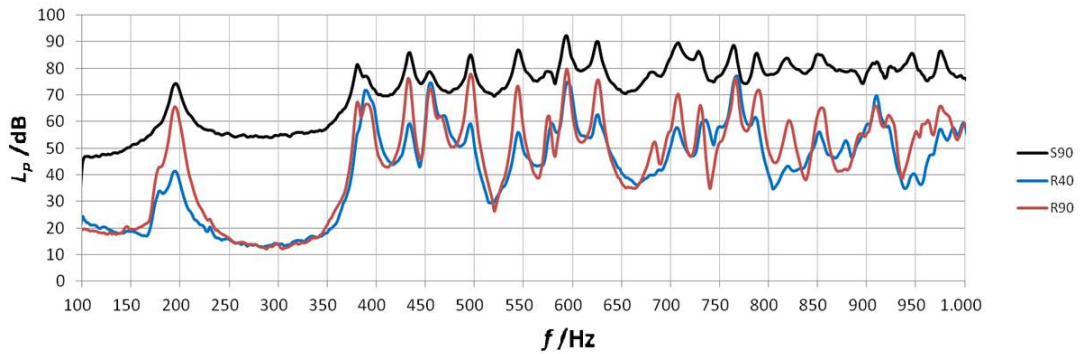


Figure 6.10: Increase of modal sound pressure levels in the receiving room due to volume coupling.

degree, i.e. their frequency distance ( $\Delta f = f_{n,source} - f_{n,rec}$ ), or  $L_x$  length difference between source and receiving rooms ( $\Delta x = L_{x,source} - L_{x,rec}$ ), is studied. For this purpose, source room  $L_x$  is fixed at 70 cm and receiving room  $L_x$  is changed from 50 cm to 90 cm with an exponential decrease/increase of steps approaching/distancing equal sizes. 248 Hz source room transmitted mode (first axial mode associated to  $L_x=70$  cm dimension) increases its sound pressure level as source and receiving room  $L_x$  lengths become similar, as shown in Fig. 6.11.

As depicted in Fig 6.12 and 6.13, the increase of modal sound pressure level as function of length or frequency differences between source and receiving room is exponential, as the Kohlrausch-Williams-Watts (KWW) function:

$$y = a \cdot e^{-|bx|^c} \quad (6.1)$$

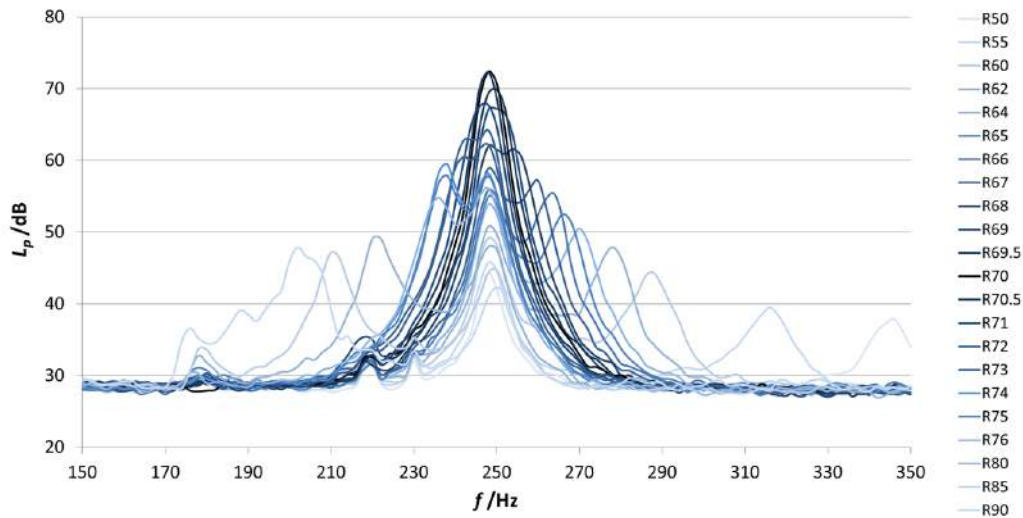


Figure 6.11: Modal sound pressure level with the increase of modal overlap degree.

The fit curve ( $a=77$ ,  $b=0.02$ ,  $c=0.5$ ), in space domain, is shown in Fig. 6.14 (frequency resolution is not high enough to perform the fit in frequency domain). This result opens the possibility to use a weighted procedure method in order to avoid problems due to modal match and get a real evaluation of laboratory modal sound insulation of a partition which could guarantee repeatable and reproducible values. In the future, it will be necessary to deepen such experimental phenomenon with further scale model measurements to validate correlation function for other modes (tangential and oblique).

Another comparison is performed with the scale model inside the anechoic chamber in order to avoid the influence of modal match. In this case, the receiving room is removed from the scale model and modal sound insulation measurements are performed with receiving space microphones placed randomly at 1 cm from the partition (see Fig. 6.15). The source room  $L_x$  length is fixed at 70 cm and microphones are placed at corners of room, according to the modal approach. In this way, receiving room modes are suppressed and source room transmitted modes are entirely evaluated with no modal match.

Result of modal sound insulation for the 248 Hz resonant frequency (the first axial mode related to  $L_x=70$  cm dimension) is 34.8 dB, a value very similar to that found in previous measurements: 35.6 dB for source room  $L_x=70$  cm and receiving room  $L_x=90$  cm, and 36.5 dB for source room  $L_x=70$  cm and receiving room  $L_x=50$  cm. This first comparison confirms that results without receiving room and without modal match are consistent each other and a weighting procedure is possible in order to assess the real modal sound insulation.

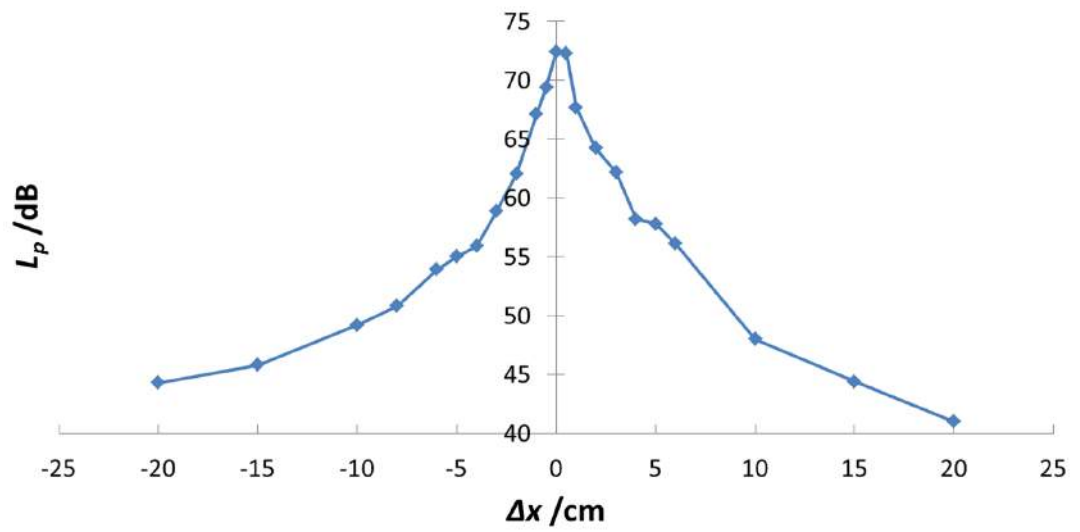


Figure 6.12: Modal sound pressure level as function of  $L_x$  length difference between source and receiving rooms.

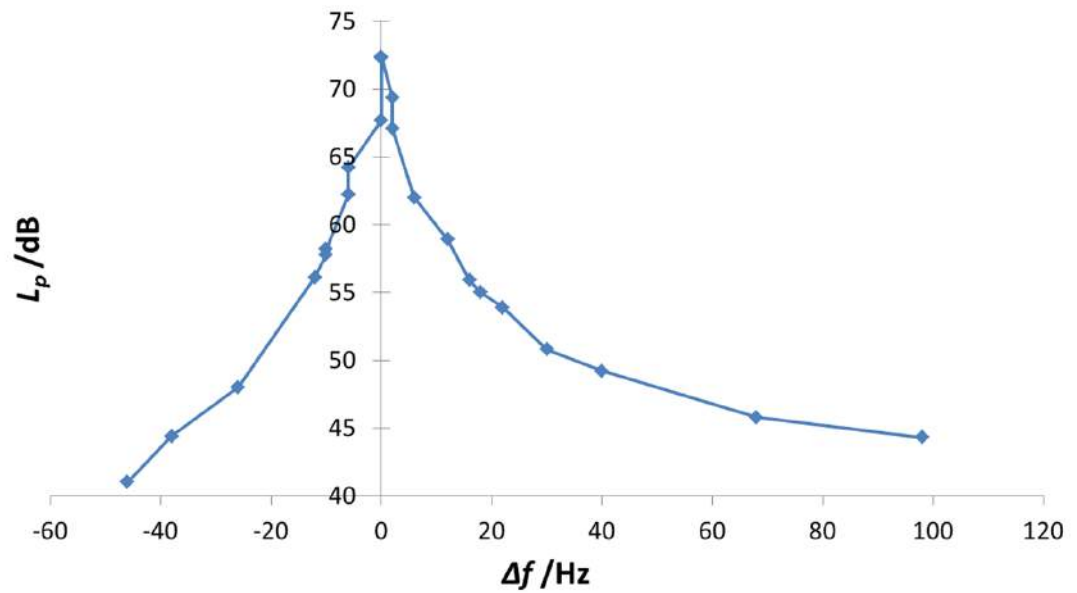


Figure 6.13: Modal sound pressure level as function of modal overlap degree in frequency.

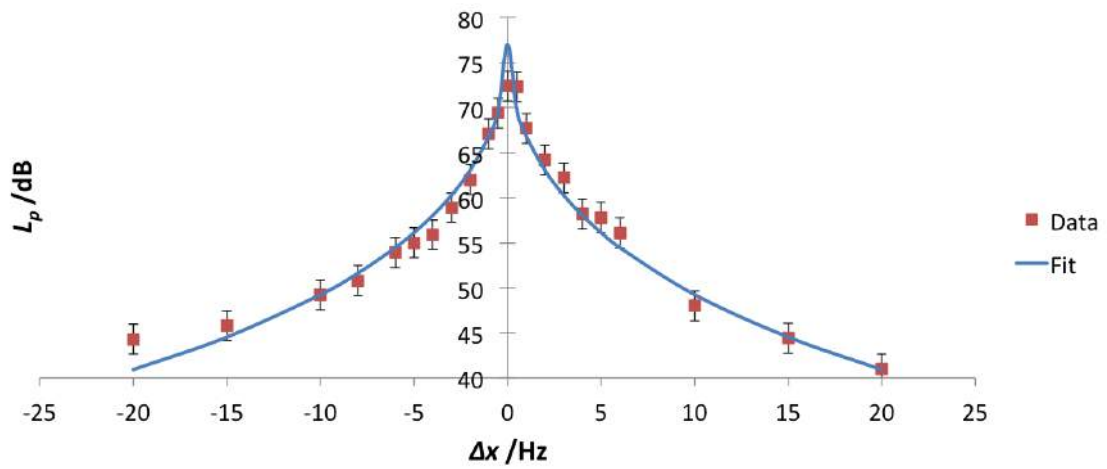


Figure 6.14: Modal sound pressure level as function of  $L_x$  length difference between source and receiving rooms and fit with a Kohlrausch-Williams-Watts function. Error bars correspond to the average of modal sound pressure level expanded uncertainties in Table 5.4.



Figure 6.15: Modal sound insulation measurement performed with the scale model in the anechoic chamber. Receiving space microphones are placed randomly at 1 cm from the partition.

## 6.4 Validation of the extension to the whole low frequency range

The discrete nature of modal sound insulation requires an extension to the whole low frequency range and a description in one-third octave bands, in this way, is possible. In order to do this, in Chapter 4.3 it is supposed that in different laboratories with different dimensions, modes move along the envelope of source and receiving room modal spectra. An experimental validation of such assumption with the use of scale model is provided in this Section. Source room  $L_x$  length is varied from 40 cm to 90 cm, with steps of 10 cm, and receiving room one is fixed at 55 cm. Spectra obtained for each size combination are depicted in Fig. 6.16.

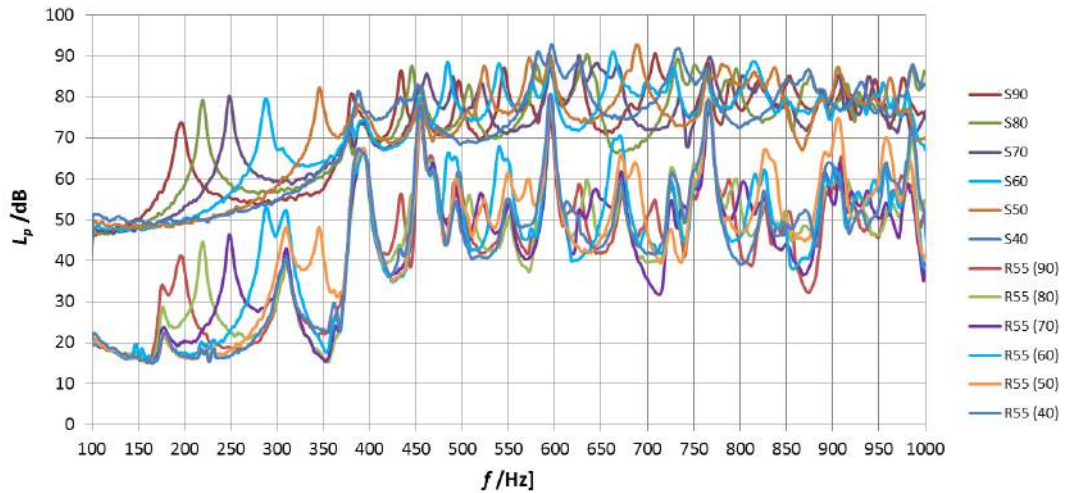


Figure 6.16: Modal spectra of source (S) and receiving (R) room with different source room volumes.

Source room modes move in frequency, as well as the transmitted ones in the receiving room. On the basis of this, envelope of source and receiving room modes is constructed (Fig. 6.17) and the main matching modes are removed on the basis of previous results. For each room combination (source room  $L_x$  fixed at 55 cm and receiving room  $L_x$  changed from 40 cm to 90 cm, and receiving room  $L_x$  fixed at 55 cm and source room  $L_x$  changed from 40 cm to 90 cm, in total 12 modal sound insulation measurements with different room combinations) modal sound insulations in one-third octave bands are determined, according to procedure explained in Chapter 4.3, in order to compare such results with the one achieved by envelope method. As depicted in Fig 6.18, modal sound insulation evaluated through spectra envelope is consistent with results from other room combinations. Such comparison provides also a first evaluation of reproducibility of modal sound insulation (12 room combinations), which is examined in depth in the following

Section.

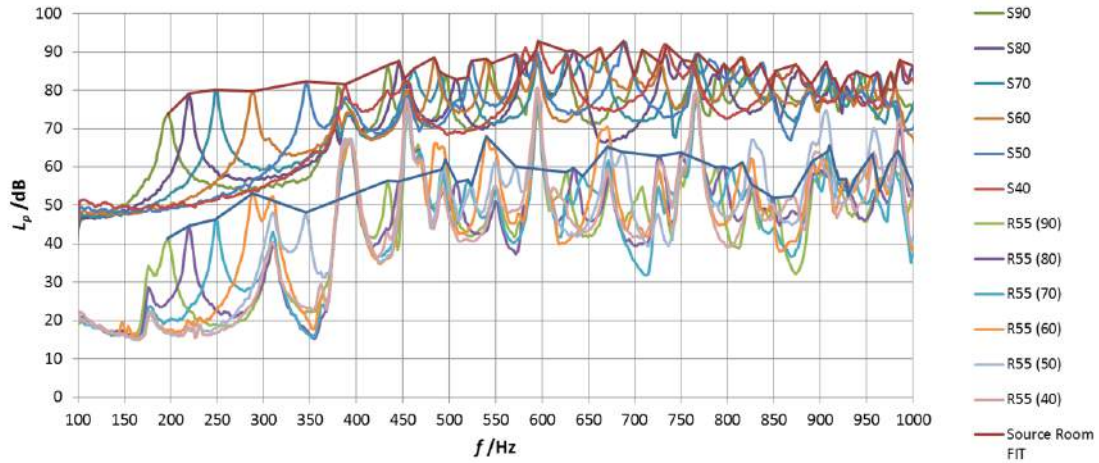


Figure 6.17: Envelope of source and receiving room modal spectra with the exclusion of matching modes.

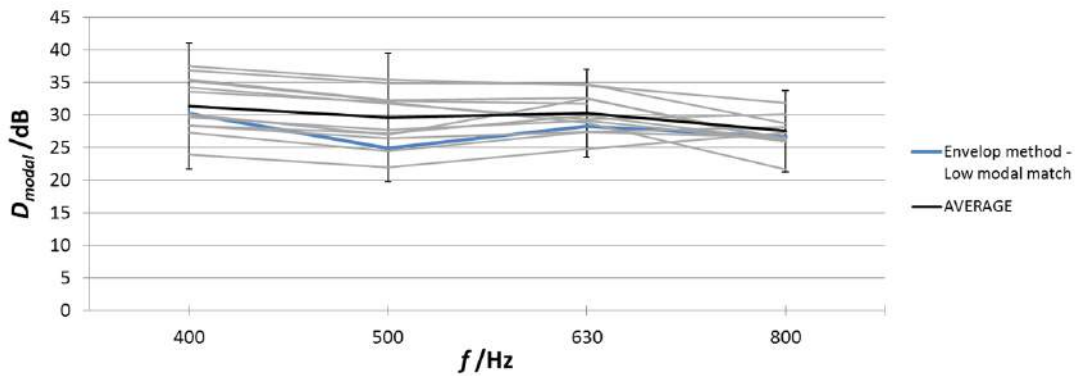


Figure 6.18: Modal sound insulation obtained with spectra envelope (blue curve) compared to average of modal sound insulation (black curve) evaluated with different room combinations (grey curves). Error bars correspond to reproducibility expanded uncertainty for the 95% confidence level.

## 6.5 Reproducibility of different methods

In this part, a first comparison of reproducibility measurements of sound insulation according to modal and standard approaches is carried out. Measurements of sound insulation  $D$ , according to ISO 10140-2:2010, with different room combinations (12, explained above) are performed in the scale model. Besides, modal

sound insulation  $D_{modal}$  values are also obtained with the same room combinations with and without the exclusion of main matching modes, as attempted in the previous Section. Comparisons are depicted in Fig. 6.19 and 6.20. Modal sound insulation with the exclusion of matching modes provides higher values, since the influence of receiving room modes, which entail an underestimation of insulation, is not taken into account. Modal sound insulation and standard sound insulation values are consistent. This is a confirmation of the validity of the extension to the whole low frequency range: both methods with such boundary conditions (source and receiving room  $L_y$  and  $L_z$  are the same) provide similar sound insulation values, although different procedures. Energetic average of sound pressure levels in one-third octave bands in the inner part of scale model rooms, following standard procedure, provides similar values obtained with maximum modal sound pressure levels measured at corner positions as required by the modal approach. Both measurement methods are mostly influenced by the highest modal sound pressure levels due to modal match of some source and receiving room modes, as outlined in Fig. 6.4 for 394 Hz, 456 Hz, 596 Hz, 766 Hz resonant frequencies. The strong and stable presence of matching modes decreases standard deviation of sound insulation  $D$  and the lowest values are achieved: since matching modes are very stable in time, standard measurement of sound insulation is less affected by uncertainties. This makes standard measurement more precise than modal sound insulation but a question about their accuracy arises since modal sound insulation is strictly connected with the real perceived sound field and the transmission of modes in small rooms. The impossibility to change  $L_y$  and  $L_z$  dimensions of scale model restricts the comparison of reproducibility standard deviations due to the constant presence of matching modes. It is probable that, in a scale model with more mobile walls in order to reproduce source and receiving rooms with different dimensions, as real laboratories are (see Chapter 3.3), standard deviation of sound insulation  $D$  increases, whereas modal sound insulation uncertainty decreases due to a smaller influence of modal match. In the future, further measurements on a different scale model with the possibility to change all dimensions will be more useful for such evaluation. Furthermore, selection of matching modes to be excluded is quite rough: a wider measurement campaign focused on the transmission of each mode and its interaction with receiving room modes is required in order to realize a weighted procedure, as mentioned in Section 6.3, which could remove the influence of modal match in the receiving room.

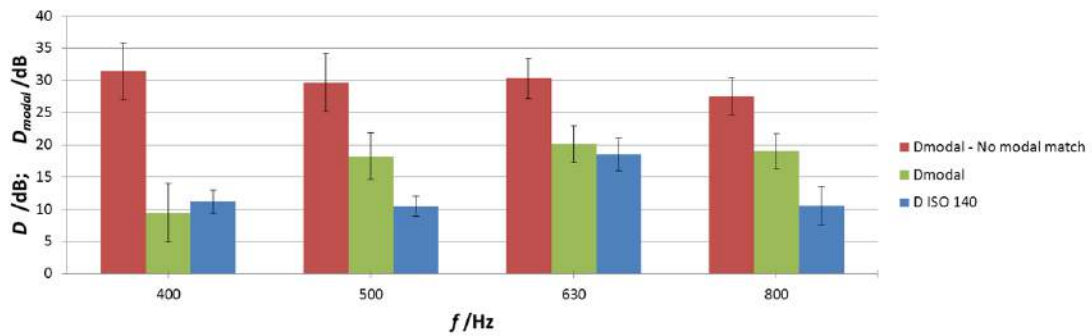


Figure 6.19: Comparison of sound insulation with the 3 methods. Error bars correspond to reproducibility standard deviations.

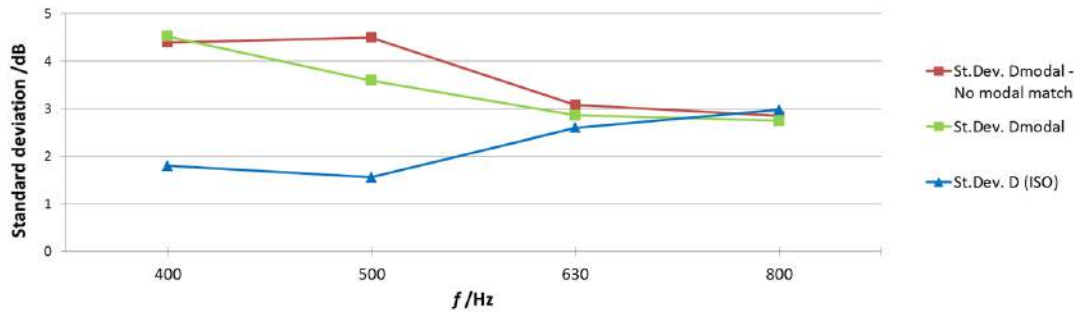


Figure 6.20: Comparison of reproducibility standard deviations for the 3 methods.



# Chapter 7

## The modal approach for reverberation time measurement

The growing interest of the international scientific community to extend the conventional building and architectural acoustics measurements to frequencies below 100 Hz requires a detailed study also on the decay of the sound pressure and the related reverberation time in small rooms (30-200 m<sup>3</sup>). In such conditions, the Standard measurement of reverberation times (see Section 2.3), related to diffuse acoustic field, involves high measurement uncertainties caused by the presence of the acoustic modes of the room, responsible for the annoyance as concerns the quality of listening (rumble effect) or noise from other rooms.

Reference Standard for the measurement of reverberation time is the ISO 3382-2:2008, from 100 Hz to 5000 Hz. Such Standard reports the procedure for the interrupted noise method (method to obtain the decay curves directly from the evaluation of the sound pressure level decay after the interruption of the broadband noise signal) and the integrated impulse response method (method to obtain the decay curves by the backward integration of the squared impulse responses). It is important to underline that these measurement methods evaluate the acoustic response of the room to an interrupted force. For what concerns the interrupted noise method, the Standard states that the signal provided to the loudspeaker shall be derived from broadband random electrical noise, the source shall be able to produce a sound level sufficient to ensure a decay curve starting at least 35 dB above the background noise in the corresponding frequency band and microphone positions should cover a portion of space sufficient to determine average behaviour of the acoustic diffuse field. No mention to frequencies below 100 Hz is reported, where the diffuse field approach, considered in the Standard, is not suitable. In general, there is no frequency distinction and the considered ones are calculated by the simple average of decays within a certain bandwidth. The aim of this part is to determine a new and more suitable measurement method to describe the reverberation time at low frequencies.

The new measurement approach is based on the resonance frequencies of the rectangular room (in contrast with it is stated in ISO 3382, which requires one-third octave band measurements). The different approach compared to ISO 3382 Standard is based on the decay of individual resonance frequencies of the rectangular room (*modal reverberation times*), instead of one-third octave band analysis. The Standard method applied to low frequency in small rooms in one-third octave bands creates problems in the evaluation of decay curves: as a matter of fact, within a third octave band more resonant frequencies are present, each with its own decay. This entails non-linear decay curves due to the individual contributions of each resonance frequency (Fig. 7.1). For this reason, it is chosen to focus the analysis on those frequencies, which are the most influential on the acoustic field.

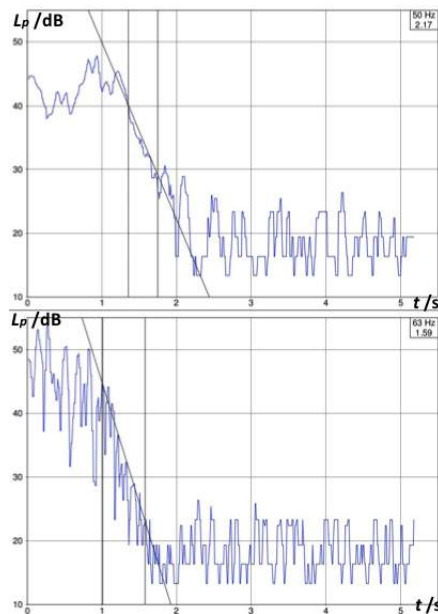


Figure 7.1: Example of decay curves in one-third octave bands at low frequencies. Interferences in the decay curves are due to the interaction of different modes.

Measurements shown below are performed in the receiving room of the impact sound insulation laboratory ( $L_x = 4.02$  m,  $L_y = 3.64$  m,  $L_z = 3.45$  m). As seen previously, under non diffuse field conditions a modal approach is preferable, rather than statistical, due to the non-homogeneity of the acoustic field in frequency. For the same reason, the guidelines for spatial averages and measurement points are not applicable in this case. Two methods are presented. The first is the *direct* measurement method of the modal reverberation time, based on the guidelines of ISO 3382, but using different guidelines for what concerns the measurement points and the acoustic force (statistical or sinusoidal). The interrupted noise method, which is often used for building acoustics measurements in laboratory, is considered

as the reference one. The integrated impulse response method, instead, is normally used in architectural acoustics to study the response of large rooms such as theatres and concert halls. The second is an *indirect* measurement of reverberation time based on Eq. 2.72 and evaluates the half bandwidth of resonance frequencies of the spectrum [43]. This is the first experimental verification of modal reverberation time expressed in Eq. 2.72. Different source signals are also evaluated.

## 7.1 Preliminary measurements

Preliminary measurements are necessary in order to evaluate resonant frequencies of the room. Measurement devices and analysis are described in Chapter 3. Considering the studies described in the previous Chapters about the modal spatial distribution, measuring points (microphone) are localized at the corners of the room (Fig. 7.2).

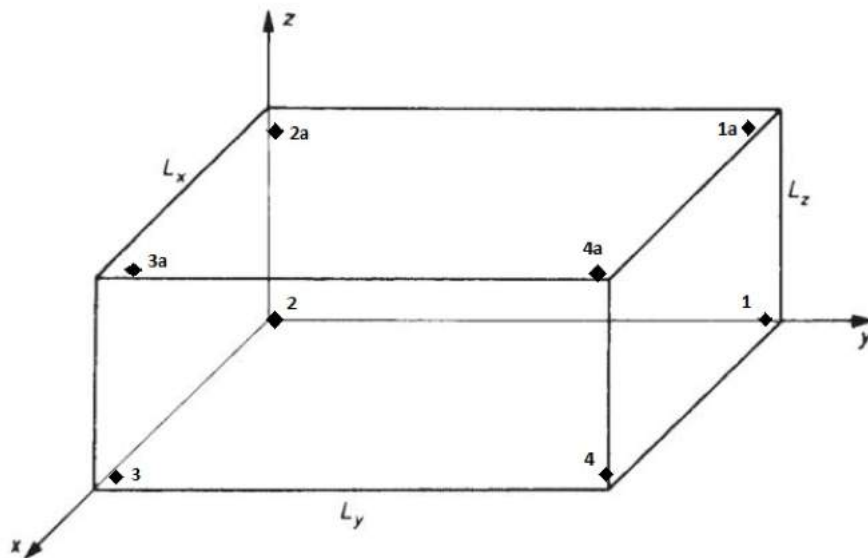


Figure 7.2: Measurement points at corners of room.

Different types of source signals to excite the acoustic field of the room are used: pink noise, sine wave and sweep signal. The first test is made using a pink noise, which is the most used for sound insulation and reverberation time measurements. Below, an example of the spectrum (resolution of 0.1 Hz), obtained by placing the microphone at one corner of the room, is shown in Fig. 7.3. Measurements at different corner positions are consistent.

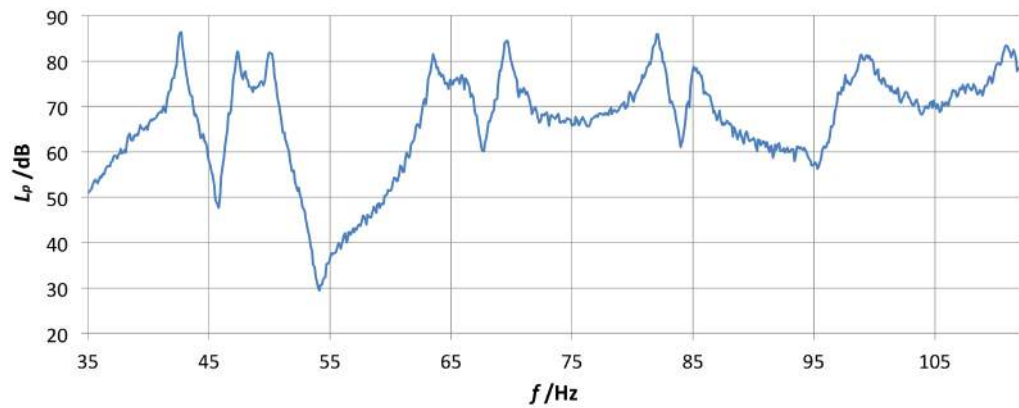


Figure 7.3: Frequency spectrum obtained with pink noise at corner 1.

The spectrum is quite disturbed and the peaks are not always easily identifiable; despite that, an assessment of modes is possible:

$f_n$ /Hz
42.7
47.4
50.1
63.6
66.1
69.6
81.2
85.2
99.3

Table 7.1: Measured modes with pink noise.

Other spectra are evaluated with different signals. Initially, a sinusoidal signal at a resonant frequency is used. The spectrum is evaluated through a temporal average long enough to obtain a stable spectrum. An example with the 42.6 Hz resonant frequency is shown in Fig. 7.4.

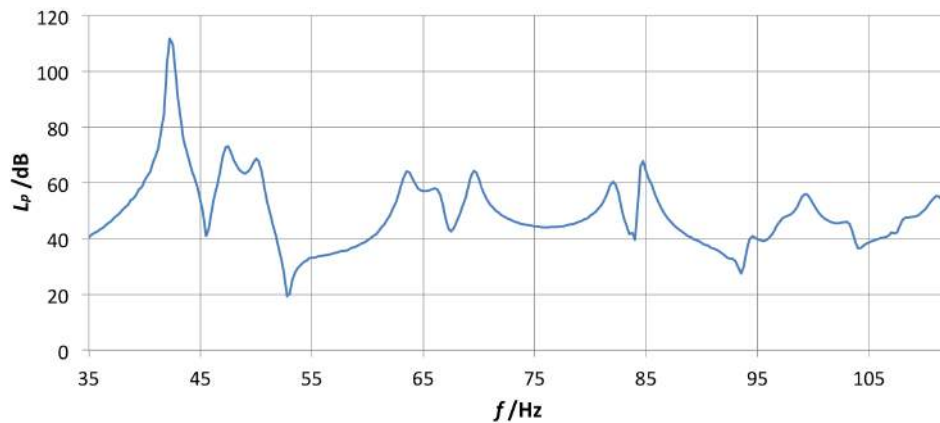


Figure 7.4: Frequency spectrum obtained with the 42.6 Hz sine wave at corner 1.

The spectrum is much more defined and smoother than the one obtained with the pink noise. Nevertheless, the problem is that the resonance peak corresponding to the frequency used as source signal is much higher than the others, and this creates possible discrepancies, since the acoustic field is not excited over all low frequency range. Furthermore, it is interesting to underline that using a sine wave, enough energy is provided to the system (room) in order to excite all the modes.

In order to excite all resonant frequencies and also to have a smoother and clearer spectrum compared to the one obtained with pink noise, a sweep signal (frequency range of 30-200 Hz and linear increase in 10 s) for the whole considered frequency range (35-112 Hz) is generated. As shown in Fig. 7.5, resonance peaks are well defined and the whole spectrum is smooth and clear.

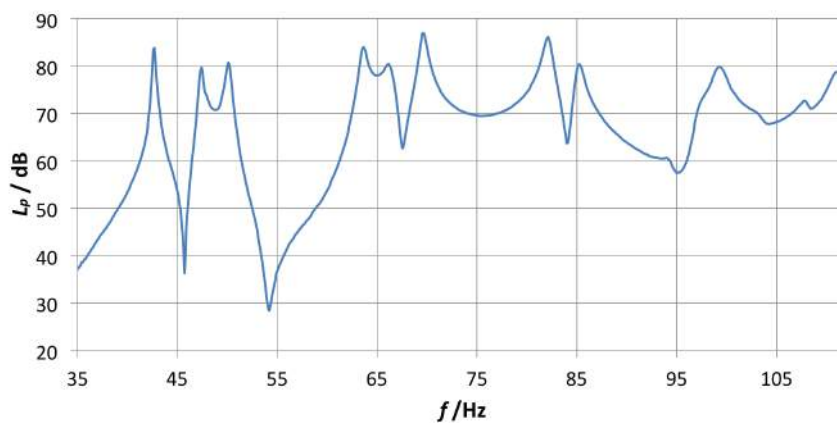


Figure 7.5: Frequency spectrum obtained with a sweep signal at corner 1.

Values are reported in Table 7.2.

These results are useful for the following measurements, as it allows to get a starting point to determine the reverberation time at low frequencies.

$f_n$ /Hz
42.6
47.4
50.1
63.7
66.2
69.6
82
85.4
99.2

Table 7.2: Measured modes with sweep signal.

## 7.2 Direct method

In the introduction of this Chapter two different measurement methods for reverberation time in non-diffuse field condition are mentioned. This Section refers to the first method, the so-called *direct method*. This first estimate of modal reverberation times is based on the interrupted noise method, indicated by the ISO 3382. Direct measurement of the modal decays entails waterfall measurements with source and microphone placed at corners of room (respectively in corners 1 and 3). In this first step, spatial measurements are neglected (see Section 7.5) as it is focused just on the determination of the most suitable signal source for decay measurements. Different tests are made, using basically two types of source signals: a random noise (pink noise) and a sinusoidal signal. For sinusoidal signals, more frequencies are tested on the basis of the spectrum obtained in preliminary measurements: two resonant frequencies (47.5 Hz and 63.5 Hz) and two nonresonances (56 Hz and 75 Hz). The source signals are listed below:

- Pink noise
- 47.5 Hz sine wave (resonance frequency)
- 56 Hz sine wave (nonresonance frequency)
- 63.5 Hz sine wave (resonance frequency)
- 75 Hz sine wave (nonresonance frequency)

In the following pages, decays are analysed and compared to determine the most suitable one.

From waterfall data, referred to the whole temporal evolution of the spectrum (resolution of 0.25 Hz), only modal sound pressure level decays are considered. For each one, a linear interpolation on the decay curve, considering the starting

point at -5 dB from the peak until at least 5 dB above the level of background noise, is performed. The interpolation returns the equation of a straight line  $y = -ax + b$  and a confident parameter, the correlation coefficient  $0 < r^2 < 1$ . The reverberation time is computed as

$$T_x = \frac{60}{a} \cdot 0.1 \quad (7.1)$$

where  $x$  indicates the range of sound pressure level  $\Delta L_p$  considered for the linear interpolation, and the factor 0.1 is due to a time resolution of 0.1 seconds. It is not possible to determine directly the  $T_{60}$  (decay of 60 dB), due to the impossibility to have a sufficient signal-to-noise ratio. In most of cases,  $T_{30}$  and, in few cases,  $T_{20}$  are calculated. The attention is focused on a range from 35 Hz to 112 Hz, which are the bounds of the low frequency interval.

### 7.2.1 Pink noise

First test is performed with pink noise. The spectrum decay is shown in Fig. 7.8. It is evident the presence of prevalent peaks in the spectrum corresponding to resonance frequencies. This confirms the validity of the approach used, as these frequencies have different decays and heavily affect the reverberation time of the room. Due to the statistical nature of the source signal, the spectrum is quite disturbed. It is clearer in single decay curves of some resonance frequencies (see an example in Fig. 7.6 and 7.7): correlation coefficient is not very high and decay curve is not perfectly straight. In Table 7.3, reverberation times of modes are reported.

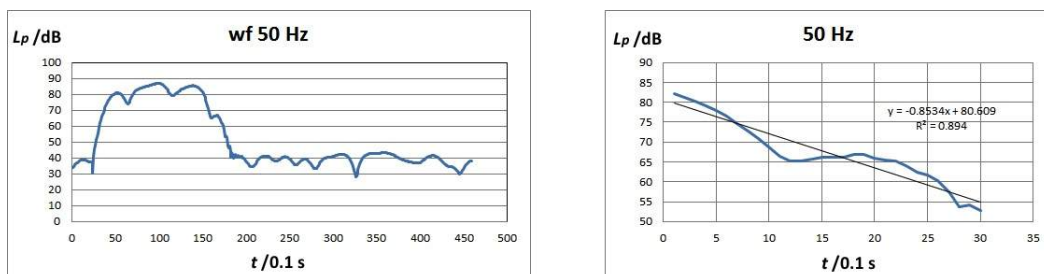


Figure 7.6: Decay curve of 50 Hz resonance frequency.

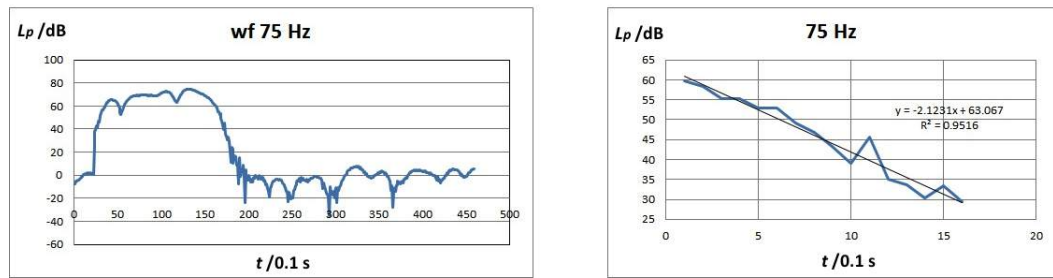


Figure 7.7: Decay curve of 75 Hz resonance frequency.

$f_n$ /Hz	$T_n$ /s
42.5	6.43
47.5	4.19
50	7.03
63.5	3.49
66	1.89
69.5	3.53
82	3.33
85.5	2.53
99.25	2.81

Table 7.3: Modal reverberation times with pink noise.

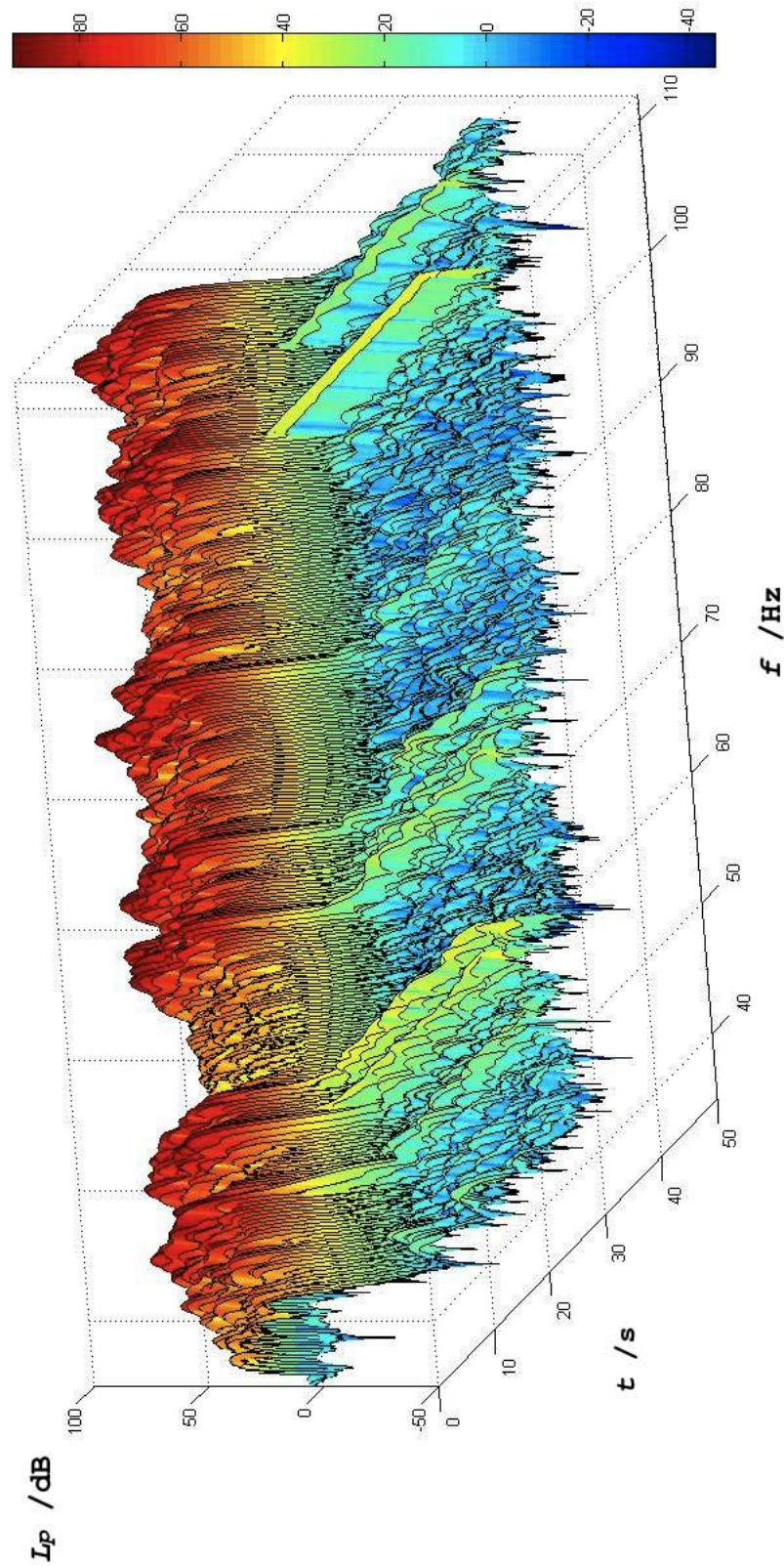


Figure 7.8: Waterfall with pink noise source signal.

### 7.2.2 Sine waves

Given the results obtained in preliminary measurements outlined in Section 7.1, sine waves corresponding to resonance frequencies are used as source signal (47.5 Hz and 63.5 Hz). The methodology is the same used for the pink noise: a signal is sent to the sound source in the room and the decay of the frequency spectrum is recorded. In Fig. 7.9 and 7.10 the waterfall spectra, obtained with 47.5 Hz and 63.5 Hz forcing sine waves respectively, are shown.

The graphs are less disturbed and the peaks referred to the modal frequencies are clearer than those obtained with pink noise. In addition, a different behaviour is visible: this kind of measure requires to feed power into the system (through the acoustic source) up to a stable situation and, later, to interrupt such energy supply to study how energy decays. With pink noise, also the part of waterfall which should be stable is very fluctuating due to the statistical nature of pink noise. In this case the achievement of a stable situation is evident: a constant plateau is visible in correspondence of the driving resonance frequencies. It is also visible the presence of two transients with respect to previous measurements: the sound pressure level of modes reaches a maximum, decreases to a certain value and then increases again when the source signal is interrupted (up to the maximum reached before). This phenomenon allows to get cleaner and clearer modal decays (Fig. 7.11 and 7.12, Table 7.4).

	56 Hz driving frequency	75 Hz driving frequency
$f_n$ /Hz	$T_n$ /s	$T_n$ /s
42.5	7.75	8.12
47.5	4.36	4.25
50	3.94	3.72
63.5	3.53	3.02
66	3.76	2.99
69.5	3.61	3.34
82	3.43	3.26
85.5	3.31	3.26
99.25	3.41	2.58

Table 7.4: Modal reverberation times with 47.5 Hz and 63.5 Hz resonance driving frequencies.

Analysing the individual decays, the transient is less pronounced than the one corresponding to the resonant frequency used as source signal, in which the transient reaches higher values of sound pressure level. For modes corresponding to the driving frequency, an interference between the modal field of the room and the direct wave produced by the source entails also a shift of maximum sound pressure level to adjacent frequencies: the membrane of the loudspeaker is obstructed by

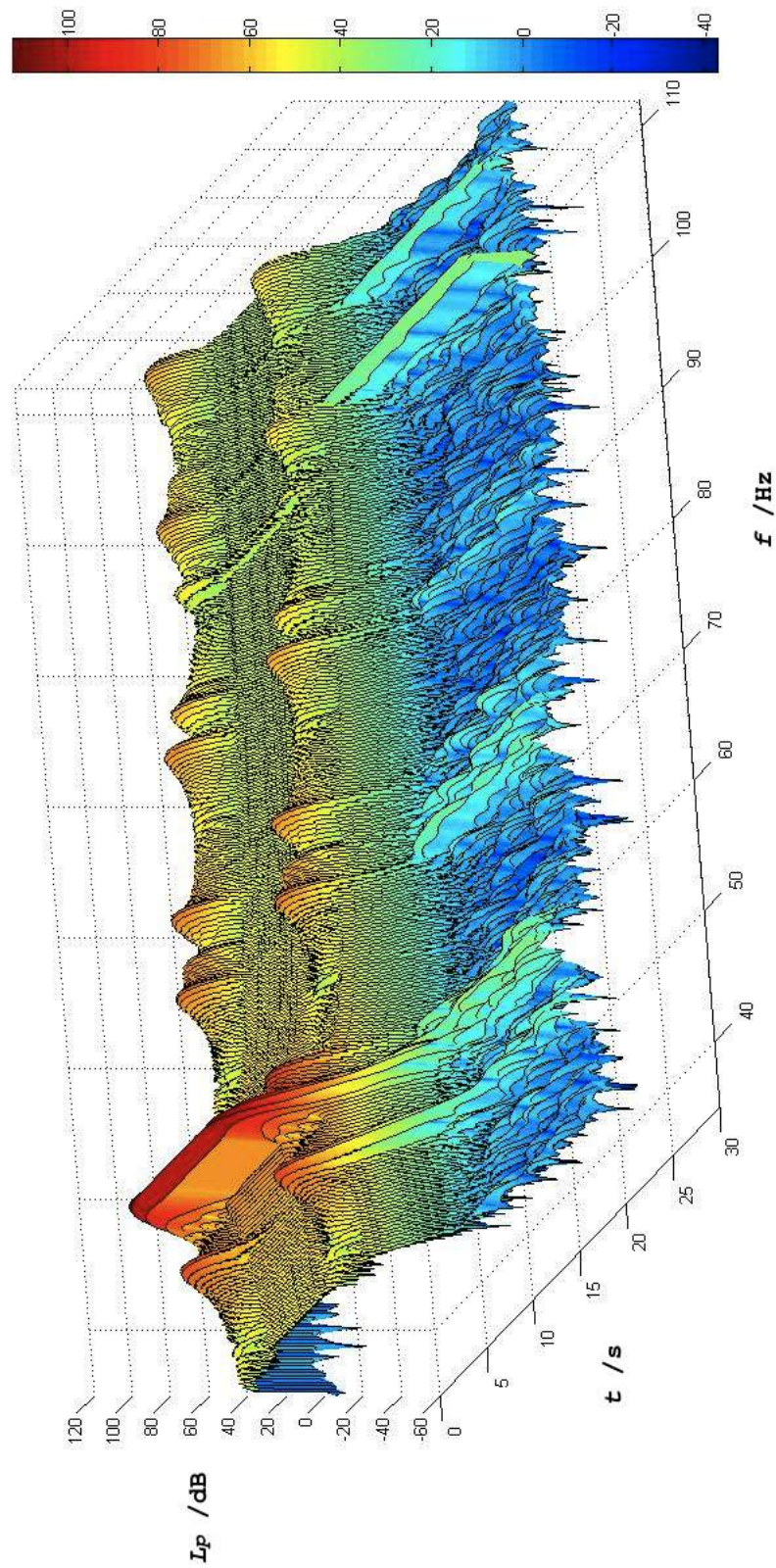


Figure 7.9: Waterfall with the 47.5 Hz resonance sine wave as source signal.

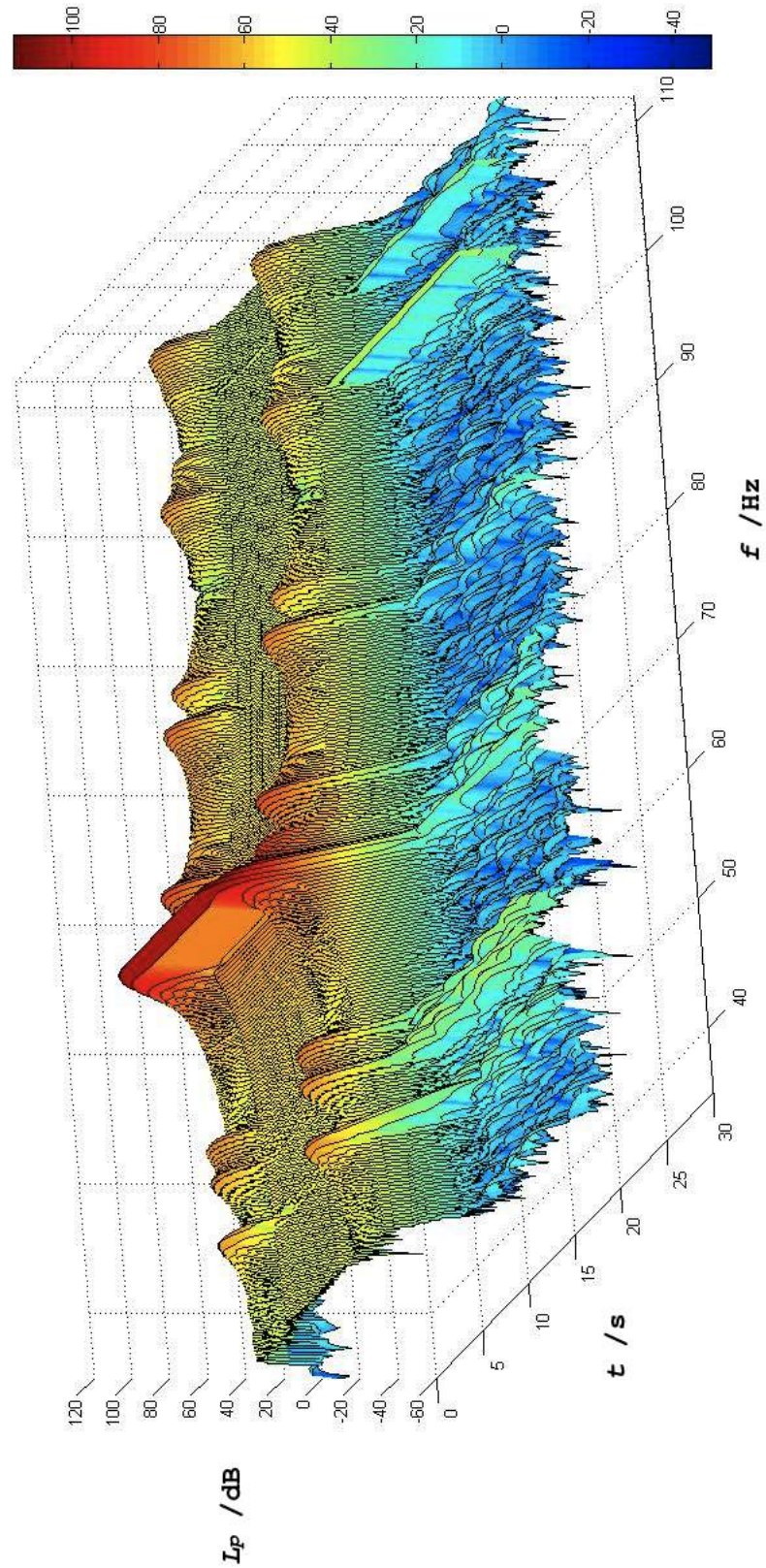


Figure 7.10: Waterfall with the 63.5 Hz resonance sine wave as source signal.

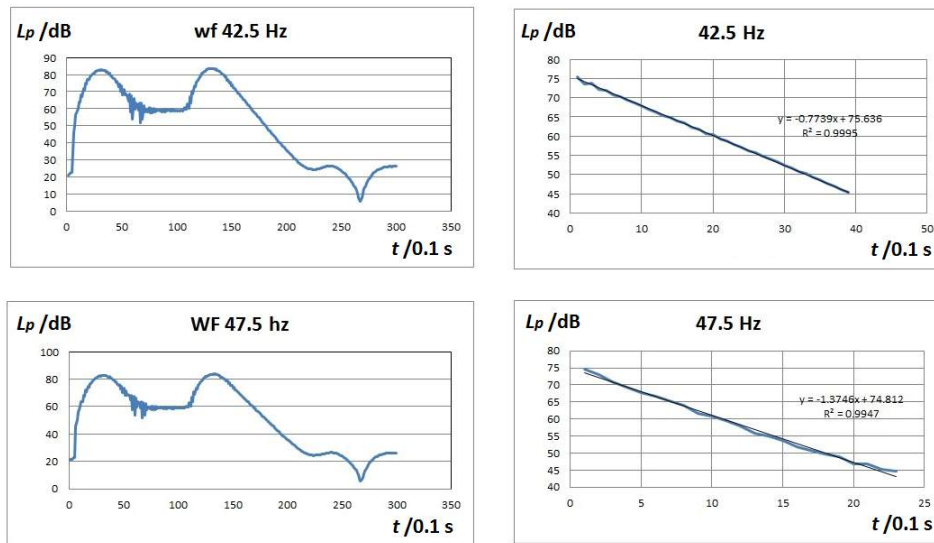


Figure 7.11: Examples of 42.5 Hz and 47.5 Hz modal decay curves measured with the 47.5 Hz resonance sine wave as source signal.

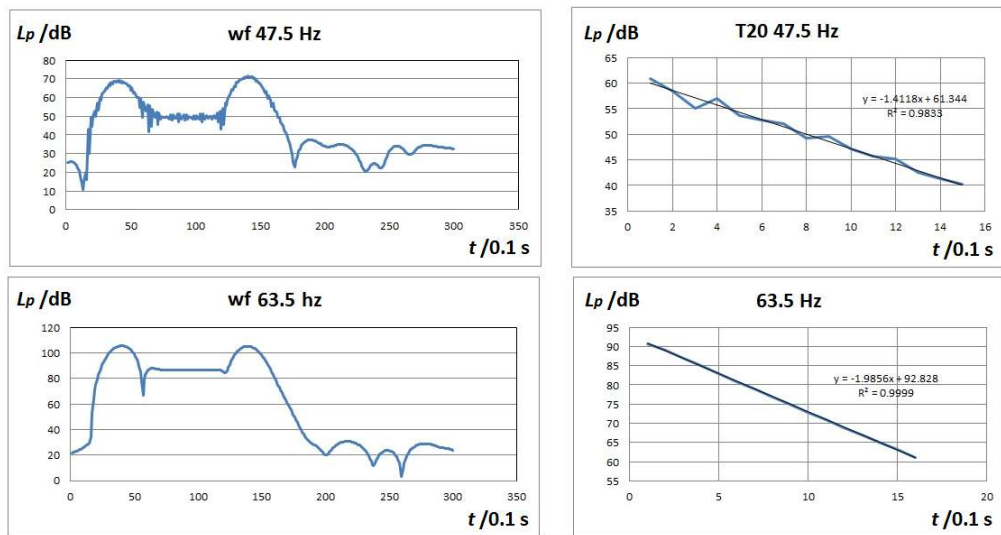


Figure 7.12: Examples of 47.5 Hz and 63.5 Hz modal decay curves measured with the 63.5 Hz resonance sine wave as source signal.

the generated modal field that vibrates at that frequency. This can induce to a distortion of the modal behaviour of the room.

To overcome this problem, another measurement is attempted using, as source signals, *nonresonance* sine waves. The idea, given the previous measures, is to feed power into the vibrating system without the introduction of a random signal as pink noise. By the waterfall obtained with these sine waves (56 Hz and 75 Hz) a slightly different behaviour compared to previous measurement emerges: it is evident the presence of room modes and the two transients with plateau (Fig. 7.14 and 7.15). Compared to the previous case, the difference between the sound pressure level of the plateau and the maximum level reached by the transients is decreased and higher signal-to-noise ratios are reached (Fig. 7.13).

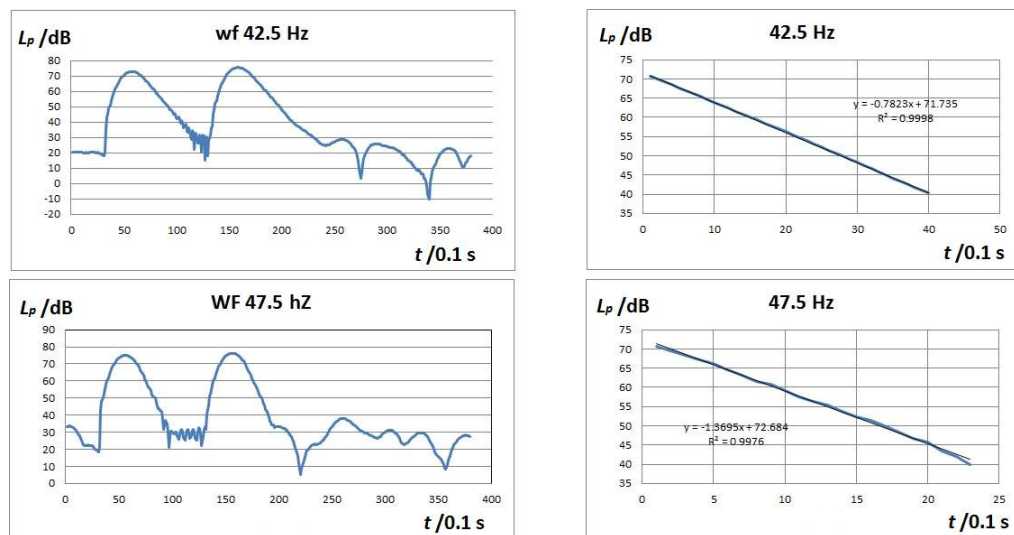


Figure 7.13: Decay curves of 42.5 Hz and 47.5 Hz resonance frequencies with nonresonance sine wave at 56 Hz as source signal.

Curves are less disturbed and the typical decays of modal frequencies are more evident. This is due to the fact that, using a nonresonance as source signal, the system is forced to resonate at a different frequency: at the beginning, when this energy is still low, the system vibrates according to its resonance frequencies, but the more the energy input increases, the more the system is unable to resonate according to its modes but is forced to resonate at the driving frequency. When the energy supply is interrupted, the system stops resonating at the driving frequency and dissipates energy vibrating again according to its modes, until the energy is not completely dissipated. When the energy input is high enough, the system is unable to distribute energy throughout the whole spectrum (as seen in the two previous cases), but it is focused entirely on the driving frequency. Since modal decays are very clean and clear, this source signal (nonresonance) results to be the most appropriate one to study modal decays in the room, without the interference,

seen previously, due to the use of a resonance sine wave as source signal. The values obtained with the two nonresonance sine waves are reported in Table 7.5. Modal reverberation times obtained are similar and this confirms the relevance of such direct method.

	56 Hz driving frequency	75 Hz driving frequency
$f_n$ /Hz	$T_n$ /s	$T_n$ /s
42.5	7.67	7.51
47.5	4.38	4.27
50	3.66	4.08
63.5	3.17	2.89
66	2.25	2.46
69.5	3.58	3.39
82	3.24	3.21
85.5	2.91	2.74
99.25	2.73	2.03

Table 7.5: Modal reverberation times with 56 Hz and 75 Hz nonresonance driving frequencies.

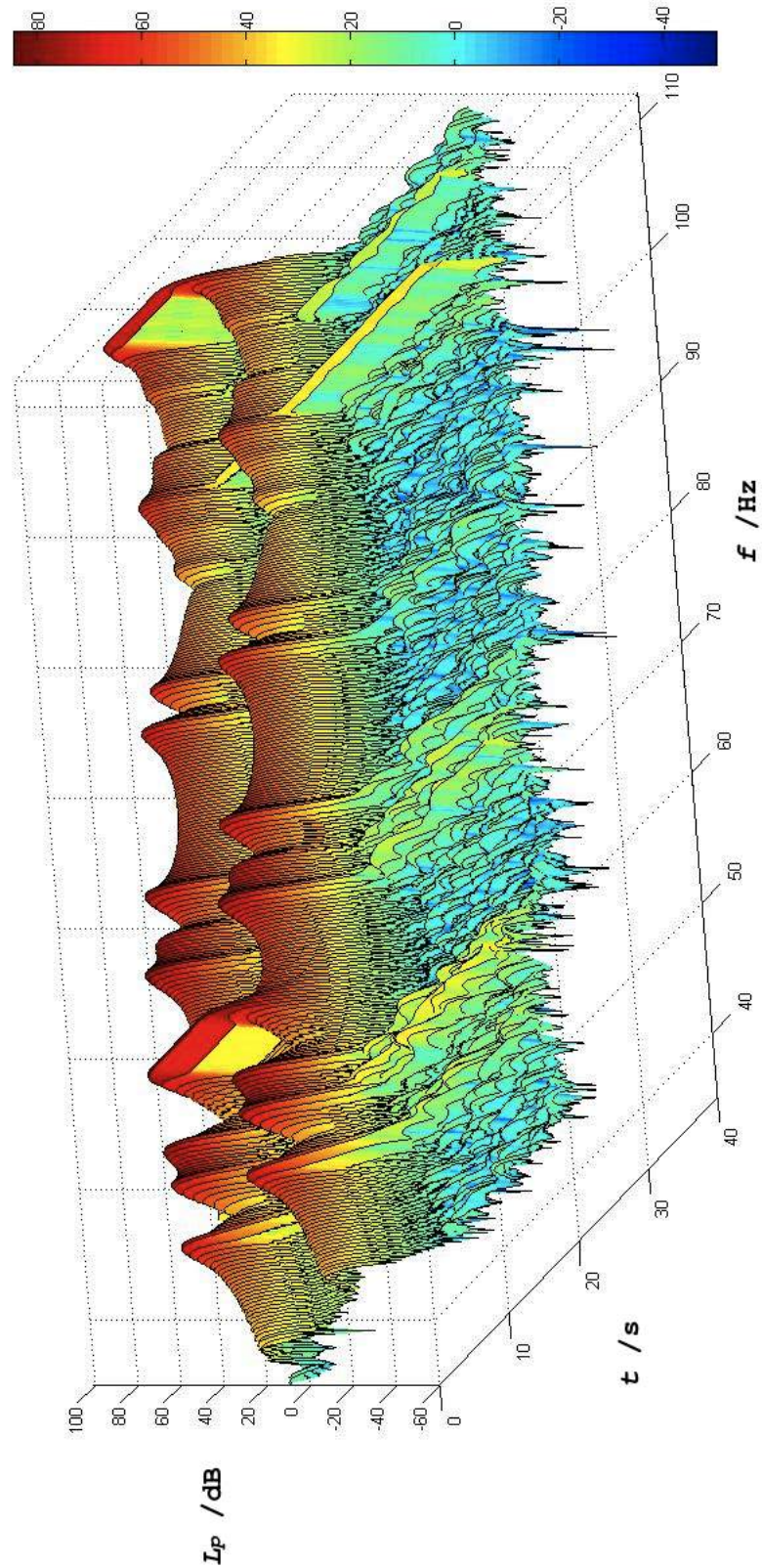


Figure 7.14: Waterfall with the 56 Hz nonresonance sine wave as source signal.

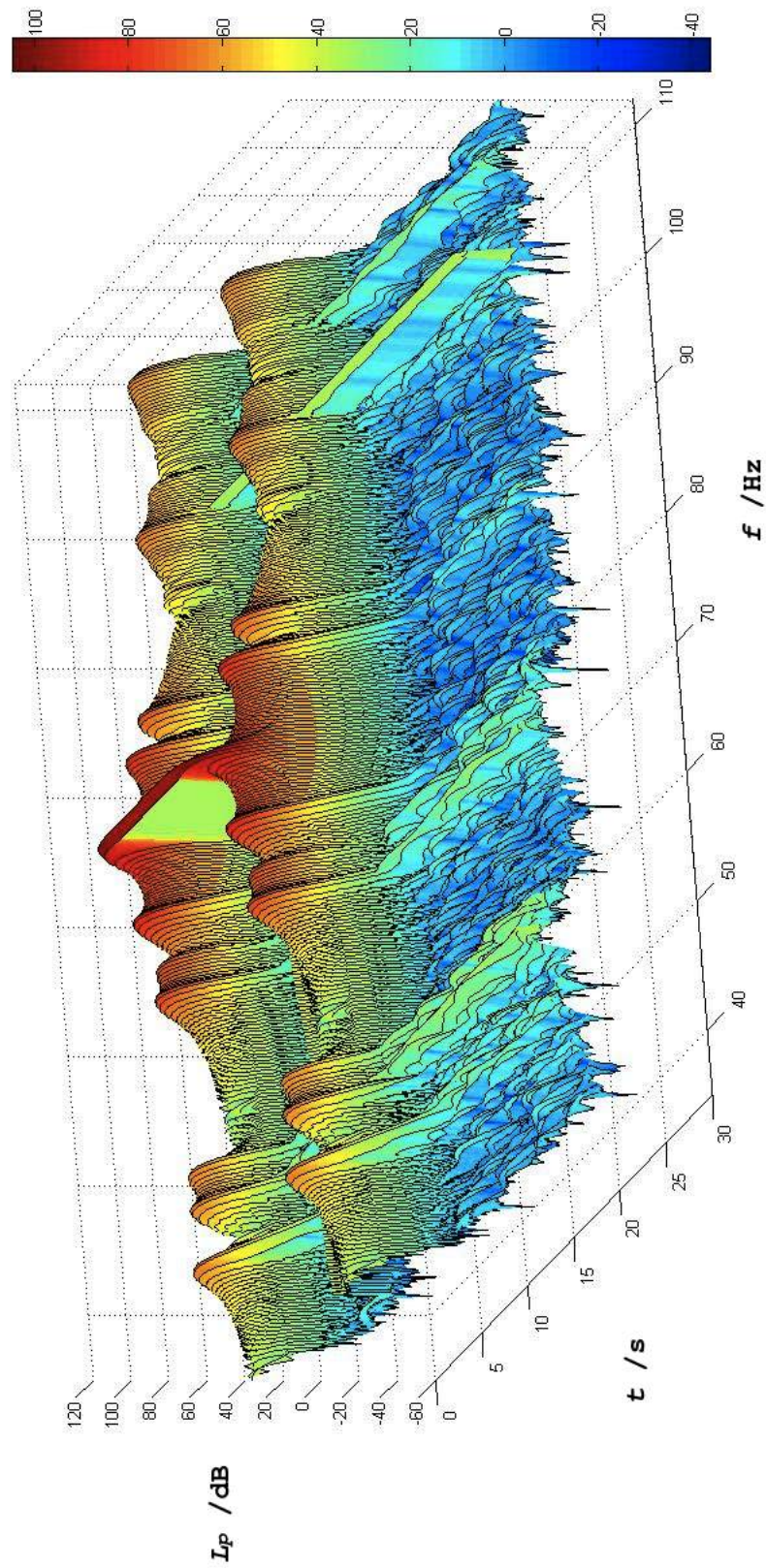


Figure 7.15: Waterfall with the 75 Hz nonresonance sine wave as source signal.

### 7.2.3 Comparison between different source signals

$f_n$ /Hz	source signal/Hz	$T_n$ /s	$f$ /Hz	source signal/Hz	$T_n$ /s	$f$ /Hz	source signal/Hz	$T_n$ /s
42.5	47.5	7.75	63.5	47.5	3.53	82	47.5	3.43
	56	7.67		56	3.17		56	3.24
	63.5	8.12		63.5	3.02		63.5	3.26
	75	7.51		75	2.89		75	3.21
	noise	6.43		noise	3.49		noise	3.33
47.5	47.5	4.36	66	47.5	3.76	85.5	47.5	3.31
	56	4.38		56	2.25		56	2.91
	63.5	4.25		63.5	2.99		63.5	3.26
	75	4.27		75	2.46		75	2.74
	noise	4.19		noise	1.89		noise	2.53
50	47.5	3.94	69.5	47.5	3.53	99.25	47.5	3.41
	56	3.66		56	3.17		56	2.73
	63.5	3.72		63.5	3.02		63.5	2.58
	75	4.08		75	2.89		75	2.03
	noise	7.03		noise	3.49		noise	2.81

Table 7.6: Comparison between modal reverberation times obtained with different source signals.

The best source signal to accomplish the study of modal reverberation time measurements with a direct method is the sine wave at a nonresonance frequency. In this way, modal sound pressure level decays are clearer because when the room is no longer forced to oscillate at a nonresonance frequency (interruption of the source signal), it starts to redistribute energy to its modes and their decays are clean and well detectable. A quantitative comparison of modal reverberation times obtained with different source signals (pink noise, resonance sine waves and nonresonance sine waves) are reported in Table 7.6.

Reverberation times obtained with sine waves are different from those achieved with pink noise. This is certainly due to the fact that the pink noise fails to adequately excite the acoustic field at low frequencies, as seen previously from the waterfall spectrum (Fig. 7.8). Given such considerations, the measurement obtained with the 75 Hz nonresonance sine wave is considered as the reference direct method for the following tests. This is precisely the best way to assess the modal decays of the room at low frequencies. Furthermore, for such laboratory room, 75 Hz sine wave is localized in a flat part of the spectrum and does not influence the closest modes.

## 7.3 Indirect method

In this Section the indirect method is discussed. Modal reverberation times are calculated by half bandwidth measurements of modes according to Eq. 2.72, reported as follows:

$$T_n = \frac{2.2}{\Delta f_{-3dB}} \quad (7.2)$$

Half bandwidths are obtained by spectrum measurements (0.1 Hz of resolution). The substantial difference from direct method is that no decay measurement is performed. Also in this case, the sound source and microphone are placed at the corners of the room to maximize the modal acoustic response and the signal-to-noise ratio. Two different source signals are tested to get the modal spectrum: a pink noise, used for building acoustic measurements, and a sweep signal, tested before in preliminary measurements (see (Fig. 7.16)).

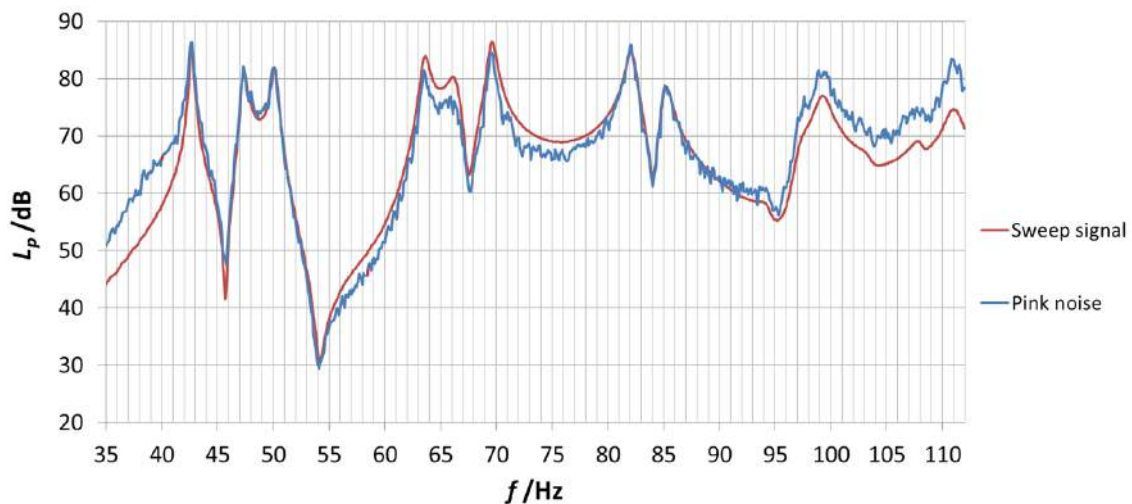


Figure 7.16: Modal spectra generated with a pink noise and a sweep signal.

Spectrum obtained with the sweep signal (30-200 Hz) is smoother and resonance peaks are well defined compared to the one achieved with pink noise. Half bandwidths of modes are then calculated through a Matlab script (see Appendix C) where the best fit, through the analysis of normalized residual sum of squares (RSS), with a Lorentzian function is implemented (Fig. 7.17 and 7.18 referred to sweep signal and pink noise respectively). In this case, resonance peaks measured with the sweep signal are well defined and the Lorentzian fit is more precise as residual analysis provides lower values. Then, through Eq. 2.72, modal reverberation times are assessed (see Table 7.7). In general, reverberation times decrease with frequency, as also confirmed by theory: first axial modes are more energetic and their decay time is longer.

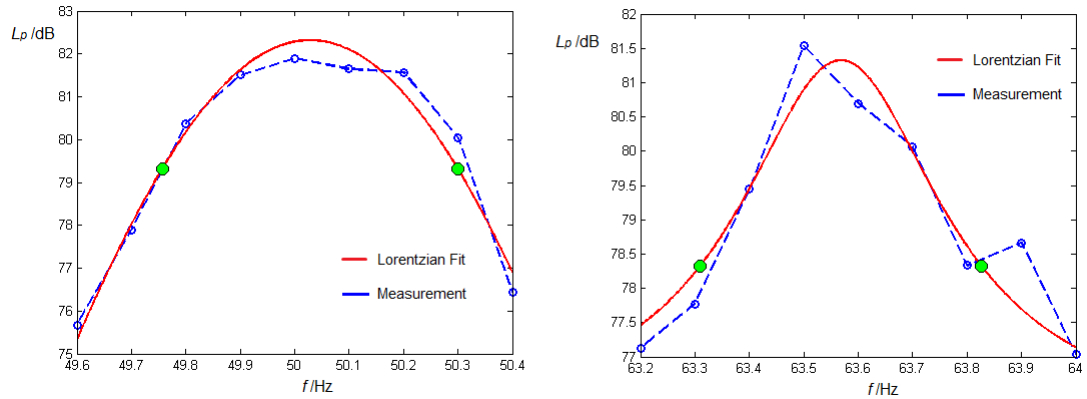


Figure 7.17: Examples of half bandwidth calculation for 50 Hz and 63.5 Hz modes using pink noise.

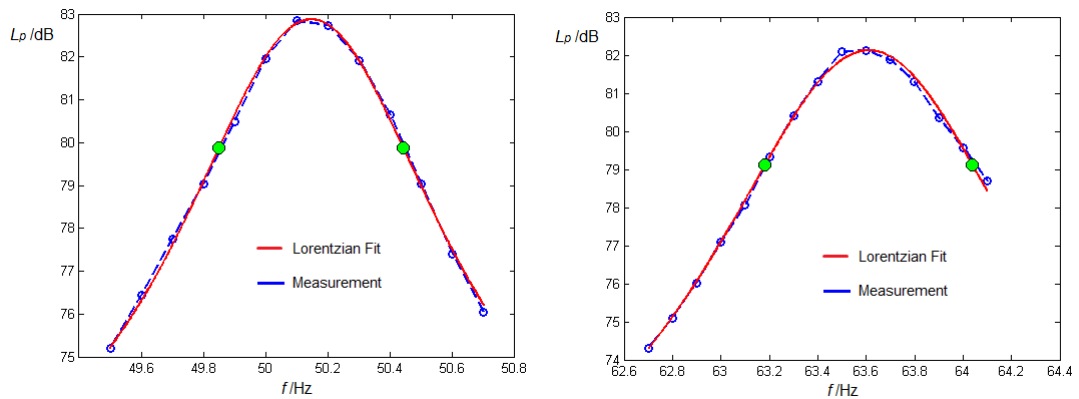


Figure 7.18: Examples of half bandwidth calculation for 50 Hz and 63.5 Hz modes using sweep signal.

Repeatability of modal reverberation times with indirect method (sweep signal) is evaluated. For this reason, 5 consecutive measurements of modal reverberation times in one corner of the room (corner 1) are performed. Results (averages and standard deviations) are reported in Table 7.8.

It is important to underline that such averages and standard deviations calculated do not want to be definitive, but are useful to give an idea of the dispersion of results. In Section 7.5, spatial measurements provide a more consistent indication of uncertainty.

$f$ /Hz	Pink noise		Sweep signal	
	$T_n$ /s	$RSS$	$T_n$ /s	$RSS$
42.5	5.83	0.20	7.46	0.19
47.5	6.34	0.17	4.38	0.18
50	4.06	0.41	3.96	0.15
63.5	4.26	0.48	2.50	0.15
66	1.49	0.80	2.19	0.11
69.5	4.12	0.34	2.99	0.05
82	4.71	0.32	2.42	0.16
85.5	2.26	0.59	2.29	0.11
99.25	1.61	0.62	1.31	0.05

Table 7.7: Summary of modal reverberation times evaluated with pink noise and sweep signal.

$f$ /Hz	56 Hz driving frequency	75 Hz driving frequency
	$\overline{T_n}$ /s	$s_{T_n}$ /s
42.5	6.43	0.81
47.5	4.21	0.32
50	3.89	0.29
63.5	2.75	0.26
66	2.98	0.46
69.5	2.89	0.28
82	2.41	0.16
85.5	2.49	0.40
99.25	1.33	0.10

Table 7.8: Repeatability of modal reverberation times with indirect method.

## 7.4 A first comparison between proposed methods

A first comparison between direct and indirect methods on the basis of previous measurements is reported as follows. In Fig. 7.19 and Table 7.9, results are depicted. Results of indirect measurements with sweep signal are close to values obtained through direct method with the 75 Hz nonresonance as source signal, while indirect measurements with pink noise deviates from both. As a consequence, the indirect measurement using the sweep signal as generating source is suitable to describe the phenomenon, and it is used as reference in the comparison with direct measurements in the next Section of spatial measurements.

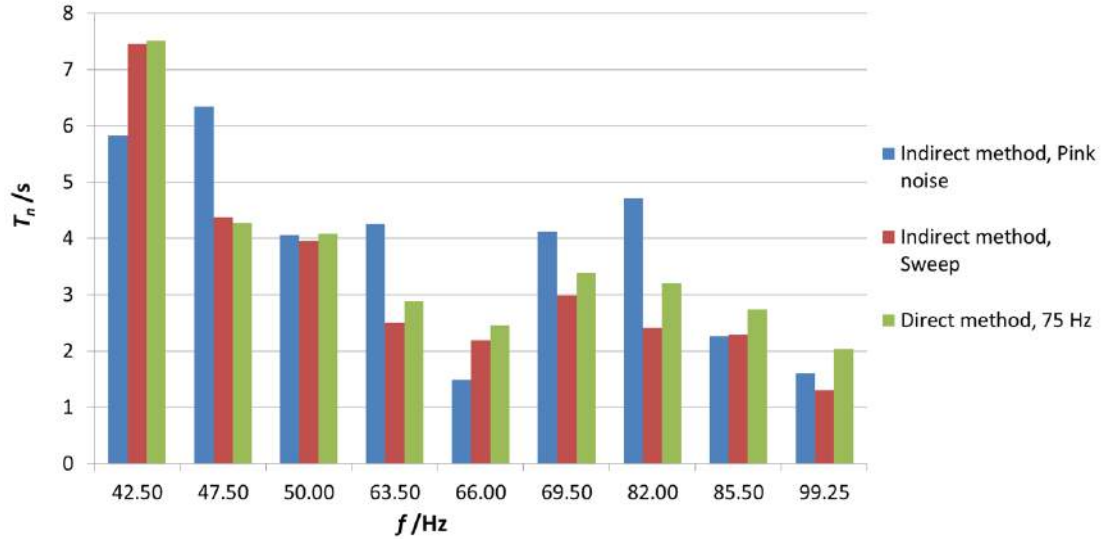


Figure 7.19: Comparison of direct and indirect methods with different source signals.

	Indirect met. Pink noise	Indirect met. Sweep sign.	Direct met. 75 Hz
$f$ / Hz	$T_n$ / s	$T_n$ / s	$T_n$ / s
42.5	5.83	7.46	7.51
47.5	6.34	4.38	4.27
50	4.06	3.96	4.08
63.5	4.26	2.50	2.89
66	1.49	2.19	2.46
69.5	4.12	2.99	3.39
82	4.71	2.42	3.21
85.5	2.26	2.29	2.74
99.25	1.61	1.31	2.03

Table 7.9: Comparison of direct and indirect methods with different source signals.

## 7.5 Spatial measurements

In previous chapters the most suitable methods for direct and indirect measurements are described. In order to get a better assessment of modal reverberation time and its uncertainty, spatial measurements (as indicated in ISO 3382) are performed. Several measurements (direct and indirect) are taken by placing microphones at 7 corners (1 is occupied by the loudspeaker) and at 3 points in the room (Fig. 7.20), 2 random points plus the center of the room, in order to have an indication of the behaviour of the acoustic field also in positions where room modes are not excited at the highest levels. In this section the 99.25 Hz mode is not considered due to the presence of a disturbance at 100 Hz that can not be excluded.

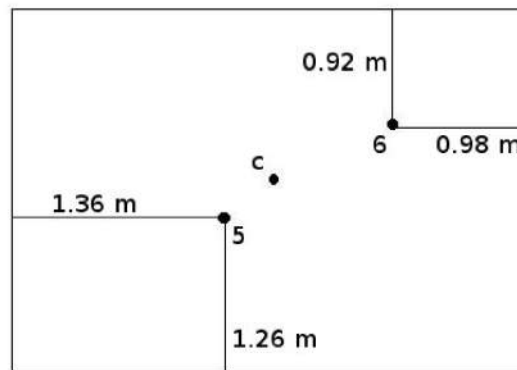


Figure 7.20: The 3 inner point of the room used for spatial measurements besides corner positions. The figure refers to  $xy$  plane.  $z$  values are  $z_5=2$  m,  $z_6=1$  m and  $z_c=1.72$  m.

On the basis of the conclusions in previous Sections, direct measurements are performed with the use of the 75 Hz nonresonance frequency as signal source, while indirect measurements are performed with a sweep signal (30-200 Hz with a linear increase in 10 s).

### 7.5.1 Indirect measurement

Spectra measurements are obtained in different points of the room (see Fig. 7.21). Spectra measurements in corner positions provide well defined resonant peaks, while at intermediate points (5 and 6) resonant peaks present lower values and at central point some modes are even completely suppressed as stated by modal theory. This justifies the fact that corner positions are the best to evaluate room modes as their intensity is maximum (high signal-to-noise ratio) and all modes are detectable.

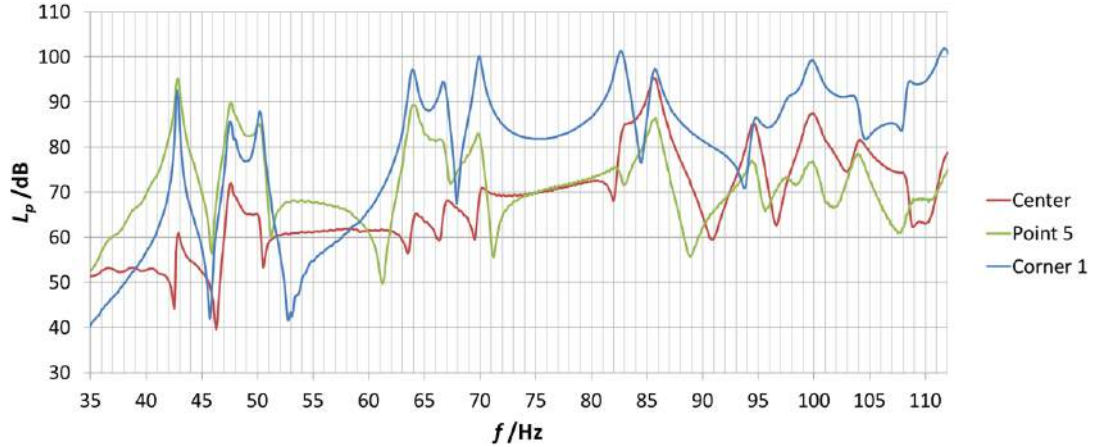


Figure 7.21: Examples of spectra obtained at a corner, at an intermediate point and at the center of the room.

Averages and standard deviations of modal measurements are then calculated considering, firstly, all spatial points and, secondly, just corner positions. Since at central point not all modes are detectable, it is excluded from the statistical analysis. In Table 7.10, results are reported.

$f$ /Hz	All spatial points		Corners	
	$\overline{T_n}$ /s	$s_{T_n}$ /s	$\overline{T_n}$ /s	$s_{T_n}$
42.5	6.26	0.54	6.29	0.62
47.5	4.36	0.33	4.46	0.28
50	4.10	0.29	4.11	0.31
63.5	3.07	0.20	3.06	0.18
66	2.95	0.40	3.01	0.26
69.5	3.18	0.17	3.19	0.17
82	2.34	0.26	2.43	0.12
85.5	2.90	0.23	2.89	0.22

Table 7.10: Spatial indirect measurements: averages and standard deviations of modal reverberation times.

Values assessed at different spatial points are consistent. Standard deviations calculated from corner measurements are lower than those evaluated in all spatial points: this is a proof of the validity of corner measurements as reference points for modal reverberation times measurement.

### 7.5.2 Direct measurement

The same spatial measurements are performed with the direct method. Also in this case, moving away from corners, intensity of resonant peaks decrease, until they mix up with background noise at the center of the room. As for indirect measurements, it is not possible to get modal reverberation times at the central point. Averages and standard deviations are evaluated considering all measurement points and only corner positions. Results are reported in Table 7.11.

$f$ /Hz	All spatial points		Corners	
	$\overline{T_n}$ /s	$s_{T_n}$ /s	$\overline{T_n}$ /s	$s_{T_n}$
42.5	6.22	0.94	6.61	0.59
47.5	3.82	0.31	3.74	0.28
50	4.21	0.51	4.34	0.53
63.5	2.66	0.13	2.69	0.12
66	2.65	0.29	2.78	0.18
69.5	3.26	0.03	3.27	0.03
82	2.67	0.26	2.75	0.13
85.5	2.77	0.19	2.71	0.16

Table 7.11: Spatial direct measurements: averages and standard deviations of modal reverberation times.

As for indirect measurements, values are consistent for different spatial averages, and standard deviations, considering only corner positions, are lower. This is a confirm of the fact that corners are the most suitable measurement points to evaluate modal reverberation times.

### 7.5.3 Comparison between direct and indirect measurements

Previous results of spatial measurements considering only the 7 corner positions are now compared in order to verify the consistency of direct and indirect measurements (Fig. 7.22). In general, the comparison shows a good agreement between the two methods since the average values are consistent (error bars correspond to expanded uncertainty with 6 degrees of freedom for the 95% confidence level). This means not only that, with the assumptions made in Section 7.2, the methodology contained in the ISO 3382 is adapted for reverberation time measurements at low frequencies, but this is also the first experimental proof of the relation between the modal reverberation time and the half bandwidth of resonant peaks in Eq. 7.2.

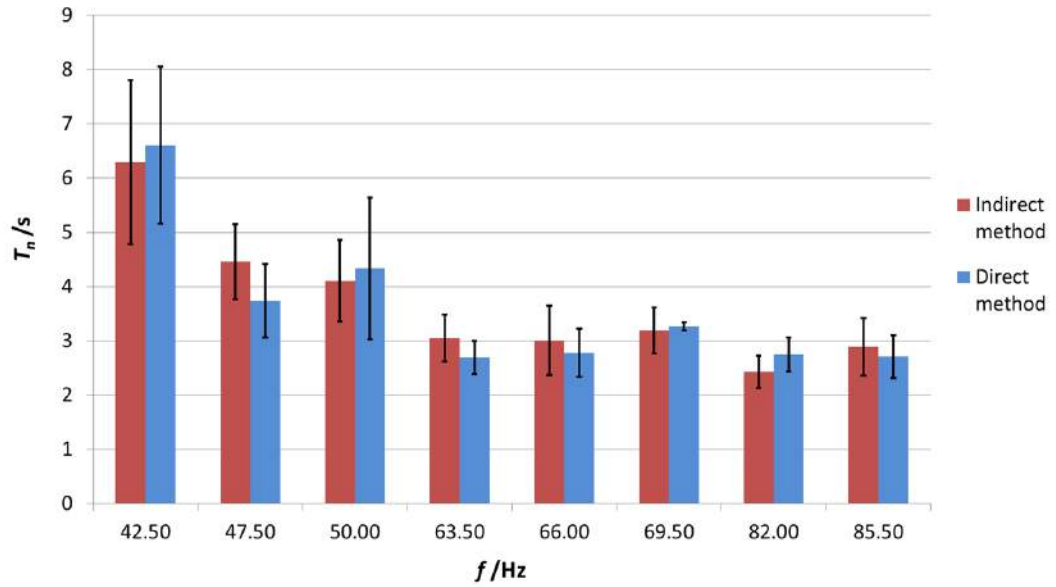


Figure 7.22: Comparison between direct and indirect spatial measurements of modal reverberation times. Error bars correspond to expanded uncertainty calculated for the 95% confidence level.

## Chapter 8

# The modal approach for impact sound insulation measurement

Among the standard building acoustics measurements, the extension to low frequencies ( $<100$  Hz) of laboratory airborne sound insulation and modal reverberation time measurements have been discussed so far. In this Chapter, the same attempt is applied for laboratory impact sound insulation measurement. In typical impact sound insulation laboratory rooms with volumes between  $50\text{ m}^3$  and  $80\text{ m}^3$ , due to modes of rooms, the acoustic field is considered non-diffuse below 100 Hz, whereas the diffuse field, in general, and for practical reasons, is assumed from 100 Hz on for all building acoustics measurements. Similarly, for the transmission of impact sound, also the floor vibrational field is considered diffuse: so it is possible to neglect the effects, on the radiated sound field, of source position, the size and boundary conditions of the slab. The current Standard (ISO 10140-3:2010) provides a measurement method and appropriate indexes for the description of impact sound insulation in diffuse field conditions (100-5000 Hz). At frequencies below 100 Hz, as expected from theory and experimentally confirmed, room modes are generated from the impact source. Therefore it is necessary, also in this case, to review the existing standard impact sound insulation descriptors (see Chapter 2.4) and adapt them in order to describe the proper physical phenomenon in connection with the human perception of noise and to ensure repeatable and reproducible values. Different authors have modelled the effect of impact sound transmission by using low frequency modal analysis and provided a good prediction of the acoustic field generated in a rectangular room by a single sound source. On the basis of these conclusions, in this Chapter, possible technical and practical solutions to evaluate, from a metrological and regulatory point of view, the acoustic performance of floating floors or floor coverings for frequencies below 100 Hz. For this purpose, new impact sound insulation descriptors for non-diffuse sound field are introduced and first experimental measurements are performed.

## 8.1 The modal impact sound insulation

Current ISO Standard (10140-3:2010) of impact sound insulation provides the measurement procedure of sound pressure levels in one-third octave bands ( $L_n$ ) in diffuse field condition, in terms of average energy radiated from the floor, excited with the ISO tapping machine (see Chapter 2.4 for deepening). As described by the theory the receiving room acoustic field, generated by the excited floor, is characterized by large fluctuation in space and frequency domains due to the presence of room modes. Applying the same modal approach described in modal airborne sound insulation (Chapter 4), it is convenient, also for impact sound insulation measurement, to move from a statistical approach typical of diffuse field (average of sound energy) to a discrete one, focused on the points of maximum noise and disturbance, i.e. the points of maximum sound pressure level in the space (corners) and frequency (resonance modes). For this reason, two descriptors are introduced: the modal impact sound pressure level,  $L_{modal} = L_{p,max}(f_n)$ , defined as the highest sound pressure level measured in the corners of the receiving room of impact sound insulation laboratory for each resonance frequency,  $f_n$ , and the improvement of modal impact sound insulation,  $\Delta L_{modal}(f_n)$ , defined as the difference between the highest sound pressure levels measured in the receiving room corners with the bare floor and the covered floor:

$$\Delta L_{modal}(f_n) = \Delta L_{p,max}(f_n) = L_{modal,0}(f_n) - L_{modal}(f_n) \quad (8.1)$$

where  $L_{modal,0}(f_n)$  is the highest modal sound pressure level measured with the bare slab and  $L_{modal}(f_n)$  is the highest modal sound pressure level measured in receiving room corners with the covered floor. Such descriptor provides an indication of transmission loss or energy absorption due to the floating floor. As stated in Chapter 2.4, for mass-spring systems (a rigid covering and the resilient layer), transmissibility curve (Fig. 2.14) has a peak around the resonant frequency of the system,  $f_0$ , given by Eq. 2.75 seen previously. Around the resonant frequency, the transmissibility is greater than 1 and higher sound pressure levels with the floating floor are obtained rather than with the bare slab. For lower frequencies, transmissibility is close to 1, and sound insulation is close to 0. The resonant frequency of the mass controls the starting insulation frequency, while the damping controls the insulation curve slope. On the basis of this, experimental measurements of modal impact sound pressure levels and improvement of modal impact sound insulation are performed with different mass-spring systems described in the next Section.

## 8.2 Experimental measurements

In order to test the new procedure, several measurements are carried out in the INRIM impact sound insulation laboratory both on the bare floor and on 3

floating floor samples.

### 8.2.1 Test elements

Since preliminary experimental measurements aim to evaluate qualitatively the new modal impact sound insulation descriptors on different floating floors, it is preferred to use small specimens, compared to the 10 m<sup>2</sup> test elements required by the ISO Standard [53]. For this reason, the approximation of locally reacting surface is applied in order to perform multiple tests. Three floating floor samples (or mass-spring systems) according to their different structural characteristics (different masses and resonant frequencies measured in INRIM laboratory with dynamic stiffness method) are tested and shown in Fig. 8.1 and described in Table 8.1. The purpose of such measurement campaign is to verify the new measurement method for the evaluation of the impact sound insulation at low frequency and compare it with the sound transmission theory.

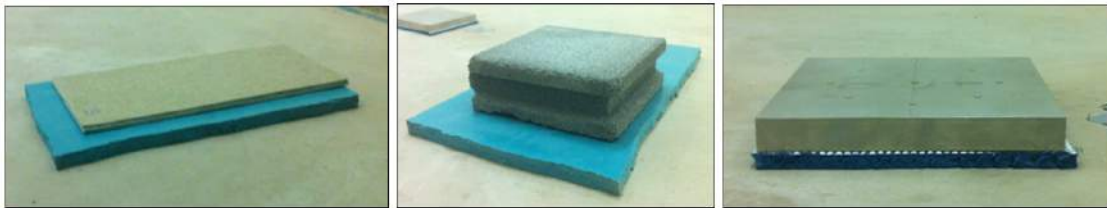


Figure 8.1: The 3 floating floor samples (M1, M2 and M3 respectively).

Name	Rigid covering	Resilient layer	$M$ /kg m <sup>-2</sup>	$S$ /m <sup>2</sup>	$f_0$ /Hz
M1	Fitted carpet	LDPE	7.65	0.1830	511
M2	Concrete	LDPE	89.95	0.0756	149
M3	Steel	LDPE	200.00	0.0400	38

Table 8.1: Technical specs of the 3 specimens.

### 8.2.2 Measurement procedure

In accordance with the definition of the new impact sound insulation descriptors and the current Standard, measurements of sound pressure level in the receiving room caused by the impact of the source on the floor are performed. With the standard tapping machine placed in three different points of the source room ( $\sim 51$  m<sup>3</sup>), the floor is mechanically stressed. The sound field radiated from the floor is measured at the four corners of the receiving room (50.5 m<sup>3</sup>) as shown in Fig. 8.2. Since it is necessary to focus on room modes, spectral analysis is performed

through a FFT from 0 Hz to 500 Hz, (0.25 Hz resolution) in order to identify the resonance frequencies. From the four spectra obtained for each corner, highest levels for each narrow band are selected in order to obtain the discrete spectrum of  $L_{p,max}(f_n)$ .

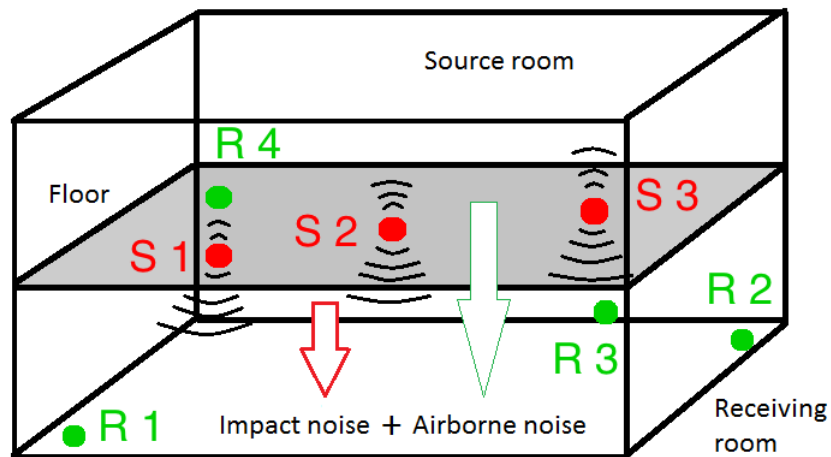


Figure 8.2: Source (S) and microphone (R) positions in the laboratory rooms.

### 8.2.3 Impact source: tapping machine or heavy/soft impact ball

In Fig. 8.3 an example of bare floor measurements is shown. The sound spectrum is strongly disturbed (blue curve), at least up to 100 Hz, by a 2 Hz occurrence, due to the harmonics of one of the five hammers of the tapping machine, probably not perfectly aligned with the others. For this reason a heavy/soft source (a 4 kg medicine ball), dropped from a 2 m height, is tested in order to excite the acoustic modes in the low frequency range. As seen in Fig. 8.3 (red curve), the spectrum is smoother and the resonance peaks are well defined. Selecting the modal sound pressure levels (red lines on the  $x$ -axis), the  $L_{modal,0}$  curve is obtained (Fig. 8.4). The weight and the drop height of the source are chosen arbitrarily as preliminary experimental measurements, and require further tests before being introduced in the Standard.

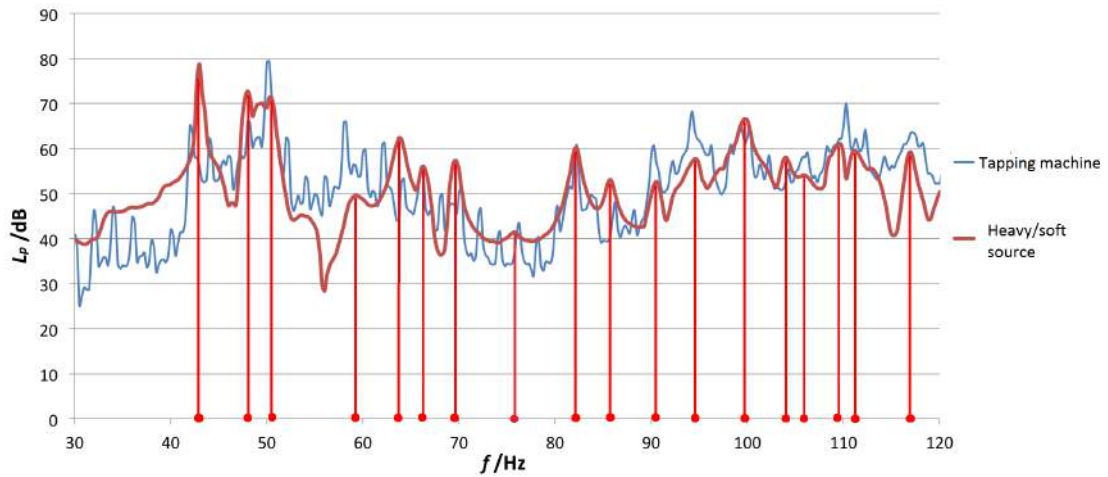


Figure 8.3: Comparison between tapping machine and heavy/soft source.

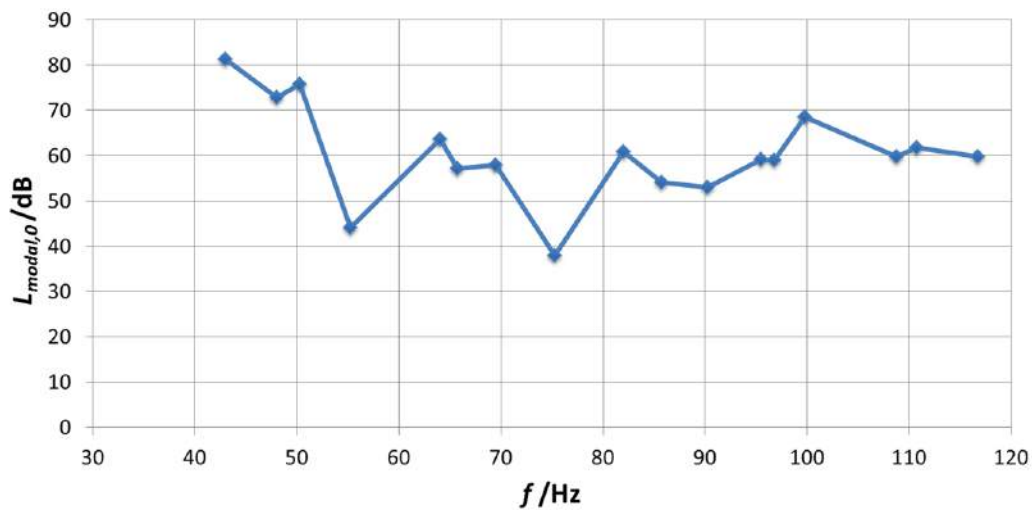


Figure 8.4: Modal impact sound pressure level on the bare floor.

### 8.2.4 Results and observations

Subsequently, measurements are performed on the three covering floors with the procedure described in the previous Section. Modal sound pressure levels obtained with the bare floor and the three floating floors are depicted in Fig. 8.5. Around the resonant frequency, the modal sound pressure level radiated from the covered floor in the receiving room is greater than the one radiated from the bare floor; for lower frequencies sound insulation tends to zero values, while for higher frequencies the sound pressure level difference between the bare and covered floor increases and the insulation starts to be visible, in agreement with theory: the

impulse force peak is damped and the mechanical power introduced into the slab is partially absorbed by the resilient surface layer [54, 55].

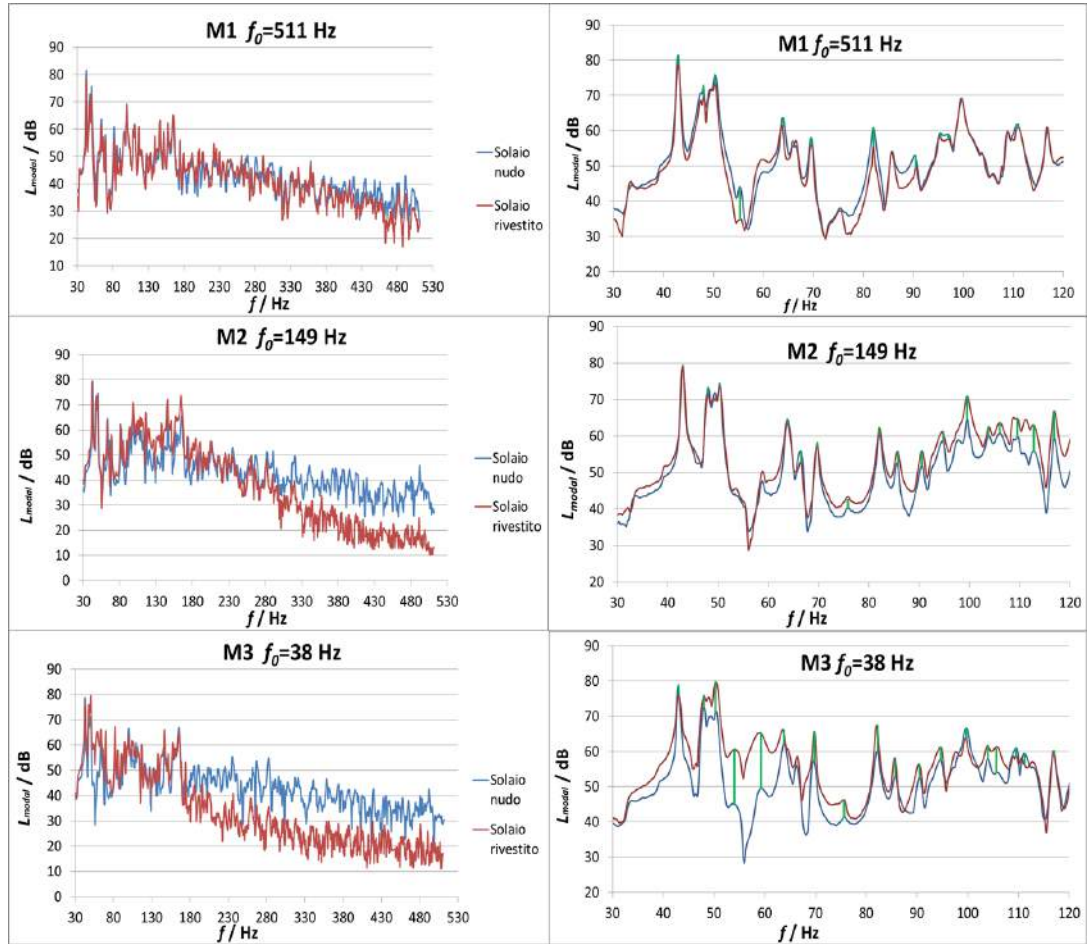


Figure 8.5: Frequency spectra obtained with each floating floor sample over the whole frequency range (left) and a zoom on the low frequency range (right). Green lines correspond to sound pressure level differences computed for each resonant frequency in order to evaluate the improvement of modal impact sound insulation  $\Delta L_{modal}$ .

Improvement of modal impact sound insulation discrete curves are depicted in Fig. 8.6. The analysed mass-spring systems, with resonance frequencies between 38 Hz and 511 Hz, do not contribute to the sound insulation in the low frequency range (M1, the curve is, on average, around zero), but, on the contrary, can cause noise amplification (M2 and M3 curves decrease approaching their resonant frequencies), as confirmed by theory [48]. Improvement of modal impact sound insulation presents negative values around resonant frequency. This is characteristic of the fact that, in construction industry, materials with very low resonance frequencies (0-10 Hz) do not exist in commerce (except for industrial spring systems which could ensure impact sound insulation in the low frequency range but cannot be used for common dwellings). As most of the common covering floors are characterized by resonance frequencies above 50 Hz, the range of low frequencies presents, in most cases, a null sound insulation and even negative in some cases. For low frequencies, it is more useful to control noise amplification rather than sound insulation.

Separate discussion, instead, concerns the case of ceilings where characterization of airborne sound insulation can be more significant even at low frequencies. As a matter of fact, airborne sound insulation can be gathered also for frequencies below the resonance frequency of the partition as stated by theory (Chapter 2.2).

A problem on measurement procedure arises when M3 curve is analysed: the negative peak is reached at 55 Hz and 65 Hz, instead of 38 Hz. Below 55 Hz, improvement of modal impact sound insulation even increases until the first mode at 43 Hz. This is probably due to the airborne transmission of first modes from the source to the receiving room through the floor. For this reason, in the future it is necessary to evaluate the influence of airborne component in impact sound insulation measurements.

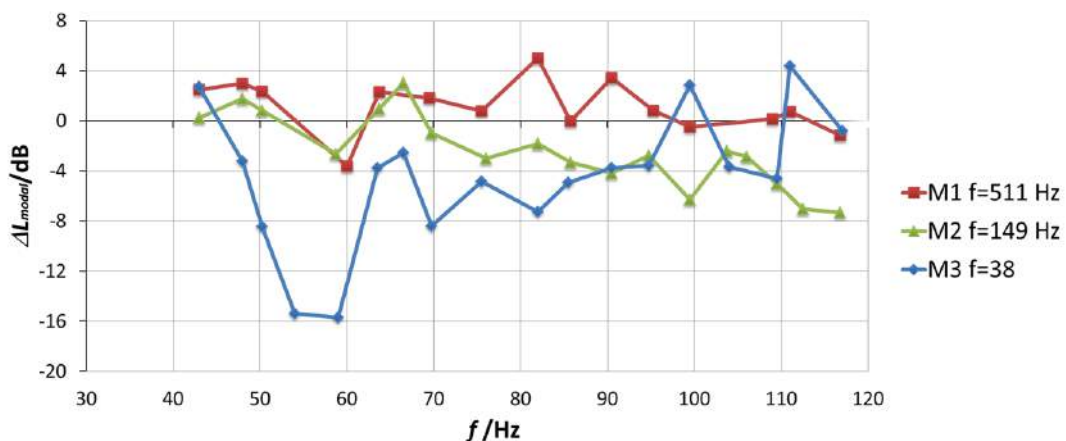


Figure 8.6: Improvement of modal impact sound insulation  $\Delta L_{modal}$  of the three floating floor samples.

The discrete form of the introduced impact sound insulation descriptor does not contain information for frequencies between two adjacent resonance frequencies. To extend these measurements to the whole low frequency range, it is assumed, in a first approximation, that in another laboratory with different dimensions, resonance peaks could move along the envelope of the measured spectra, as already proposed for modal airborne sound insulation (Chapter 4.3). In this way, a representation in one-third octave bands, as required by ISO Standard, of modal impact sound pressure levels, as well as for the improvement of modal impact sound insulation is obtained (Fig. 8.7).

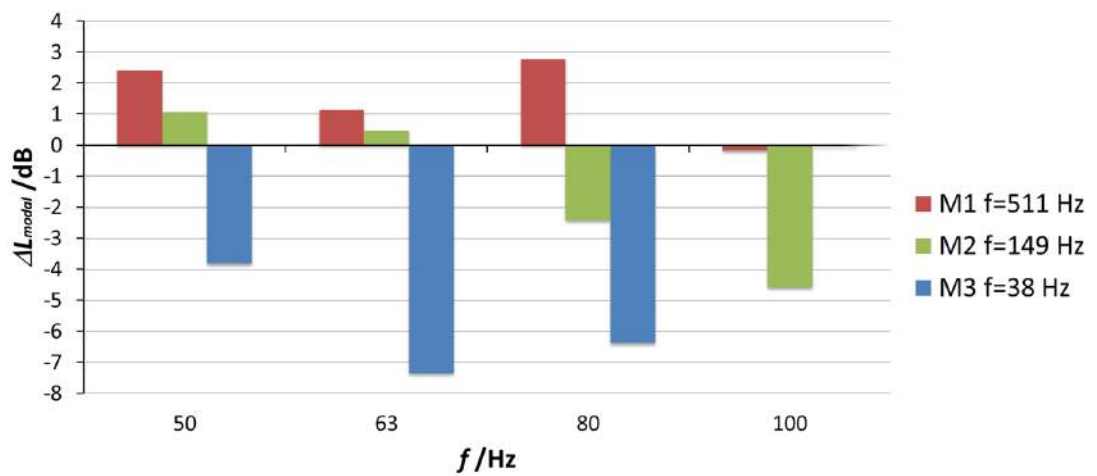


Figure 8.7: Improvement of modal impact sound insulation  $\Delta L_{modal}$  in one-third octave bands of the three floating floor samples.

New indexes of laboratory impact sound insulation and improvement of impact sound insulation at low frequencies (and in general for non-diffuse field conditions) are introduced as well as a new measurement procedure according to the modal approach. The preliminary experimental measurements, in accordance with the theory, confirm the significance of such indexes. In the future it will be necessary to introduce normalization terms that consider different boundary conditions (size of the receiving room, modal absorption, airborne transmission, etc.) in order to obtain repeatable and reproducible values and to evaluate the uncertainty budget. In the end, it is necessary to perform measurements on 10 m<sup>2</sup> specimens for further experimental tests.

## Chapter 9

# Conclusions and future works

The modal approach for the main laboratory measurements of building acoustics (airborne sound insulation, impact sound insulation and reverberation time) at low frequency (50-100 Hz) is introduced and new descriptors are investigated on the basis of theoretical analysis of non-diffuse sound field of small laboratory rooms. This new approach represents a possible solution for the required extensions of building acoustics measurements down to 50 Hz, also for field measurements in common dwellings with small volumes. Nevertheless, different practical and metrological problems have still to be solved for all the proposed measurement methods and further efforts are necessary to be overcome.

The application of modal approach to airborne sound insulation measurement entails the proposal of a new descriptor, the modal sound insulation  $D_{modal}$ , obtained by a proper measurement procedure with microphones and loudspeaker placed at room corners and differs from standard sound reduction index  $R$ , which is based on sound power measurements, still unable to be defined in a modal field and not enough accurate to evaluate sound insulation, also from the human perception point of view. It is a discrete index (focused just on source room modes) and it is an indicator of modal transmission loss, based on the transmission of source room modes into the receiving room through the partition. A comparison of modal sound insulation values with vibrational measurements on a partition, with resonant frequency at around 80 Hz, confirmed the validity of results. A proper normalization term corresponding to receiving room volume is obtained from theoretical calculations and an extension to the whole low frequency range, based on the envelope method, are proposed in order to adapt modal sound insulation to Standard requirements (results expressed in one-third octave bands). In this way, a possible solution is to provide two different insulation descriptors for technical and commercial purposes: one for diffuse field (100-5000 Hz), the standard sound reduction index  $R$ , and one for non-diffuse field (50-100 Hz), the modal sound insulation  $D_{modal}$ . Since the two descriptors can not be quantitatively related due to different physical meanings and measurements procedure, it could

be possible to provide two separate single numbers for the acoustic characterization of building elements. Analysis of uncertainty budget confirmed the higher influence of type A uncertainty due to repeatability, rather than errors related to the measurement devices (ratio of 10:1). Repeatability measurements showed that standard deviation values are within the limits fixed by ISO 12999-1:2014 for the low frequency third octave bands (50 Hz, 63 Hz, 80 Hz and 100 Hz). This result confirms the proposed extension method. A first reproducibility comparison within the 2 INRIM sound insulation laboratories is performed. The general trend of modal sound insulation in one-third octave bands is similar but differences are quantitatively evident, although the application of normalization term, introduced to improve the agreement of results. The main cause is the presence of matching modes (similar source and receiving room modes due to similar dimensions) which entails an underestimation of sound insulation and, at present, they can not be avoided. Further modal sound insulation measurements are performed in the 1:8 scale model. The peculiarity of such model is the possibility to move mobile walls facing the test specimen. In this way, changing receiving room volume (from -30% to 60% with respect to source room volume), it is possible to verify the validity of normalization term. Results show the negligible effect of the introduced normalization term and rise a question about the effective weight of receiving volume term in modal sound insulation measurements. The main influential factor is the modal match due to coupled source and receiving room lengths,  $L_y$  and  $L_z$ , unable to be changed. A first rough exclusion of such modes from the evaluation of modal sound insulation decreased the standard deviation and partially avoided underestimation of results. Another comparison is performed with the scale model, without the receiving room, inside the anechoic chamber in order to avoid the influence of modal match, as the receiving space is a free field. The comparison shows that modal sound insulation results, evaluated in free field and in modal field (without modal match), are consistent and a weighting procedure is possible. In particular, the increase of modal sound pressure level for a particular mode as function of length or frequency differences between source and receiving rooms is studied. The relation follows the Kohlrausch-Williams-Watts function. Such experimental evidence opens to the future possibility of a weighted procedure in order to avoid modal match and, thus, obtain a real representation of modal sound insulation. The same weighted procedure could be applied for field measurements when modal sound insulation is evaluated in ordinary dwellings, most of characterized by similar volumes and dimensions. Further evaluations on a different scale model with the possibility to move all boundary walls will be necessary in order to completely avoid modal match. In the end, all different volume combinations are used to validate the envelope method for the extension to the whole low frequency range in one-third octave bands. Results are consistent and the proposed method is confirmed. Inter-laboratory Round Robin Test will be useful to have further experimental confirmations in real laboratories.

---

The modal approach for impact sound insulation measurement entails two new descriptors: the modal impact sound pressure level, defined as the highest sound pressure level measured in the corners of the receiving room for each resonance frequency, and the improvement of modal impact sound insulation, defined as the difference between the highest modal sound pressure level measured in the receiving room corners with the bare floor and the covered floor. Starting from ISO Standard guidelines (ISO 10140-3:2010), the measurement procedures are modified in accordance with the new definition of indexes. The first experimental results on three different spring-mass systems confirm the significance of the introduced quantities, in accordance with the impact sound transmission theory. The same method of extension to the whole low frequency range in one-third octave bands, previously proposed for modal sound insulation, is also applied. In the future it will be necessary to introduce normalization terms that take into account different boundary conditions (size of the receiving room, modal absorption, airborne transmission of source room modes into the receiving room, etc.) and to check repeatability and reproducibility. Besides, more measurements on 10 m<sup>2</sup> specimens as required by the ISO Standard are necessary.

In non-diffuse sound field, the non-linearity of sound pressure level decays in one-third octave bands suggest to focus just on resonant frequencies, as the most influential parameters of the acoustic field and human annoyance in quality of listening (rumble effect). Following this approach the modal reverberation time is introduced. In particular two measurement methods are investigated: the direct method and the indirect method. For the first one, starting from the interrupted noise procedure stated in ISO 3382-2:2008, different source signals are compared: pink noise and sine waves (resonant and non-resonant). The last one fits better as decays are cleaner and well detectable. The indirect method, whereas, requires measurement of half bandwidths of modes, mathematically related to modal reverberation time. No experimental tests have been performed before from a literature review. The source sweep signal is preferable with respect to pink noise as spectra are smoother and half bandwidth calculations are more precise. In the end, the comparison between direct and indirect methods for modal reverberation time measurement shows a good agreement as results are consistent and comparable. This is the first experimental validation of the relation between half bandwidth of resonant frequencies and modal reverberation time. It is still necessary to further investigate this proposal and choose the method that is more comfortable for acousticians and adaptable to field measurements. Besides, the results of this study open the way to further research in a very promising and still little deepened areas: the development of particular solutions for the absorption and control of low frequencies in building acoustics, and the control of room acoustic field to guarantee the quality of listening, like recording studios or small concert halls.



# Appendices



# Appendix A

## The modal sound insulation: comparison between sweep and noise signals

A comparison between two different source signal is performed for modal sound insulation measurement on a same test object: sweep signal and pink noise. In the first case, FFT analysis is operated with the so called Max-Hold function which returns the highest sound pressure levels for each narrowband in time. In the second case, FFT analysis is performed through a linear average over 60 s. Comparison of modal sound insulation is performed according to procedure described in Chapter 4. Sweep signals results to be better for what concerns spectra measurements: peaks are well defined and source and receiving room spectra are very smooth with respect to pink noise ones (Fig. A.1 and Fig. A.2). Modal sound insulation curves are consistent and final results are similar as seen in Fig. A.3.

136 **A. The modal sound insulation: comparison between sweep and noise signals**

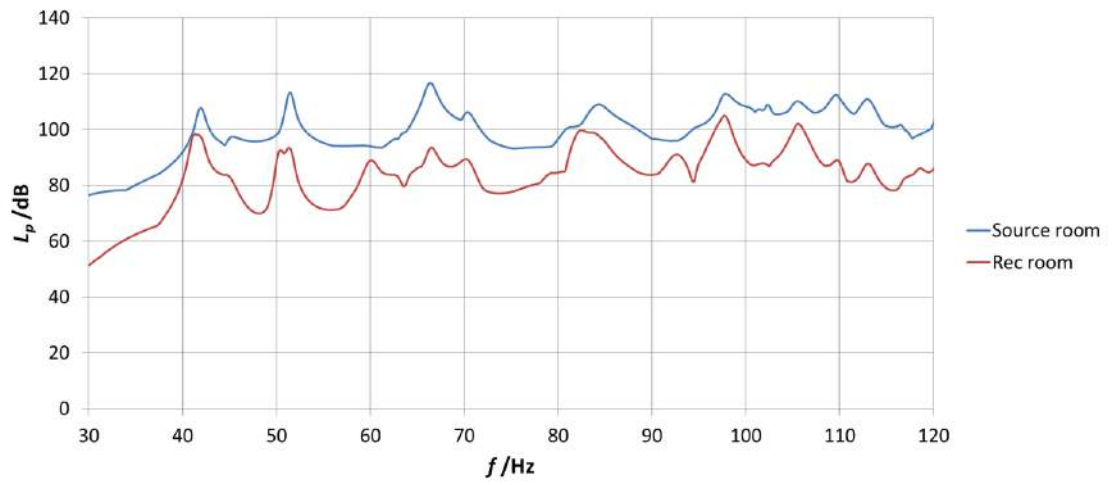


Figure A.1: Source and receiving room spectra obtained with sweep signal

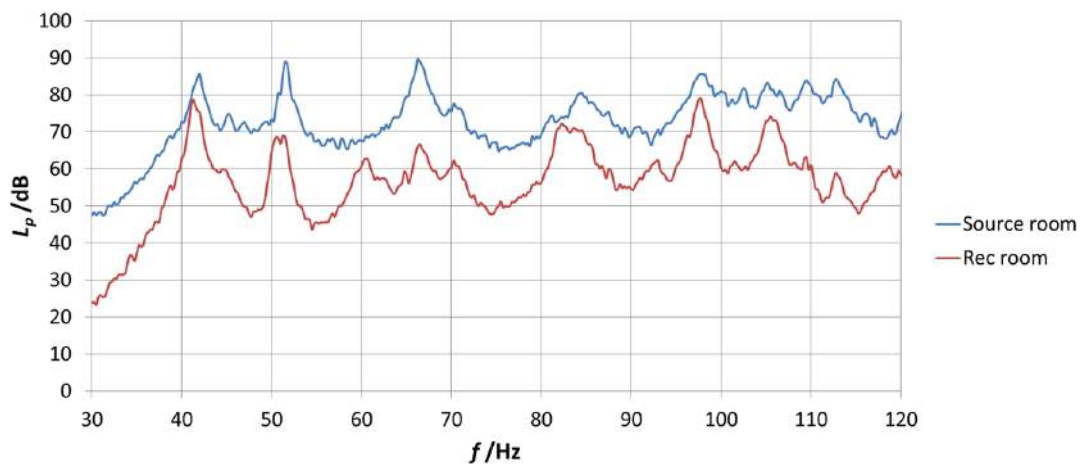


Figure A.2: Source and receiving room spectra obtained with pink noise.

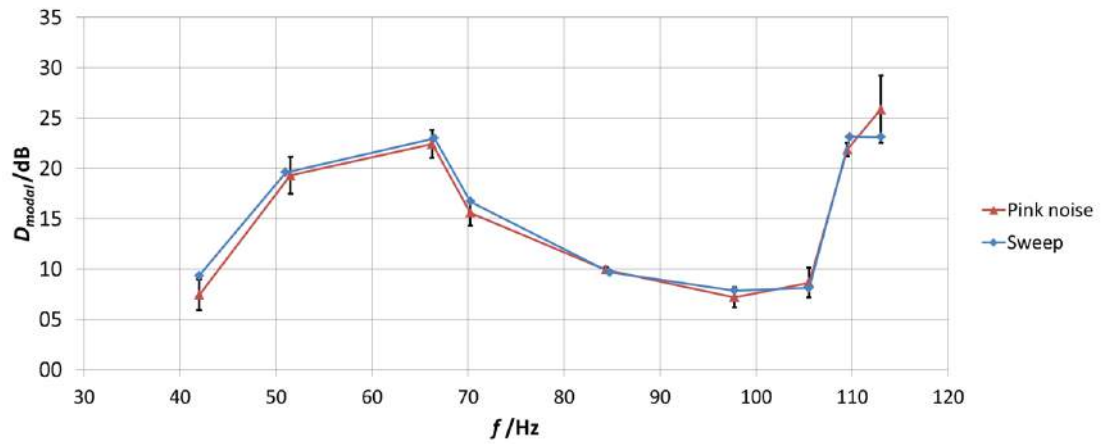


Figure A.3: Comparison between modal sound insulation curves obtained with pink noise and sweep signal. Error bars correspond to expanded uncertainty of modal sound insulation (pink noise) calculated for the 95% confidence level. Results are consistent with each other.



# Appendix B

## Normalization terms

Starting from modal theory (Section 2) for rectangular rooms, different assumptions and simplifications discussed in Section 4.2 for the modal sound insulation index  $D_{modal}(f_n) = D_{modal}(2\pi\omega_{l_1 m_1 n_1})$  are proposed and introduced:

- $\psi_{l_1 m_1 n_1}^{(2)}(x_{corner}) = \psi_{l_2 m_2 n_2}^{(2)}(x_{corner}) = 1$ .
- Summation terms in  $p_{max}^{(1)}(x_{corner}, \omega_{l_1 m_1 n_1}, t)$  and  $p_{max}^{(2)}(x_{corner}, \omega_{l_1 m_1 n_1}, t)$  reduce to one term as the other terms can be considered negligible.
- In  $G_{qr, l_2 m_2 n_2}^{(2)}(\omega_{l_1 m_1 n_1})$ , forcing the analysis it is possible to assume  $(1 - (-1)^{q+m_2})(1 - (-1)^{r+n_2}) = 1$ , otherwise it is 0.
- In  $G_{l_1 m_1 n_1, qr}^{(1)}(\omega_{l_1 m_1 n_1})$ , we assume that  $(1 - (-1)^{q+m_1})(1 - (-1)^{r+n_1}) = 1$ , otherwise it is 0.

With such assumptions and simplifications

•

$$\begin{aligned}
 p_{max}^{(1)}(x_{corner}, \omega_{l_1 m_1 n_1}, t) &\sim \\
 &\sim A_{l_1 m_1 n_1}^{(1)}(\omega) \psi_{l_1 m_1 n_1}^{(1)}(x_{corner}) e^{-i\omega_{l_1 m_1 n_1} t} \sim \\
 &\sim \frac{\rho_0 c^2 \omega Q_0}{V_1 \Lambda_{l_1 m_1 n_1} 2\omega_{l_1 m_1 n_1} \delta_{l_1 m_1 n_1}} e^{-i\omega_{l_1 m_1 n_1} t} \quad (\text{B.1})
 \end{aligned}$$

$$\begin{aligned}
p_{max}^{(2)}(x_{corner}, \omega_{l_1 m_1 n_1}, t) &\sim \\
&\sim G_{qr, l_2 m_2 n_2}^{(2)}(\omega_{l_1 m_1 n_1}) G_{l_1 m_1 n_1, qr}^{(1)}(\omega_{l_1 m_1 n_1}) \cdot \\
&\cdot A_{l_1 m_1 n_1}^{(1)}(\omega_{l_1 m_1 n_1}) \psi_{l_2 m_2 n_2}^{(2)}(x_{corner}) e^{-i\omega_{l_1 m_1 n_1} t} \sim \\
&\sim \frac{2S_p \rho_0 c^2 \omega_{l_1 m_1 n_1}}{V_2 \Lambda_{l_2 m_2 n_2} 2\omega_{l_2 m_2 n_2} \delta_{l_2 m_2 n_2}} \cdot \frac{q}{(q^2 - m_2^2)} \frac{r}{(r^2 - n_2^2)} \\
&\cdot \frac{2\omega_{l_1 m_1 n_1}}{\Lambda_{l_1 m_1 n_1} \pi^2 i L_y^{(p)} L_z^{(p)}} \cdot \frac{q}{(q^2 - m_1^2)} \frac{r}{(r^2 - n_1^2)} \cdot \\
&\cdot \frac{1}{M[(1 + i\eta)\omega_{qr}^2 - \omega_{l_1 m_1 n_1}^2]} \cdot \frac{\rho_0 c^2 \omega_{l_1 m_1 n_1} Q_0 e^{-i\omega_{l_1 m_1 n_1} t}}{V_1 \Lambda_{l_1 m_1 n_1} 2\omega_{l_1 m_1 n_1} \delta_{l_1 m_1 n_1}} \quad (B.2)
\end{aligned}$$

and it is possible to demonstrate that evaluation of  $D_{modal}$  in different laboratories depends, in first approximation, on receiving room volume  $V_2$ , since partition properties can be considered the same. Influence of coupling indexes ( $\frac{q}{(q^2 - m_1^2)}$  and  $\frac{r}{(r^2 - n_1^2)}$ ) and environmental parameters ( $\rho_0$  and  $c$ ) is negligible with respect to the main ones and gets into measurement uncertainty.

$$\begin{aligned}
D_{modal}(f_n) &= D_{modal}(2\pi\omega_n) = D_{modal}(2\pi\omega_{l_1 m_1 n_1}) = \\
&= 20 \log_{10} \left( \frac{|p_{max}^{(1)}(x_{corner}, \omega_{l_1 m_1 n_1}, t)|}{|p_{max}^{(2)}(x_{corner}, \omega_{l_1 m_1 n_1}, t)|} \right) = \\
&= 20 \log_{10} \left( \frac{|\sum_{l_1 m_1 n_1=0}^{\infty} A_{l_1 m_1 n_1}^{(1)}(\omega_{l_1 m_1 n_1}) \cdot \psi_{l_1 m_1 n_1}^{(1)}(x_{corner}) e^{-i\omega_{l_1 m_1 n_1} t}|}{|\sum_{l_1 m_1 n_1=0}^{\infty} \sum_{qr=1}^{\infty} \sum_{l_2 m_2 n_2=0}^{\infty} G_{qr, l_2 m_2 n_2}^{(2)}(\omega_{l_1 m_1 n_1}) \cdot G_{l_1 m_1 n_1, qr}^{(1)}(\omega_{l_1 m_1 n_1}) A_{l_1 m_1 n_1}^{(1)}(\omega_{l_1 m_1 n_1}) \psi_{l_2 m_2 n_2}^{(2)}(x_{corner}) e^{-i\omega_{l_1 m_1 n_1} t}|} \right) \\
&\sim 20 \log_{10} \left( \frac{|A_{l_1 m_1 n_1}^{(1)}(\omega_{l_1 m_1 n_1})|}{|G_{qr, l_2 m_2 n_2}^{(2)}(\omega_{l_1 m_1 n_1}) G_{l_1 m_1 n_1, qr}^{(1)}(\omega_{l_1 m_1 n_1})|} \cdot \frac{1}{A_{l_1 m_1 n_1}^{(1)}(\omega_{l_1 m_1 n_1})} \right) \sim \\
&\sim 20 \log_{10} \left( \frac{1}{|G_{qr, l_2 m_2 n_2}^{(2)}(\omega_{l_1 m_1 n_1}) G_{l_1 m_1 n_1, qr}^{(1)}(\omega_{l_1 m_1 n_1})|} \right) \\
&\qquad \qquad \qquad \propto 20 \log_{10}(V_2) \quad (B.3)
\end{aligned}$$

Fixing a standard value for receiving room volume ( $V_{2,0}$ ),  $p_{0,max}^{(2)}(x_{corner}, \omega_{l_1 m_1 n_1}, t) \propto 1/(V_{2,0})$  and normalized modal sound insulation  $D_{modal, nV}$  becomes:

$$\begin{aligned}
D_{\text{modal},nV}(f_n) &= D_{\text{modal}}(2\pi\omega_n) = D_{\text{modal}}(2\pi\omega_{l_1m_1n_1}) = \\
&= 20\log_{10} \left( \frac{|p_{\text{max}}^{(1)}(x_{\text{corner}}, \omega_{l_1m_1n_1}, t)|}{|p_{0,\text{max}}^{(2)}(x_{\text{corner}}, \omega_{l_1m_1n_1}, t)|} \right) = \\
&= 20\log_{10} \left( \frac{|p_{\text{max}}^{(1)}(x_{\text{corner}}, \omega_{l_1m_1n_1}, t)|}{|p_{0,\text{max}}^{(2)}(x_{\text{corner}}, \omega_{l_1m_1n_1}, t)|} \cdot \frac{V_2}{V_2} \right) = \\
&= 20\log_{10} \left( \frac{|p_{\text{max}}^{(1)}(x_{\text{corner}}, \omega_{l_1m_1n_1}, t)|}{|p_{\text{max}}^{(2)}(x_{\text{corner}}, \omega_{l_1m_1n_1}, t)|} \frac{V_{2,0}}{V_2} \right) = \\
&= D_{\text{modal}} - 20\log_{10} \left( \frac{V_2}{V_{2,0}} \right) \quad (\text{B.4})
\end{aligned}$$



# Appendix C

## Matlab scripts

### C.1 Extension of modal sound insulation envelope to one-third octave bands

```
\%\%\%\%\%\%\%\%\%\% INPUT \%\%\%\%\%\%\%\%\%\%\%\%\%\%  
f = [43  
48  
50.25  
54  
59  
63.5  
66.5  
69.75  
75.5  
82  
85.5  
90.5  
94.75  
99.5  
104  
109.5  
111  
117  
];  
  
Lp = [76.0  
75.9  
79.7  
60.6
```

```

65.3
66.1
58.6
65.6
46.2
67.3
58.0
56.4
61.2
63.7
61.7
58.7
56.6
60.1
];
fc = 0.25;

```

```

%%%%%%%%%%%%%%%%%% OUTPUT %%%%%%%%%%%%%%%%%%%

```

```

for i=1:length(f)-1
    fFit{i} = f(i)+fc:fc:f(i+1);
end

for n=1:length(f)-1
    LpFit{n} = (Lp(n+1)-Lp(n))/(f(n+1)-f(n))*(fFit{n}-f(n)) + Lp(n);
end

NO=0;
for l=1:length(f)-1
    N=length(LpFit{1})+NO;
    NO=N;
end

fTOT(1:length(fFit{1}),1)=fFit{1};
LpTOT(1:length(LpFit{1}),1)=LpFit{1};

```

```

for n=1:length(f)-2

    fTOT(length(fTOT(:,1))+1:length(fTOT(:,1))+length(fFit{n+1}),1)
    =fFit{n+1};

    LpTOT(length(LpTOT(:,1))+1:length(LpTOT(:,1))+length(LpFit{n+1}),1)
    =LpFit{n+1};
end

fitTOT(:,1)=fTOT(:,1);
fitTOT(:,2)=LpTOT(:,1);

plot(fitTOT(:,1),fitTOT(:,2))

fitTOTlin = 10.^(fitTOT(:,2)/10);

Ni_50 = find (fitTOT(:,1)==44.75);
Nf_50 = find (fitTOT(:,1)==56.25);
N_50 = Ni_50:1:Nf_50;
Ni_63 = Nf_50 + 1;
Nf_63 = find (fitTOT(:,1)==70.75);
N_63 = Ni_63:1:Nf_63;
Ni_80 = Nf_63 + 1;
Nf_80 = find (fitTOT(:,1)==89);
N_80 = Ni_80:1:Nf_80;
Ni_100= Nf_80 + 1;
Nf_100= find (fitTOT(:,1)==112.25);
N_100 = Ni_100:1:Nf_100;

Lp_50 = fitTOTlin(N_50);
Lp_63 = fitTOTlin(N_63);
Lp_80 = fitTOTlin(N_80);
Lp_100 = fitTOTlin(N_100);

Lp_50 = 10*log10(sum(Lp_50));
Lp_63 = 10*log10(sum(Lp_63));
Lp_80 = 10*log10(sum(Lp_80));
Lp_100 = 10*log10(sum(Lp_100));

fitThirdOctBand = [ 50 Lp_50; 63 Lp_63; 80 Lp_80; 100 Lp_100]

```

## C.2 Calculation of resonant peak half bandwidth

```
\% \% \% \% \% \% \% \% \% \% INPUT \% \% \% \% \% \% \% \% \% \%
x=[
98.7000
98.8000
98.9000
99.0000
99.1000
99.2000
99.3000
99.4000
99.5000
99.6000
99.7000
99.8000
99.9000
100.0000
100.1000
100.2000
100.3000
100.4000
];

y=[
82.961733
83.151709
84.366271
84.171198
84.354853
85.905975
85.459873
86.131221
86.633704
87.086933
87.2495
86.731214
87.882006
86.949463
86.622885
87.090484
86.045234
```

```

85.843365
];

%%%%%%%%%%%%%%%%%% OUTPUT %%%%%%%%%%%%%%%%%%%

if (max(y)-y(length(y))<3 && max(y)-y(1)<3)

a=find(y==max(y));
x1=x(1)-(x(2)-x(1));
y1=y(1)-(y(2)-y(1));
x2=x(length(x))+x(length(x))-x(length(x)-1));
y2=y(length(x))+y(length(y))-y(length(y)-1));

x=[x1 x' x2];
y= [y1 y' y2];
x=x'
y=y'

[prime params resnorm residual] = lorentzfit(x,y);

xfit= min(x):0.001:max(x);

yfit=params(1)./((xfit - params(2)).^2 + params(3)) + params(4);

indxfc = find(yfit == max(yfit) );
indx3dBsup = indxfc+1:length(yfit);
yfitsup = abs(yfit(indx3dBsup)-max(yfit)+3);
ind3dBsup = find(yfitsup == min(yfitsup));
indxsup = indx3dBsup(ind3dBsup);
fsup = xfit (indxsup)
SPLsup = yfit (indxsup)

fc = params(2);
D3dB = 2*(fsup - fc)
finf = fsup - D3dB
SPLfc = max(yfit)

plot(x,y,'--o','LineWidth',2)
hold on
plot (xfit, yfit,'r','LineWidth',2)

```

```

hold on
plot(fsup, SPLsup, 'o', 'MarkerEdgeColor','k',
'MarkerFaceColor','g','MarkerSize',10)
hold on
plot(fin, SPLsup, 'o', 'MarkerEdgeColor','k',
'MarkerFaceColor','g','MarkerSize',10)

xlabel({'frequency [Hz]'})
ylabel({'SPL [dB]'})

else
if (max(y)-y(length(y))>3)
[yprime params, resnorm residual] = lorentzfit(x,y);

xfit= min(x):0.001:max(x);

yfit=params(1)./((xfit - params(2)).^2 + params(3)) + params(4);

indxfc = find(yfit == max(yfit));
indx3dBsup = indxfc+1:length(yfit);
yfitsup = abs(yfit(indx3dBsup)-max(yfit)+3);
ind3dBsup = find(yfitsup == min(yfitsup));
indxsup = indx3dBsup(ind3dBsup);
fsup = xfit (indxsup)
SPLsup = yfit (indxsup)

fc = params(2)
D3dB = 2*(fsup - fc)
fin = fsup - D3dB
SPLfc = max(yfit)

plot(x,y,'--o','LineWidth',2)
hold on
plot (xfit, yfit,'r','LineWidth',2)
hold on
plot(fsup, SPLsup, 'o', 'MarkerEdgeColor','k',
'MarkerFaceColor','g','MarkerSize',10)
hold on
plot(fin, SPLsup, 'o', 'MarkerEdgeColor','k',

```

```
'MarkerFaceColor','g','MarkerSize',10)

xlabel({'frequency [Hz]'})
ylabel({'SPL [dB]'})

else
[yprime params, resnorm residual] = lorentzfit(x,y);

xfit= min(x):0.001:max(x);

yfit=params(1)./((xfit - params(2)).^2 + params(3)) + params(4);

indxfc = find(yfit == max(yfit) );
indx3dBinf = 1:indxfc-1;
yfitinf = abs(yfit(indx3dBinf)-max(yfit)+3);
ind3dBinf = find(yfitinf == min(yfitinf));
finf = xfit (ind3dBinf)
SPLinf = yfit (ind3dBinf)

fc = params(2)
D3dB = 2*(fc - finf)
SPLfc = max(yfit)
fsup = finf + D3dB
plot(x,y,'--o','LineWidth',2)
hold on
plot (xfit, yfit,'r','LineWidth',2)
hold on
plot(fsup, SPLinf, 'o', 'MarkerEdgeColor','k',
'MarkerFaceColor','g','MarkerSize',10)
hold on
plot(finf, SPLinf, 'o', 'MarkerEdgeColor','k',
'MarkerFaceColor','g','MarkerSize',10)

xlabel({'frequency [Hz]'})
ylabel({'SPL [dB]'})

end
```

```
end

Res0=0;

xfit=round(xfit*10000000)/10000000;

for indx=1:length(x);

    indRes= find(xfit==x(indx));
    yfitRes = yfit(indRes);
    yx = y(indx)
    Res = (yx-yfitRes)^2;
    Res = Res + Res0;
    Res0 = Res;

end

Res=sqrt(Res0/length(y))
Tr = 2.2/D3dB
```

# Bibliography

- [1] Berglund B, Hassmn P, Job RF, *Sources and effects of low-frequency noise*, J. Acoust. Soc. Am., 99(5), pp. 2985-3002, 1996.
- [2] Persson Waye K, Rylander R, *The prevalence of annoyance and effects after long-term exposure to low-frequency noise*, Journal of Sound and Vibration, 240(3), pp. 483-497, 2001.
- [3] Rasmussen B, Machimbarrena M, *COST Action TU0901 Building acoustics throughout Europe. Volume 1: Towards a common framework in building acoustics throughout Europe*, DiScript Preimpresion, 2014, ISBN: 978-84-697-0158-4.
- [4] Peterson A, *Handbook of noise measurements*, General Radio Company, 1980, Form No: 5301-8111-0.
- [5] Harding G W, Bohne B A, *Temporary DPOAE level shifts, ABR threshold shifts and histopathological damage following below-critical-level noise exposures*, Hear. Res., 196, pp. 94108, 2004.
- [6] Tomei G, Anzani M F, Casale T, Tomei Fa, Piccoli F, Cerratti D, Paolucci M, Filippelli M, Fioravanti M, Tomei Fr, *Effetti extrauditivi del rumore*, G. Ital. Med. Lav. Erg., 31:1, pp. 37-48, 2009.
- [7] Persson Waye K, Aggea A, Clowb A, Hucklebridgeb F, *Cortisol response and subjective sleep disturbance after low-frequency noise exposure*, J. Acoust. Soc. Am., 277, pp. 453457, 2007.
- [8] Saeki T, Fujii T, Yamaguchi S, Harima S, *Effects of acoustical noise on annoyance, performance and fatigue during mental memory task*, Applied Acoustics, 65, pp. 913921, 2004.
- [9] Hensel J, Scholz G, Hurttig U, Mrowinski D, Janssen T, *Impact of infrasound on the human cochlea*, Hearing Research, 233(1-2), pp. 67-76, 2007.
- [10] ISO 226:2003. *Acoustics - Normal equal-loudness-level contours*.

- [11] DIN 45631:1991. *Berechnung des Lautstärkepegels und der Lautheit aus dem Geräuschspektrum Verfahren nach E. Zwicker.*
- [12] Watanabe, T., Müller, H., *Low frequency hearing thresholds in pressure field and free field*, J. Low Frequency Noise Vibrat., 9, pp. 106115, 1990.
- [13] General Federal Environment Agency survey (UBA), *Noise annoyance*, International Noise Awareness Day, 27 April 2011.
- [14] Regulation (EU) No 305/2011 of the European Parliament and of the Council, *Harmonised conditions for the marketing of construction products*, Official Journal of the European Union, 2011.
- [15] World Health Organization (WHO), *Burden of disease from environmental noise*, JRC European Commission, 2011, ISBN: 978-92-890-0229-5.
- [16] Rasmussen B, Machimbarrena M, *COST Action TU0901 Building acoustics throughout Europe. Volume 2:Housing and construction types country by country*, DiScript Preimpresion, 2014, ISBN: 978-84-697-0159-1.
- [17] Meier A, Schmitz A, Raabe G, *Inter-laboratory test of sound insulation measurements on heavy walls: part II - results of main test*, Building Acoustics, 6, pp. 171-186, 1999.
- [18] Di Bella A, Pontarollo C M, *Comparison of uncertainties in acoustic measurements in building with different test methods*, Forum Acusticum 2011, Aalborg, Denmark.
- [19] Wittstock V, *Uncertainties in building acoustics*, Forum Acusticum 2005, Budapest, Hungary.
- [20] Simmons C, *Uncertainty of measured and calculated sound insulation in buildings - Results of a Round Robin test*, Forum Acusticum 2005, Budapest, Hungary.
- [21] Roland J, Villenave M, Gagliardini L, Soubrier D, *Inter-comparison of measurements of noise attenuation by double glazed windows in frames*, ECC-BCR study, Contract No. 3165/1/0/078/87/7 BCR-B(30), 1991.
- [22] Masovic D, *Low frequency measurements in building acoustics Analysis of reverberation time field measurement results*, 20th Telecommunications forum TELFOR 2012, Belgrade, Serbia.
- [23] Hagberg K, Thorsson P, *Uncertainties in standard impact sound measurement and evaluation procedure applied to light weight structures*, Proceedings of 20th International Congress on Acoustics, ICA 2010, Sydney, Australia.

- [24] ISO 10140:2010. *Acoustics - Laboratory measurement of sound insulation of building elements - Part 2: Measurement of airborne sound insulation.*
- [25] Kuttruff H, *Room acoustics*, Taylor & Francis, Abingdon, 2000.
- [26] Hopkins C, Turner P, *Field measurement of airborne sound insulation between rooms with non-diffuse sound fields at low frequencies*, Applied Acoustics, 66, pp. 1339-1382, 2005.
- [27] Kropp W, Pietrzyk A, Kihlman T, *On the meaning of sound reduction index at low frequencies*, Acta Acustica, 2, pp. 379-392, 1994.
- [28] Roland J, *Adaptation of existing test facilities to low frequencies measurements*, Proceedings of InterNoise 1995, Newport Beach, California, USA.
- [29] Simmons C, *Measurement of sound pressure levels at low frequencies in rooms. Comparison of available methods and standards with respect to microphone positions*, NT Techn Report 385, 1997.
- [30] Mullholland K A, Lyon R H, *Sound insulation at low frequencies*, J. Acoust. Soc. Am., 54, pp. 867-878, 1973.
- [31] Osipov A, Mees P, Vermeir G, *Low-frequency airborne sound transmission through single partitions in buildings*, Applied Acoustics, 52, pp. 273-288, 1997.
- [32] Pedersen D B, Roland J, Raabe G, Maysenhoder W, *Measurement of the low-frequency sound insulation of building components*, Acta Acustica, 86, 495-505, 2000.
- [33] ISO 717:2013. *Acoustics - Rating of sound insulation in buildings and of building elements - Part 1: Airborne sound insulation.*
- [34] Scholl W, Lang J, Wittstock V, *Rating of sound insulation at present and in future. The revision of ISO 717*, Acta Acustica, 97, pp. 686-698, 2011.
- [35] Granzotto N, Di Bella A, *Analysis between weighted sound reduction index according to ISO 717-1 and indices according to ISO 16717-1*, Proceedings of AIA-DAGA 2013, Merano, Italy.
- [36] ISO 10140:2010. *Acoustics - Laboratory measurement of sound insulation of building elements - Part 3: Measurement of impact sound insulation.*
- [37] Neves e Sousa A, Gibbs B M, *Parameters influencing low frequency impact sound transmission in dwellings*, Applied Acoustics, 78, pp 77-88, 2014.

- [38] Bradley J S, *Annoyance caused by constant-amplitude and amplitude-modulated sounds containing rumble*, Noise Control Engineering Journal, 42 (6), pp. 203-208, 1994.
- [39] Landstrom U, Akerlund E, Kjellberg A, Tesarz M, *Exposure levels, tonal components, and noise annoyance in working environments*, Environment International, 21 (3), pp. 265-275, 1994.
- [40] Stephenson M, *Assessing the quality of low frequency audio reproduction in critical listening spaces*, Degree of Doctor of Philosophy, School of Computing, Science & Engineering, University of Salford, Salford, UK, May 2012.
- [41] ISO 3382:2008, *Acoustics - Measurement of room acoustic parameters - Part 2: Reverberation time in ordinary rooms*.
- [42] Cingolani S, Spagnolo R, *Acustica musicale e architettonica*, UTET, Torino, 2009.
- [43] Hopkins C, *Sound insulation*, Elsevier, Oxford, 2007.
- [44] Jo C H, Elliott S J, *Active control of low-frequency sound transmission between rooms*, J. Acoust. Soc. Am., 92, pp. 1461-1472, 1992.
- [45] Morse P, *Vibration and sound*, McGraw-Hill, New York, 1948.
- [46] Jo C H, *Active control of low frequency sound transmission*, M.S. thesis, University of Southampton, 1990.
- [47] ISO 10140:2010. *Acoustics - Laboratory measurement of sound insulation of building elements - Part 5: Requirements for test facilities and equipment*.
- [48] Cremer L, Heckl M, Ungar E E, *Structure-Borne Sound*, Springer, Heidelberg, 1988.
- [49] Duarte E, Moorhouse A, Viveiros E B, *Indirect measurement of acoustic power into a small room at low frequencies*, Applied Acoustics, 73(3), pp. 248-255, 2012.
- [50] JCGM 100:2008, *Evaluation of measurement data Guide to the expression of uncertainty in measurement*.
- [51] ISO 12999:2014. *Acoustics - Determination and application of measurement uncertainties in building acoustics - Part 1: Sound insulation*.
- [52] Wittstock V, Schmelzer M, Kling C, *On the use of scaled model in building acoustics*, Proceedings of Euronoise 2008, Paris, France.

- 
- [53] ISO 10140:2010. *Acoustics - Laboratory measurement of sound insulation of building elements - Part 1: Application rules for specific products - Annex H: Floor coverings - Improvement of impact sound insulation.*
- [54] Ver I L, *Impact noise isolation of composite floors*, J. Acoust. Soc. Am., 50. pp. 1043-1050, 1971.
- [55] Beranek L L, *Noise and Vibration Control*, Institute Noise Control Eng., 1988.



# Acknowledgements

I wish to express my sincere gratitude to my supervisor, Dr. Alessandro Schiavi, for his patient guidance and his expert scientific support. I benefit a lot from his valuable experience and knowledge, not only scientific, but also literary and human. I wish to thank Dr. Arianna Astolfi, from Politecnico di Torino, for including me in different projects, acoustics field measurements and for giving me the possibility to teach at Politecnico di Torino; Dr Pavoni Belli, for his precious support in laboratory measurements and his wise and priceless teaching; Dr Laura Rossi, for her fruitful knowledge and collaboration in many projects and ideas; M.S. thesis students, Federico Casassa and Anna Ruatta for their fundamental help and the great work developed with me; the members of INRIM Acoustics Department for these 3 years together, in alphabetic order: Dr. Antonio Agostino, Dr. Alberto Giuliano Albo, Dr. Giuliana Benedetto, Dr. Elisabetta Chirivi', Dr. Mario Corallo, Dr. Rugiada Cuccaro, Dr. Gianni Durando, Dr. Roberto Gavioso, Dr. Claudio Guglielmone, Dr. Simona Lago, Dr. Daniele Madonna Ripa, Dr. Chiara Magnetto, the pitied colleague Dr. Francesco Russo, Prof. Renato Spagnolo, Dr. Paolo Tarizzo, Dr. Adriano Troia; Dr. Louena Shtrepi and Dr. Giuseppina Puglisi from Politecnico di Torino, for sharing with me courses, measurements and conferences. A special thank to the whole Acoustic Department of PTB (Braunschweig, Germany) for their kind welcome, availability and scientific support, especially to Dr. Werner Scholl and Dr. Volker Wittstock. I am also grateful to Federica, my family and my friends for their steady support.